Colorado State University
Fall Session 2011

CHEM 475
Physical Chemistry Laboratory - 1

Notes for
Determination of Rotational Barrier via Nuclear Magnetic Resonance (NMR)

The following is a set of short notes to outline the experiment in question and to provide helpful guidance to those executing the experiment.

A. Nuclear Magnetic Resonance (NMR) is capable of probing chemically distinct species in a molecule and to provide information on the molecular dynamics of those species.

B. In substituted amido compounds 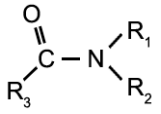

, the C–N bond displays a substantial barrier to rotation and the nitrogen substituents, R_1 and R_2, are found to be co-planar with the carbonyl group.

C. The compounds N,N-dimethylacetamide and N,N-dimethylformamide are examplars of this behavior and suitable for study via NMR.

D. The rotational isomerization of N,N-dimethylacetamide about the C–N bond has been studied with moderately low field NMR (1.4 T or 60 MHz for ^{1}H resonance). Varying the sample temperature causes the rotational rate about the C–N to vary in turn. At sufficiently high rates motional averaging of the NMR signals corresponding to these to methyl groups occurs and they coalese into a single signal.

E. At the higher field available in this laboratory (7.1 T or 300 MHz for ^{1}H resonance), the minimum rate necessary for coalescense and the temperature required for the attainment of this rate is significantly higher than at low field.

F. The observation of these various signals is the experimental target of this experiment. The simulation and analysis of these signals using NMR processing software followed by the interpretation of this analysis in terms of suitable thermodynamic variables will be performed. The theoretical explanation of the origin of the rotational barrier will be discussed in the Laboratory Report.

G. The dynamic analysis to be performed requires accurate knowledge of the sample temperature throughout the experiment and a separate calibration of this experimental variable is required.

H. The elevated temperatures required by this experiment may necessitate sealing of NMR tubes containing samples.

Francis P. Gasparro
Department of Biochemical Sciences
Princeton University
Princeton, New Jersey 08540

and Nancy H. Kolodny
Wellesley College
Wellesley, Massachusetts 02181

NMR Determination of the Rotational Barrier in N,N-dimethylacetamide

A physical chemistry experiment

Nuclear magnetic resonance spectroscopy has long been taught at the undergraduate level as an effective tool for structural studies. Although it has been almost 20 years since the first studies of rate processes by nmr spectroscopy were reported (*1*) little about this technique has filtered down to the undergraduate level. Consider, for example, the lack of dynamic nmr experiments in the current physical chemistry laboratory manuals (*2*). In this experiment the barrier to rotation in N,N-dimethylacetamide is determined by measuring changes in nmr line shapes as a function of temperature. This study is an example of dynamic nuclear magnetic resonance spectroscopy.

The beauty of this method is twofold. First, dynamic aspects of systems which are at chemical equilibrium can be studied. For example, rate information can be obtained for virtual reactions, such as the cis-trans isomerization of N,N-dimethylacetamide in which reactants and products are chemically identical

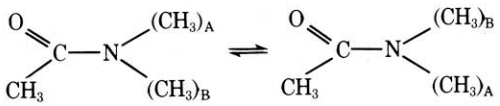

Second, due to the characteristic period of the nmr measurement, a range of reaction rates usually encountered in the laboratory is easily accessible (10^{-1}–10^{-5} s^{-1}). In addition, rotational barriers in the range 3–20 kcal/mole can be studied by this method (*3*).

Theory

Line Shape Analysis

If two groups of chemically equivalent nuclei are exchanged by an intramolecular process, the nmr spectrum is a function of the difference in their resonance frequencies, $\nu_A - \nu_B = \Delta\nu$, and of the rate of exchange, k. (A typical value for $\Delta\nu$ is about 10 Hz.) The effects of exchange at several temperatures on the linewidths at ν_A and ν_B are shown in Figure 1. At low temperatures the exchange is slow and $k \ll \Delta\nu$. The spectrum thus consists of two sharp singlets at ν_A and ν_B (Fig. 1 *A*). At high temperatures the exchange is fast; i.e. $k \gg \Delta\nu$ and a single sharp peak is observed (Fig. 1 *D*). There is also an intermediate temperature range over which the spectrum consists of two significantly broadened overlapping lines (Fig. 1 *B*).

Usually spin-spin and spin-lattice relaxation determine the width of an nmr absorption peak (*7*). Here we are concerned with the additional effect of exchange of two groups of chemically equivalent nuclei on linewidth. The Heisenberg uncertainty principle states that the product of the uncertainty in the measurement of the energy of a particular state, ΔE, and the uncertainty in the lifetime of the state, Δt, is approximately equal to $\hbar$; i.e

$$\Delta E \Delta t \simeq \hbar \tag{1}$$

Since

$$\Delta E = h\Delta\nu_{1/2} \tag{2}$$

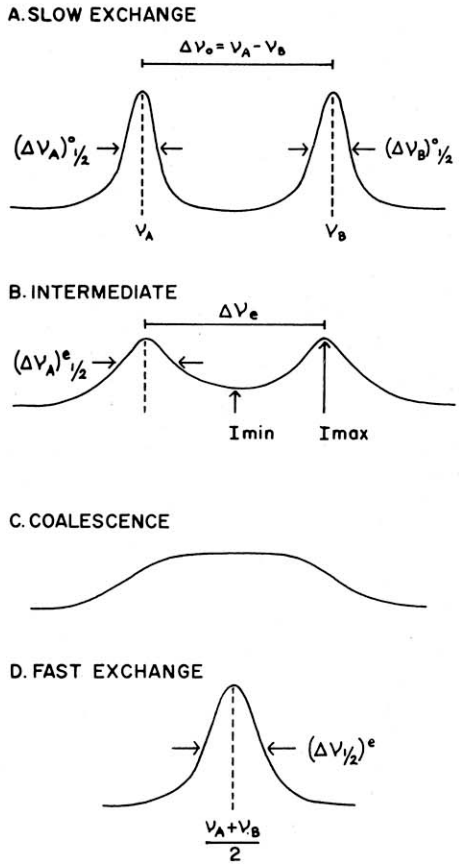

Figure 1. Effect of exchange of chemically equivalent nuclei on nmr line shapes.

$\Delta\nu_{1/2}$, the absorption linewidth for the transition, is inversely proportional to the lifetime of the excited state

$$\Delta\nu_{1/2} = \frac{\Delta E}{h} = \frac{\Delta E \Delta t}{h \Delta t} = \frac{1}{2\pi\Delta t} \tag{3}$$

An exact analysis of the line broadening produced by the exchange process is derived from the Bloch equations (*4*). The Bloch equations describe the motion of the bulk magnetic moment of a sample in the presence of a static field, H_0, and a rotating field, H_1, perpendicular to H_0.

The exact function for the lineshape (*5*) in the case of two equivalent exchanging groups with no coupling is given by

$$g(\nu) = \frac{K\tau(\nu_A - \nu_B)^2}{\left[\frac{1}{2}(\nu_A - \nu_B) - \nu\right]^2 + 4\pi^2\tau^2(\nu_A - \nu)^2(\nu_B - \nu)^2} \tag{4}$$

where $g(\nu)$ is the intensity at the frequency, ν; K is a normalization constant and $\tau = 1/2k$ where k is the rate constant for the exchange. τ, ν_A, and ν_B are functions of temperature and cannot be determined separately. Computer programs are available in which estimated values for τ, ν_A, and ν_B are used to generate $g(\nu)$ which is then compared to the experimental spectrum.[1] Values for τ, ν_A, and ν_B are chosen such that the deviation between the experimental and calculated lineshapes is minimized. Alternatively various approximations can be made which apply over different ranges of exchange rates.

[1] For example, see Program 140 or 165, Quantum Chemistry Program Exchange, Indiana University, Bloomington, Indiana 47401.

Approximate Methods for Evaluation of Rate Constants (6).

Direct calculation of the lifetime of a specific spin state from eqn. (4) can be made over a limited temperature range. Beyond a certain temperature, the rate of exchange is so fast that the magnetic environments of the two sets of nuclei are identical and any possible distinction between the two sets of nuclei is lost. Thus we have only one set of spins with a lifetime determined by spin-spin and spin-lattice relaxation mechanisms.

As the temperature is varied from values at which the rate of exchange is low through values of intermediate exchange rates, to rapid exchange, a series of approximations is available for the calculation of lifetimes. Although these approximate methods provide somewhat less accurate results than does eqn. (4), they present the student with a meaningful treatment of the data obtained by an nmr study of a chemical rate process.

Slow and Intermediate Exchange: At slow exchange rates the spectrum consists of two lines. In this region $\tau \gg (\nu_A - \nu_B)^{-1}$, and eqn. (4) reduces to

$$g(\nu)_A = g(\nu)_B = \frac{KT_{2A}'}{1 + T_{2A}'^2(\nu_A - \nu)^2} \tag{5}$$

where T_{2A}' is the spin-spin relaxation time. Comparison of eqn. (5) to the exact function shows that the linewidth of the line at ν_A is

$$(\Delta\nu_A)_{1/2} = \frac{1}{\pi}\left(\frac{1}{T_{2A}'} + \frac{1}{\tau_A}\right) \tag{6}$$

In the absence of exchange the linewidth is $(\Delta\nu_0)_{1/2} = (\pi T_{2A}')^{-1}$. Exchange results in *broadening* equal to $(\pi\tau_A)^{-1}$. A value for k $(= 1/2\tau)$ is determined by comparing linewidths at half height of exchanging peaks to those of peaks recorded at temperatures where the rate of exchange is very small

$$k = \pi[(\Delta\nu_e)_{1/2} - (\Delta\nu_0)_{1/2}] \tag{7}$$

For slow exchange, the rate can also be related to the change in *peak separation.* Equation (8) applies over the limited range where there is extensive overlap between the two separate peaks (but not too close to coalescence, see below)

$$k = \frac{\pi}{\sqrt{2}}(\Delta\nu_0^2 - \Delta\nu_e^2)^{1/2} \tag{8}$$

where $\Delta\nu_i$ is the peak separation in Hz, and the subscripts (i = e or 0) have the previously defined meanings.

A third method applies in the slow exchange region. In the *ratio method,* k is calculated from the ratio of the intensities of the peaks, I_{max}, to the intensity midway between the peaks, I_{min}, $r = I_{max}/I_{min}$ and

$$k = \frac{\pi\Delta\nu_0}{\sqrt{2}}(r + (r^2 - r)^{1/2})^{-1/2} \tag{9}$$

Coalescence Temperature: The coalescence temperature is defined as the temperature at which the appearance of the spectrum changes from that of two separate peaks to that of a single, flat-topped peak (see Fig. 1*C*). At this temperature

$$k = \frac{\pi\Delta\nu_0}{\sqrt{2}} \tag{10}$$

Fast Exchange: At temperatures above the coalescence temperature, the spectrum consists of a single peak. In this region $\tau \ll (\nu_A - \nu_B)^{-1}$ and eqn. (4) reduces to

$$g(\nu) = \frac{KT_2'}{1 + \pi T_2'(\nu_A + \nu_B - 2\nu)^2} \tag{11}$$

If the signal is not completely collapsed, i.e., the process is slow enough to contribute to its width but is still well beyond the rate corresponding to separate signals, the following approximation results

$$k = \frac{\pi\Delta\nu_0^2}{2}[(\Delta\nu_e)_{1/2} - (\Delta\nu_0)_{1/2}]^{-1} \tag{12}$$

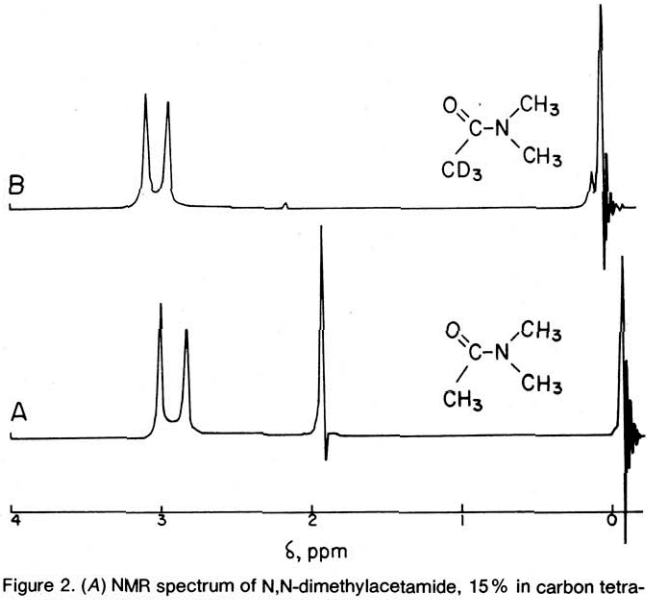

Figure 2. (*A*) NMR spectrum of N,N-dimethylacetamide, 15% in carbon tetrachloride (2% TMS). (*B*) NMR spectrum of acetyl deuterated N,N-dimethylacetamide, 15% in carbon tetrachloride (2% TMS).

Experimental

A 15 volume percent solution of freshly distilled N,N-dimethylacetamide (NNDMA) is prepared gravimetrically in carbon tetrachloride containing 2% tetramethylsilane (TMS). The sample is transferred to a clean and dry nmr tube, degassed, and permanently sealed. Degassing is required in order to remove paramagnetic oxygen which, if not removed, would result in an additional, indeterminate line broadening factor. To be sure that the sealed nmr tube can withstand exposure to high temperatures, the tube should be immersed in an oil bath and heated to ~160°C.

Any nmr spectrometer equipped with a variable temperature probe may be used for the spectral measurements. A series of spectra is recorded at each temperature until no further change in spectral characteristics (line-width or peak separation) is observed. The resolution of the instrument should be checked at each temperature by recording the methyl resonance of TMS. The temperature is most conveniently determined using either a sample of ethylene glycol (above ambient): $T = 466.4 - 1.705\,(\Delta\nu) - 63.4\,(\Delta\nu/100)^2$ or methyl alcohol (below ambient): $T = 406.0 - 0.551\,(\Delta\nu)$ (*8*).

Exact peak positions and linewidths are determined using the sideband technique (*7*). This technique may also be used to calibrate the chart paper. Typical full scale spectra obtained with a Perkin-Elmer R12 nmr spectrometer are shown in Figure 2. Figure 3 shows results at temperatures ranging from 259–368°K. These results were obtained with the spectrometer set on the 50 Hz scale.

The data are divided into three groups corresponding to slow exchange and intermediate exchange, coalescence temperature, and fast exchange. Then eqns. (7) through (12) are used to calculate k (Table 1). Figure 4 shows a plot of log k versus $(T\ (°K))^{-1}$. The slope of this plot yields a value for the activation energy. Using values of k extending over the entire temperature range, 279–485°K, E_a was found to be 14 kcal/

Table 1. Typical Values for *k*

T (°K)	k (s^{-1})
279	1.45
288	2.35
308	5.95
325	19.8
331	24.1
334	27.8
348	129
368	598
485	805

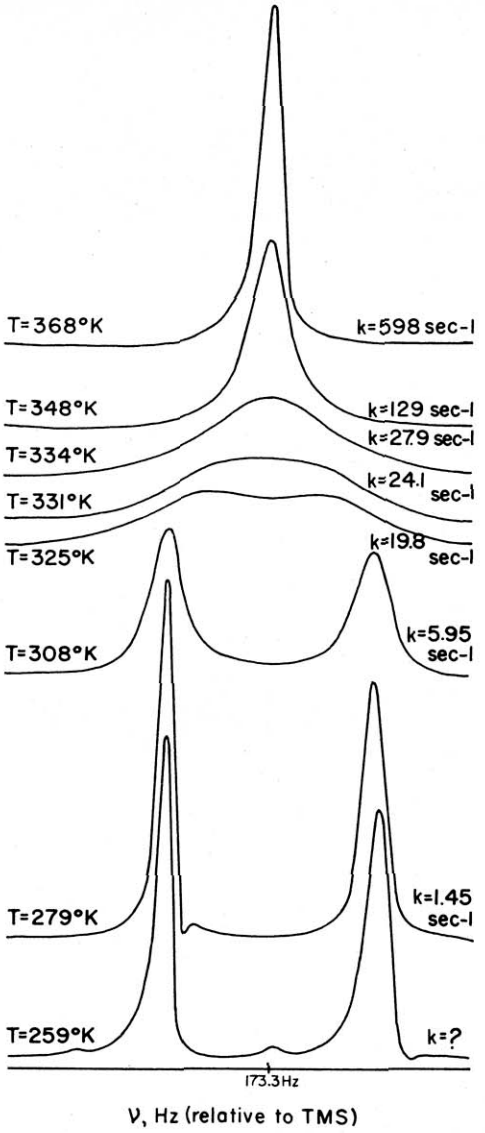

Figure 3. Effect of temperature on line shapes and values for k, the exchange rate for the two N-methyl groups.

Table 2. Comparison to Values of Reeves, et al. (9)

	This study	Reeves et al. (9)
T_c, (°K)	331	339
E_a (kcal/mole)	17(14)[a]	16.8
$\Delta G^{\ddagger}$ (kcal/mole)	17	17.3
$\Delta H^{\ddagger}$ (kcal/mole)	16	16.3
$\Delta S^{\ddagger}$ (e.u.)	−2.1	−3.59

[a] See Discussion Section.

mole. Eliminating values for k at the two lowest temperatures yielded a value for E_a = 17 kcal/mole, in much better agreement with the 16.8 kcal/mole determined by Reeves et al. (*9*) in an identical study. The quantity, $\Delta G^{\ddagger}$, is obtained from a plot of log (k/T) versus T^{-1}. From values for E_a and $\Delta G^{\ddagger}$, $\Delta H^{\ddagger}$ and $\Delta S^{\ddagger}$ can be evaluated. See Table 2 for a comparison of the results of this study with the values obtained by Reeves et al. (*9*).

Discussion

Amides are the simplest model compounds for the peptide bond in proteins. The conformation of the peptide bond plays an important role in determining the backbone structure of proteins (*10*). X-Ray crystallographic results indicate that the trans configuration (*11*) is the predominant form in amides, polypeptides, and proteins. However, recent work has shown

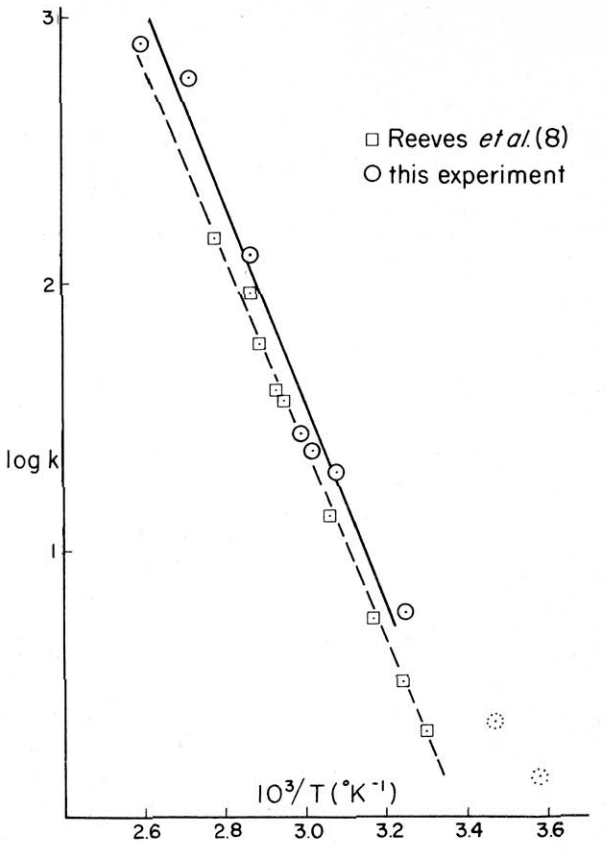

Figure 4. Log k versus $10^3/T$ (°K).

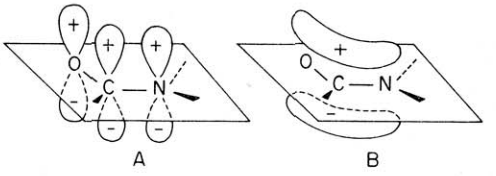

Figure 5. (*A*) Sigma-bonding skeleton for peptide group. (*B*) Pi-bonding molecular orbital for peptide group.

that the cis form does occur in some proteins and polypeptides (*12*).

The planarity of the peptide bond originates from the delocalization of the carbonyl electrons and two resonance structures, (I) and (II), can be drawn

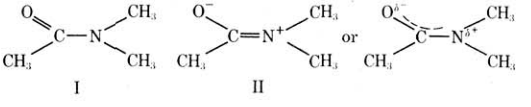

Alternatively, the origin of this rotational barrier can be viewed in terms of molecular orbital theory. After constructing the sigma bonding skeleton, the carbon, nitrogen, and oxygen atoms each have a p orbital "left over." (See Figure 5*A*.) One possible linear combination of these p orbitals leads to a π bonding molecular orbital which extends over the three atoms, Figure 5*B*.

If the $-N(CH_3)_2$ moiety rotates freely, we would expect the complete nmr spectrum of NNDMA to consist of two singlets, with an intensity ratio of 2:1 (2 methyls on nitrogen, 1 methyl on the carbonyl carbon). The nmr spectrum shown in Figure 2*A* is thus not consistent with free rotation about the peptide bond. Instead of one peak at 3 ppm and one at 2 ppm, there are two peaks at ~3 ppm in addition to the one at 2 ppm. This is thought to result from the two $-N-CH_3$ groups being in magnetically nonequivalent environments. One methyl group is cis to the carbonyl bond and the other is cis to the acetyl

methyl group. The upfield resonance at ~3 ppm is assigned to the $-NCH_3$ group cis to the acetyl methyl; the downfield resonance at ~3 ppm is assigned to the $-NCH_3$ group cis to the carbonyl bond. The 2 ppm resonance is assigned to the acetyl methyl protons.

The effects of the rotational barrier, i.e. different magnetic environments for the two N-methyl groups, observed at low temperatures (Fig. 3) vanish at higher temperatures. The rate of exchange between the two magnetic environments increases as the temperature is increased. The lifetime of each state thus decreases and hence the absorption peak is broadened. At temperatures below the coalescence temperature few molecules have sufficient energy to overcome the barrier to rotation. However, at temperatures greater than the coalescence temperature, many molecules have sufficient thermal energy to overcome the barrier and therefore rotation occurs. Thus there is no longer a preferred configuration (cis or trans) and the spectrum is the single line characteristic of free rotation about a single bond. Further increases in temperature cause the line to narrow.

Our results are in good agreement with those of Reeves et al. (*9*). One experimental difficulty plagued our attempts to accurately determine k at low temperatures (<288°K). A significant amount of drift was noted as the doublet was recorded at these temperatures, thus introducing an indeterminate uncertainty in both the linewidths and peak separations. Elimination of the two values for k at 279°K and 288°K resulted in marked improvement in the value for E_a which increased from 14 to 17 kcal/mole. The drift could be eliminated by using an instrument provided with a locking mode.

To avoid the effects of coupling between the trans N-methyl group and the acetyl methyl group, linewidth measurements were made on the cis peak only. This coupling effect can be almost completely eliminated by studying the acetyl deuterated analog of NNDMA, because proton-deuterium coupling is markedly smaller than proton-proton coupling (*13*). (Compare the peaks centered at ~3 ppm in Fig. 2*A* and 2*B*.)

Related Projects

The magnitude of the rotational barrier in NNDMA has been shown to be both solvent and concentration dependent. At high concentrations and in the presence of polar solvents, molecular complex formation leads to values for E_a significantly greater than 17 kcal/mole (*14*).

The scope of this experiment can be broadened by including the synthesis and purification (*15*) of the acetyl deuterated analog of NNDMA. As such it would be an experiment suitable for project-type laboratories currently in vogue. Infrared spectroscopy (*16*) and dielectric studies (*17*) can also supplement the nmr results.

Literature Cited

(1) Gutowsky, H. S., and Holm, C. H., *J. Chem. Phys.*, **25,** 1228 (1956). For a quick overview see Sandstrom, J., *Endeavour*, **23,** 111 (1974).
(2) Shoemaker, D. P., Garland, C. W., and Steinfeld, J. I., "Experiments in Physical Chemistry," 3rd Ed., McGraw-Hill, New York, **1974;** Daniels, F., Williams, J. W., Bender, P., Alberty, R. A., and Cornwell, C. D., "Experimental Physical Chemistry," 7th Ed., McGraw-Hill, New York, **1974;** for descriptions of two nmr kinetics experiments see Oelke, W. C., "Laboratory Physical Chemistry," Van Nostrand Reinhold Co., New York, **1969;** and Socrates, G., J. CHEM. EDUC. **44,** 575 (1967).
(3) Bovey, F. A., "Nuclear Magnetic Resonance Spectroscopy," Academic Press, New York, **1969,** Chapter VII.
(4) Ref. (*3*), pp. 184–188.
(5) Carrington, A., and McLachlan, A. D., "Introduction to Magnetic Resonance," Harper and Row, New York, **1967,** pp. 205–208.
(6) Johnson, E. S., *in* "Advances in Magnetic Resonance," (*Editor:* Waugh, J. S.), Academic Press, New York, **1966,** Volume 1, Chapter 2, pp. 64–68.
(7) Pople, H. A., Schneider, W. G., and Bernstein, H. J., "High Resolution Nuclear Magnetic Resonance," McGraw-Hill, New York, **1967,** pp. 74–77.
(8) Van Geet, A. L., *Anal. Chem.*, **40,** 2227 (1968).
(9) Reeves, L. W., Shaddick, R. C., and Shaw, K. N., *Can. J. Chem.*, **49,** 3683 (1971).
(10) Stewart, W. E., and Siddall, T. H., *Chem. Rev.*, **70,** 517 (1970).
(11) Pauling, L., "The Nature of the Chemical Bond," Cornell University Press, Ithaca, New York, **1948,** p. 207.
(12) Torchia, D. A., *Biochemistry*, **11,** 1462 (1972).
(13) Newman, R. C., and Jonas, V., *J. Amer. Chem. Soc.*, **90,** 1970 (1968).
(14) Calzolari, A., Conti, F., and Franconi, C., *J. Chem. Soc., B,* 555 (1970).
(15) Vogel, A. I., "Textbook of Organic Chemistry," 3rd Ed., John Wiley & Sons, New York, **1956,** p. 394. (Modification of synthesis of acetamide using dimethyl ammonia.)
(16) Hallam, H. E., and Jones, C. M., *J. Mol. Struct.*, **5,** 1 (1970).
(17) Moffat, J. B., J. CHEM. EDUC., **43,** 74 (1966).

Rate Processes and Nuclear Magnetic Resonance Spectra. II. Hindered Internal Rotation of Amides*

H. S. GUTOWSKY AND C. H. HOLM†
Noyes Chemical Laboratory, University of Illinois, Urbana, Illinois
(Received January 30, 1956)

Mathematical methods are presented for calculating rate constants of processes which narrow nuclear magnetic resonance absorption lines having discrete components. High resolution proton spectra show that the $R_1CO\text{-}NR_2R_3$ skeletons of N,N-dimethylformamide (DMF) and N,N-dimethylacetamide (DMA) are planar and suggest that N-methylformamide, N-methylacetamide, N-methylformanilide and N-methylacetanilide exist predominantly in one configuration. The presence of a significant amount of double bond character in the C—N amide bond is proved by the temperature dependent coalescence observed for the chemically shifted proton doublet of the $N(CH_3)_2$ groups in DMF and DMA, which gives values of about 22 and 19 kcal respectively for the free energy of activation required for reorientations about the bond.

I. INTRODUCTION

MOST characteristics of nuclear magnetic resonance spectra[1] are influenced to some extent by the various motions of the molecules, ions or atoms containing, or in the vicinity of, the nuclei observed. These effects provide several methods of studying a wide range of kinetic phenomena. Bloombergen, Purcell, and Pound[2] (BPP) made the first extensive theoretical and experimental analysis demonstrating the importance of "lattice motions" as a mechanism for spin-lattice relaxation and for narrowing the absorption lines. This article is concerned with a line narrowing phenomenon differing superficially from that described by BPP[2] but identical in principle; both belong to a general class containing a number of such effects.

In the case investigated by BPP the widths and structure of the absorption line were determined directly by the local magnetic dipole fields of the magnetic nuclei. The dipole fields depend upon the direction and distance of the observed nuclei from the neighboring dipoles; and it is this dependence which leads to the motional effects, as may be seen from the following qualitative argument. Suppose two nuclei have Larmor precessional and resonance frequencies differing by $\Delta\nu$ because of differences in the local dipole fields. If the nuclei are precessing in phase at a given instant they will be 180° out of phase $(\frac{1}{2}\Delta\nu)$ sec later. However, if the local fields change during this time, then the rate of getting out of phase changes and the difference in precessional and resonance frequency is modified. The spectrum of the dipole fields is symmetric, with negative as well as positive values, so the lattice motions will reduce the effective dipolar splitting or broadening, providing the frequency of the motions is comparable to the frequency equivalent of the perturbation to be reduced. The detailed analysis of this motional narrowing[2] is complicated by the continuous character of the local field spectrum.

Similar arguments apply to other perturbations which are time dependent. A motional model was proposed to account for the absence in certain liquids of the multiple NMR spectra produced by the local magnetic fields from electrons polarized by magnetic nuclei.[3] In this case, the resonance absorption of one group of nuclei is split into discrete components depending on the spin coordinates of a second group of nuclei in the same molecule. Fluctuations in the spin coordinates of one group, if fast enough, will average out the splitting and narrow the resonance of the second group to a single line. Ogg has reported[4,5] several instances in which such a transition from a multiple to a single resonance can be effected by adjusting the chemical exchange rate of one of the interacting groups. Estimates of specific rate constants for the exchange were made[5] by applying the qualitative criterion outlined above to the conditions under which the transitions occurred. In a related experiment, an rf field at the resonance frequency can be used to change "artifically" the spin coordinates of one group of nuclei at a known and adjustable rate while observing the multiplet resonance of the other group. Multiplet resonances have been observed to coalesce in a predictable manner in such experiments,[6] which differ from the "naturally occurring" processes such as chemical exchange in that the latter produce random rather than coherent fluctuations in the spin coordinates.

In this paper we are concerned primarily with differences in the local magnetic fields and resonance positions produced by chemical differences in the magnetic shielding of nuclei in different electronic environments, which also can be averaged by the proper rate processes.[7] This case is equivalent to that of the multiplets. In the first paper of this series,[7] the

* Supported by the U. S. Office of Naval Research.
† Presently at the Shell Development Company, Emeryville, California.
[1] E. R. Andrew, *Nuclear Magnetic Resonance* (Cambridge University Press, Cambridge, 1955), gives a general introduction to the field.
[2] Bloombergen, Purcell, and Pound, Phys. Rev. **73**, 679 (1948).
[3] Gutowsky, McCall, and Slichter, J. Chem. Phys. **21**, 279 (1953).
[4] R. A. Ogg, Jr., J. Chem. Phys. **22**, 560 (1954).
[5] R. A. Ogg, Jr., Discussions Faraday Soc. **17**, 215 (1954).
[6] A. L. Bloom and J. N. Shoolery, Phys. Rev. **97**, 1261 (1955).
[7] H. S. Gutowsky and A. Saika, J. Chem. Phys. **21**, 1688 (1953).

theory developed for the multiplets was used to interpret the single proton resonance lines with concentration dependent positions resulting from proton exchange among the various chemical species in aqueous solutions of HNO_3, H_2SO_4 and others. Line shapes were computed for several exchange rates in the transition region and it was pointed out that rate constants could be calculated directly from observations of such line shapes. Details of these calculations are given here, and the methods are used to analyze the proton spectra observed for several amides, yielding numerical values for the rate at which internal molecular reorientations take place about the C—N bond in N,N-dimethylformamide and N,N-dimethylacetamide.

II. MATHEMATICAL METHODS

Our starting point is very nearly the model used previously.[7] More general theories of motional effects have since been developed.[8,9] However, the analysis[3] based on the Bloch equations[10] is much simpler yet entirely adequate for handling most cases of immediate chemical interest. We consider a liquid in which there is negligible dipolar broadening of a proton (or other) resonance because of motional narrowing, but in which there are sites with different local fields giving a resonance with two components A and B shifted by $+\delta\omega/2$ and $-\delta\omega/2$ from their average angular frequency. The relative intensities of these components are directly proportional to the proton fractions p_A and p_B contributing to each component.

The process in question interchanges protons between sites A and B, so if the protons N_A and N_B at each site are labeled N_A^* and N_B^* at some instant

$$dN_A^*/dt=-k_AN_A^* \quad \text{and} \quad dN_B^*/dt=-k_BN_B^*, \quad (1)$$

where $k_Ap_A=k_Bp_B$. The average lifetime of protons at each site is therefore

$$\tau_A=1/k_A=\tau/p_B \quad \text{and} \quad \tau_B=1/k_B=\tau/p_A, \quad (2)$$

where $\tau=\tau_A\tau_B/(\tau_A+\tau_B)$. The proton absorption line shape is described by the imaginary part of the total rf nuclear magnetization of the two states. When averaged over the proton interchange, the total magnetization M is that given by Eq. (18) of reference 7,

$$M=\frac{i\omega_1M_0[(\tau_A+\tau_B)+\tau_A\tau_B(\alpha_Ap_B+\alpha_Bp_A)]}{(1+\alpha_A\tau_A)(1+\alpha_B\tau_B)-1}, \quad (3)$$

where ω_1 describes the applied rf field, M_0 is the static nuclear magnetization at thermal equilibrium, while $\alpha_A=(1/T_2)-i(\Delta\omega+\delta\omega/2)$ and $\alpha_B=(1/T_2)-i(\Delta\omega-\delta\omega/2)$. This assumes the resonance absorption is plotted at a constant static magnetic field as a function of the different $\Delta\omega$ between the applied radiofrequency and the frequency at the center of the two resonance components. T_2 is related to the line width. In the absence of exchange effects or overlap of the components $\Delta\omega_{\frac{1}{2}}$ the width of each component at half-maximum is $2/T_2$; this includes all contributions to the line width such as field inhomogeneities and implies a Lorentzian line shape. $\delta\omega$ is the separation of the components assuming no exchange and no overlap of the components.

Expanding Eq. (3) and retaining only the imaginary part v, we find

$$v=\frac{\omega_1M_0[(1+\tau/T_2)P+QR]}{P^2+R^2} \quad (4)$$

where

$$P=\tau[(1/T_2^2)-(\Delta\omega)^2+(\delta\omega/2)^2]+1/T_2$$
$$Q=\tau[\Delta\omega-(\delta\omega/2)(p_A-p_B)]$$
$$R=\Delta\omega[1+(2\tau/T_2)]+(\delta\omega/2)(p_A-p_B).$$

Experimentally, the separation of the two components is measured and from such values we wish to find τ. The positions of the two components and their dependence on τ are given by the maxima of Eq. (4), which can be located by solving the fifth order equation obtaining upon differentiating v with respect to $\Delta\omega$. For the case of immediate interest, $p_A=p_B$, $\tau_A=\tau_B=2\tau$, and the result is

$$\frac{\tau^4}{T_2}(\Delta\omega)^5+2\tau^2S\left(1+\frac{\tau}{T_2}\right)(\Delta\omega)^3$$
$$+\left[\left(1+\frac{\tau}{T_2}\right)\left(1+\frac{2\tau}{T_2}\right)^2-\tau S\left(2+\frac{3\tau}{T_2}\right)\right]S(\Delta\omega)=0 \quad (5)$$

where

$$S=\left[\frac{1}{T_2}+\frac{\tau}{T_2^2}+\tau\left(\frac{\delta\omega}{2}\right)^2\right].$$

One solution of Eq. (5) is always at $\Delta\omega=0$, which corresponds to either a minimum or a maximum depending on whether τ is long or short.

If the line widths ($\sim 1/T_2$) are small compared to the separation $\delta\omega$ (i.e., if $T_2\delta\omega$ is large), the terms in T_2 in Eq. (5) can be neglected; the observed separation is not influenced by overlap of the components and depends only on τ. This gives the particularly simple result that $\delta\omega_e$, the experimentally observed separation, is

$$\delta\omega_e\equiv 2\Delta\omega=(1-2/\tau^2\delta\omega^2)^{\frac{1}{2}}\delta\omega \quad \text{if} \quad \tau\delta\omega>\sqrt{2},$$
and (6)
$$\delta\omega_e=0 \quad \text{if} \quad \tau\delta\omega\lesssim\sqrt{2}.$$

This simple result for the limiting case is the same as Eq. (60) of reference 8. The general nonzero solution

[8] P. W. Anderson, J. Phys. Soc. Japan **9**, 316 (1954).
[9] R. Kubo, J. Phys. Soc. Japan **9**, 935 (1954).
[10] F. Bloch, Phys. Rev. **70**, 460 (1946).

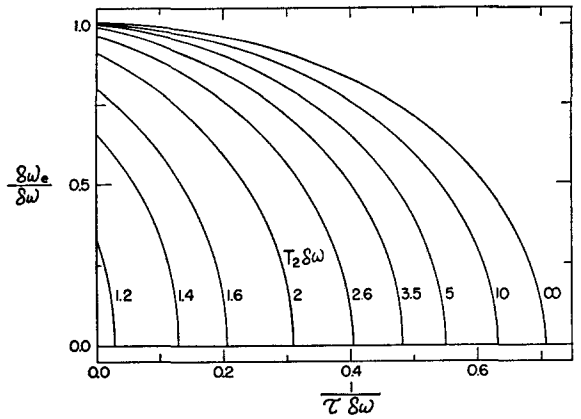

FIG. 1. The separation, $\delta\omega_e$, of two equally intense resonance components, relative to $\delta\omega$, as a function of exchange rate, $1/\tau\delta\omega$, for several values of $T_2\delta\omega$. The separation between the components in the absence of exchange, with no overlap of the components, is $\delta\omega$.

of Eq. (5), which includes the effects of overlap is

$$\Delta\omega=\pm\left\{-S\left(\frac{1}{\tau}+\frac{T_2}{\tau^2}\right)\pm S^{\frac{1}{2}}\left(\frac{\delta\omega}{2}\right)\left(\frac{T_2^2}{\tau^3}+\frac{4T_2}{\tau^2}+\frac{4}{\tau}\right)^{\frac{1}{2}}\right\}^{\frac{1}{2}}. \quad (7)$$

The dependence of $\delta\omega_e$ on τ and T_2 has been computed using Eqs. (6) and (7); the results are shown in Fig. 1 which gives plots of the positions of the components, relative to $\delta\omega$, as a function of $1/\tau\delta\omega$ for several values of $1/T_2\delta\omega$. The curves in this figure show the coalescence of the two components as the exchange time decreases.

The curves in Fig. 1 also show that if $1/T_2\delta\omega$ is greater than about $\frac{1}{3}$, overlap of the components reduces their apparent separations by an appreciable amount. This means that the limiting value of $\delta\omega_e$, when the exchange is slow, does not equal $\delta\omega$. This overlap effect was important in the study of the amides. If we let $\delta\omega_\infty$ be the observed separation of the components as $\tau\rightarrow\infty$, we find from Eq. (7) that the true limiting separation, $\delta\omega$, is given by

$$\delta\omega=\frac{\delta\omega_\infty}{\sqrt{3}}\left[2\left(\frac{1}{T_2^4(\Delta\omega_\infty)^4}+\frac{1}{T_2^2(\Delta\omega_\infty)^2}+1\right)^{\frac{1}{2}}+\left(1-\frac{1}{T_2^2(\Delta\omega_\infty)^2}\right)\right]^{\frac{1}{2}}, \quad (8)$$

where $\delta\omega_\infty\equiv 2\Delta\omega_\infty$. In practice T_2 was found by measuring the line width under conditions such that the resonance components had coalesced to a single line ($\tau\rightarrow 0$), while $\delta\omega_\infty$ was the limiting separation observed for long exchange lifetimes ($\tau\rightarrow\infty$). $\delta\omega$ can be calculated with Eq. (8) from the experimental $\delta\omega_\infty$ and T_2 values, or obtained from the graph of $\delta\omega/\delta\omega_\infty$ as a function of $2/T_2\delta\omega_\infty$ in Fig. 2. For all practical cases $2/T_2\delta\omega_\infty$ will not exceed the value one. The experimental values of the separation of the components, $\delta\omega_e$, in the transition region can be applied to Fig. 1 and the values of $1/\tau\delta\omega$ read off from the curve for the proper $1/T_2\delta\omega$ value. Figure 1 gives a good representation of the actual coalescence of the resonance components, but it is not very satisfactory for interpolating for different values of $1/T_2\delta\omega$. Figure 3 gives plots of $1/T_2\delta\omega$ *versus* $1/\tau_2\delta\omega$ for various values of $\delta\omega_e/\delta\omega$; and $1/\tau_2\delta\omega$ is more readily obtained from this figure. Equation (8) is a general form and can be applied to any pair of equally intense spectral lines with Lorentzian shapes to correct for overlap, provided of course the T_2 is known or can be estimated for the components.

The above analysis assumes that the exchange rate does not influence T_2. This may or may not be true depending on the system and experimental conditions. For the results reported in this work the exchange rate was varied by changing the temperature and strictly speaking the temperature dependence[1,11] of T_2 should be included. However, the line widths in the absence of exchange effects were most likely due mainly to inhomogeneities in the magnetic field so any temperature dependence of the effective T_2 was slight.

III. RESULTS AND DISCUSSION

Experimental Procedure

The high resolution NMR spectrometer and experimental techniques used in these experiments have been described previously,[12] except for certain modifications. A new field sweep system incorporates a well regulated saw tooth generator (non-linearity <1%), with an adjustable period from 0.1 to 100 sec, which is connected to two 1000 turn coils mounted about the pole caps and produces sweep fields from 2 to 1500 milligauss. Spectra can be recorded automatically by means of a dc amplifier driving a Sanborn Model 127 Oscillograph. A thermally insulated box has been placed about the permanent magnet and the temperature of the in-

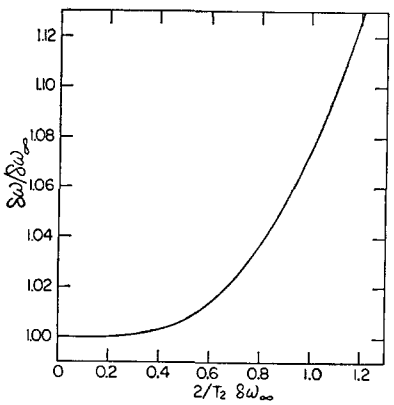

FIG. 2. The effect of overlap of two equally intense resonance components on their apparent separation, as a function of line width $2/T_2$. The observed separation is $\delta\omega_\infty$ while the separation corrected for overlap is $\delta\omega$.

[11] R. Kubo and K. Tomita, J. Phys. Soc. Japan **9**, 888 (1954).
[12] Gutowsky, Meyer, and McClure, Rev. Sci. Instr. **24**, 644 (1953).

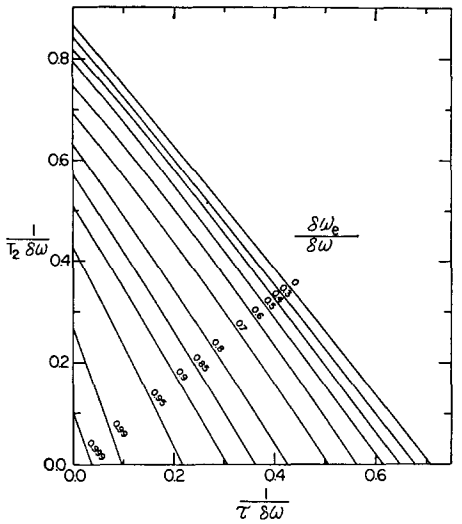

FIG. 3. A plot of Eq. (7), in a form different from Fig. 1, to permit easier interpolation in determining values of $1/\tau\delta\omega$ from experimental observations of $\delta\omega_e/\delta\omega$.

closure regulated in order to minimize drifts in the magnetic field with changes in room temperature.

The samples used in the studies of temperature effects were contained in melting point tubes (1.5 mm ID and 2 mm OD) and the sample volume in the rf coil was about 0.01 cm^3. Larger samples, ~0.03 cm^3, were used in obtaining the room temperature spectra. The samples themselves were Eastman Kodak Co. white label grade chemicals, except for the N-methyl formamide ($n_D^{20}=1.4300$) which was very kindly synthesized and provided for us by Mr. R. A. Vierling and Dr. C. S. Marvel. A simple air driven device was used to spin the samples as a means of averaging out inhomogeneities in the applied field and improving resolution.[13]

The temperature of the sample was controlled by putting the entire rf probe into a Dewar vessel in the magnet gap, with a Styrafoam plug as insulation at the top of the Dewar. The outer part of the probe is a copper box into the bottom of which a copper rod is screwed; a heating coil of Teflon coated copper wire is wound non-inductively about the rod. The copper box serves both as an rf shield and also as a means of maintaining a uniform temperature throughout the probe. The temperature of the probe was measured with a copper-constantan thermocouple; this gave the temperature of the sample to within ±1°, sufficient for the present purpose. Temperatures below that of the room were obtained by placing dry ice or liquid nitrogen in the bottom of the Dewar.

[13] Bloch, Anderson, and Arnold, Phys. Rev. **94**, 496 (1954). An earlier experiment using spinning sample techniques has been described by H. Y. Carr, Ph.D Thesis, Free Precession Techniques in Nuclear Magnetic Resonance (Harvard University, 1952).

N,N-Methylformamide and N,N-Methylacetamide

The proton magnetic resonance spectra of several substituted amides at room temperature are given in Fig. 4. The structural formula that has usually been used for these compounds is (I),

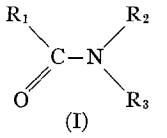

(I)

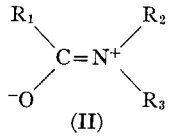

(II)

but it was postulated by Pauling[14] that form (II), with a nitrogen-carbon double bond rather than a single bond makes a significant contribution to the actual electronic structure of the compounds. The various components in the observed spectra are readily assigned to the particular substituents on the basis of relative intensities and the known chemical shift values characteristic of the substituents.[15] In N,N-dimethylformamide (DMF) the weak single component at a δ of +0.29 is assigned to the proton (R_1) in the HCO− group while the much stronger absorption at −0.22 corresponds in position to N−CH_3 groups in other compounds. The main point of interest is the doublet structure in this region which must be due to a nonequivalence of the two CH_3 groups (R_2 and R_3). This doublet was apparently first observed by Meyer

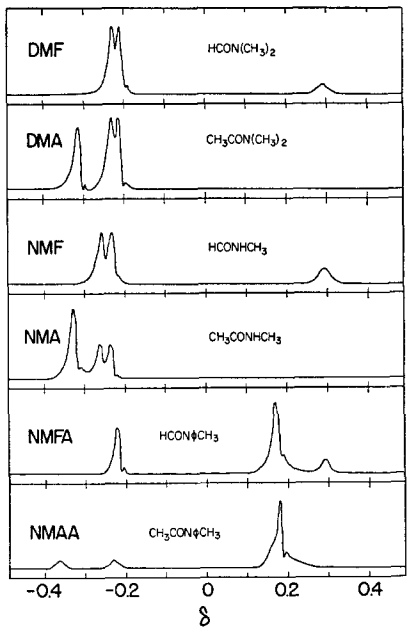

FIG. 4. Proton magnetic resonance spectra recorded at 29°C, as a function of applied magnetic field, at a fixed frequency of 17.735 Mc. δ is defined as $10^5(H_r-H_c)/H_r$ with H_2O the reference compound. The total sweep is 40.7 milligauss; the sweep period, 21 sec. The N-methylacetanilide (NMAA) was a saturated solution in benzene; all other samples were the pure liquids.

[14] L. Pauling, The Nature of the Chemical Bond (Cornell University Press, Ithaca, New York, 1948), 2nd Edition, p. 207.

[15] Meyer, Saika, and Gutowsky, J. Am. Chem. Soc. **75**, 4567 (1953).

TABLE I. Temperature dependence of $1/\tau\delta\omega$.

N,N-dimethylformamide			N,N-dimethylacetamide		
T°K	$\delta\omega_e$ radian sec^{-1}	$1/\tau\delta\omega$ radian^{-1}	T°K	$\delta\omega_e$ radian sec^{-1}	$1/\tau\delta\omega$ radian^{-1}
236	20.1±0.3[a]	0.00±0.03[b]	249	24.4±0.9[a]	0.00±0.1 [b]
322.5	19.2±0.9	0.08±0.04	293	23.7±0.7	0.08±0.07
325	18.5±1.2	0.11±0.04	303	22.8±0.9	0.14±0.07
344	17.3±0.6	0.17±0.03	307	21.9±1.1	0.19±0.07
347	16.6±1.2	0.20±0.03	310.5	21.7±0.9	0.20±0.06
354.5	15.4±0.6	0.24±0.02	313	20.4±0.9	0.25±0.04
359	13.8±0.6	0.29±0.01	316.5	17.5±0.7	0.34±0.03
360.5	15.4±0.6	0.24±0.02	319.7	15.4±0.9	0.39±0.03
362.5	13.2±0.3	0.30±0.01	321.2	13.4±1.3	0.43±0.03
367	12.6±0.6	0.32±0.01	322.5	9.8±0.7	0.48±0.01
369	11.9±0.6	0.33±0.01			

[a] The error given is the standard deviation from the average of about ten measurements.
[b] The error in $1/\tau\delta\omega$ is obtained from Fig. 3 using the error given for $\delta\omega_e$.

although it was not explicitly reported in the summary of his results.[15]

If the doublet were a result of electronic coupling of the CH_3 group protons with the HCO-proton, the resonance of the latter would be a multiplet, which is not the case. Moreover, N,N-dimethylacetamide (DMA) in which R_1 is itself a CH_3 group has a similar doublet, as shown in Fig. 4, while a quartet would be predicted for the electronic coupling mechanism. So we assign the doublets in both DMF and DMA to a chemical shift in the resonance positions of protons in the two methyl groups. This assignment was confirmed by measuring the separation of the doublet at 6300 gauss as well as at 4165 gauss; the separation in milligauss was proportional to the field, whereas a multiplet splitting would have been field independent.[3] The chemical shifts originate in differences in electronic environment of the nuclei, and in DMF and DMA such differences will occur if the double bonded form (II) makes a significant contribution to the structure of the amides. In this event the skeleton of the molecule is coplanar, one of the CH_3 groups (R_2) is *trans* and the other (R_3) is *cis* to the oxygen atom. The double bond character provides a potential barrier to reorientations about the C—N bond, and as reported qualitatively by Phillips[16] the hindrace to such internal rotation must be "high" in order that the reorientation rate be too slow at room temperature to average out the small resonance shift between the two methyl groups.[17]

At higher temperatures the rate of reorientation increases and, as shown in Fig. 5 for DMA, the doublet coalesces to give a single line. Table I summarizes the experimentally observed doublet separations $\delta\omega_e$ as a function of temperature for DMF and DMA and also gives the values of $1/\tau\delta\omega$ calculated from these observations using the methods of Sec. II. The experimental values of T_2 and $\delta\omega_\infty$ applying to these calculations are in Table II along with the value for $\delta\omega$ calculated from $\delta\omega_\infty$, and also the temperature T_c at which the components were observed to coalesce. In practice the measurements at various temperatures for a given sample were made by holding constant the field sweep amplitude, sweep rate, recorder speed and position of the sample in the magnetic field, throughout a run. All parameters in the calculation of $1/\tau\delta\omega$ are dimensionless, so the line widths (T_2) and separations were measured in units of centimeters on the recorder paper. A calibration was made for each run, relating chart distance to field sweep, in order to obtain $\delta\omega$ in radian sec^{-1} and calculate τ in sec.

If the reorientations can be treated as a typical rate process, their temperature dependence should be of the form

$$k=\nu_0\exp(-E_a/RT), \tag{9}$$

where k is the reorientation rate constant; ν_0 is a frequency factor; and the activation energy E_a is the potential barrier hindering the internal rotation. Equation (2) gives $k=1/2\tau$, so Eq. (9) can be rewritten as

$$\log_{10}(1/\tau\delta\omega)=\log_{10}(2\nu_0/\delta\omega)-E_a/2.3RT. \tag{10}$$

The data of Table I are plotted in Fig. 6 as $\log_{10}(1/\tau\delta\omega)$ *versus* $1/T$, giving points which are fitted reasonably well by Eq. (10). The values of E_a and ν_0 which fit the data best are listed in Table II. The activation energies are 7±3 and 12±2 kcal mole^{-1} for DMF and DMA respectively.

The errors were estimated by trial calculations with idealized data. For example, a 10% error in the value of T_2, when carried through the calculations for a $\delta\omega$ of about 20, introduces an error of approximately 1 kcal in E_a; whereas the same percentage error in $\delta\omega_\infty$ gives a non-linear plot for Eq. (10) and the best straight line fit has an E_a about 5 kcal in error. So special care should be taken in measuring $\delta\omega_\infty$. It should be noted that while the errors in measuring $\delta\omega_e$ are the order of 0.15 cps throughout, the resulting percentage error in determining $1/\tau\delta\omega$ becomes very large when $\delta\omega_e$ approaches the limiting value $\delta\omega_\infty$. In general, the errors in the final results of these experiments are quite large. One of the main reasons for this is the small value of $\delta\omega$. At higher magnetic fields $\delta\omega$ would be proportionately larger, and more accurate results could be obtained providing the other experimental parameters were no worse.

TABLE II. Summary of results for N,N-dimethylformamide and N,N-dimethylacetamide.

	T_2 sec radian^{-1}	$\delta\omega_\infty$ radian sec^{-1}	$\delta\omega$ radian sec^{-1}	T_c °K	E_a kcal	ν_0 sec^{-1}
DMF	0.14±0.03	20.1±0.3	20.4±0.3	372[a]	7±3	10^3 to 10^7
DMA	0.18±0.04	24.4±0.9	24.6±1.1	325	12±2	10^7 to 10^{10}

[a] This is the temperature at which the doublet coalesces to a single line.

[16] W. D. Phillips, J. Chem. Phys. **23**, 1363 (1955).
[17] A preliminary estimate, based on our work, of 15 kcal for the barrier was reported at the April, 1955, Discussion of the Faraday Society [**19**, 247 (1955)], assuming a normal frequency factor for the rate process.

N-Methylformamide and N-Methylacetamide

Superficially, the spectra of these compounds, NMF and NMA in Fig. 4, are very similar to the spectra of DMF and DMA. The resonances of the N-methyl groups are split into doublets; however, the splitting was checked at 6300 gauss as well as at 4165 gauss and was found not to be proportional to the applied field. So the splitting is not a simple chemical shift but is caused by the indirect coupling[3] of the N—H proton with the protons in the CH_3 group. No resonance attributable to the N—H proton was found. In the parent compound formamide,[15] $HCONH_2$, the NH_2 and HCO— proton resonances at δ's of 0.29 and 0.37 are weak and broad at room temperature, about 3 to 4 milligauss, perhaps because of molecular association and hydrogen bonding or due to unresolved chemical shifts and splittings. In the N-methyl derivatives the N—H resonance would be split into a quartet by coupling with the CH_3 group protons with further splitting by the nitrogen nucleus possible, and this in addition to broadening by molecular association is a plausible explanation for not detecting the resonance.

Phillips[16] mentions observing single methyl proton resonances in the two N-methyl amides and concludes that only one of the two possible rotational isomers is present. In the sense that the doublets we find are not caused by a chemical shift, this conclusion is a reasonable one. Mizushima[18] has reported a detailed study of the infrared and Raman spectra of N-methylacetamide,

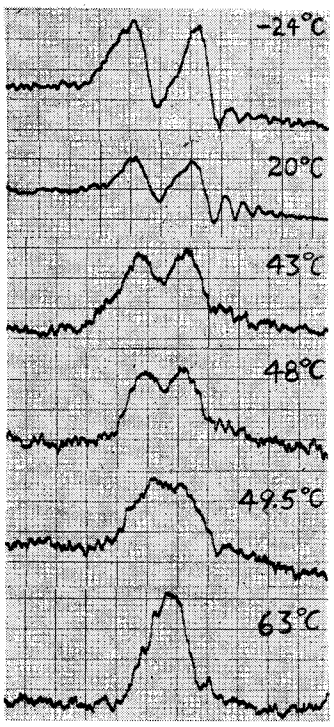

FIG. 5. The proton magnetic resonance spectrum of N-methyl groups in N,N-dimethylacetamide at several temperatures. The spectra were recorded at a fixed frequency of 17.735 Mc; the magnetic field sweep amplitude corresponds to 19.5 cps.

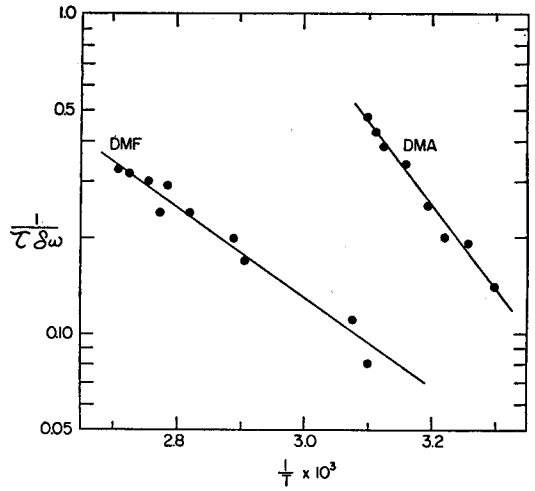

FIG. 6. Temperature dependence of the reorientation rate constant ($1/2\tau$) for N,N-dimethylformamide (DMF) and N,N-dimethylacetamide (DMA). The energy barriers to reorientation obtained from these plots are 7 ± 3 and 12 ± 2 kcal mole^{-1} for DMF and DMA respectively.

from which it was concluded that almost all of the molecules are in the configuration with the N—H bond *trans* to the C—O. Arguments based on the proton spectra as to which is the stabler form appear to be rather indirect. However, it is clear that the form of the N-methylformamide is the same as that of the N-methylacetamide.

This is seen by comparing the spectra of the N-methyl amides with the N,N-dimethyl amides. For the latter, Fig. 4 shows that replacement of the HCO— group with CH_3CO— produces no discernible shift in the $N(CH_3)_2$ group. Therefore, the chemical shift observed between the two CH_3 groups on the nitrogen is due to a *cis-trans* difference in their interaction with the oxygen. On going from the N,N-dimethyl amides to the N-methyl amides there is a chemical shift of the N—CH_3 group resonance because the other CH_3 group on the nitrogen is replaced with a hydrogen. However, the N—CH_3 resonance positions are the same in both N-methyl amides, so the configuration of the N—CH_3 group with respect to the oxygen must be the same in the two compounds. If the N-methylacetamide has a stable *trans* configuration, then so does the N-methylformamide.

Another interpretation of the present NMR data may be made. If the *cis* and *trans* forms were of about the same energy, and the barrier to reorientation were low enough, the internal reorientations could average out the chemical shift leaving the observed indirect spin-spin coupling. In this regard, it is of interest that preliminary experiments by A. Saika in this laboratory show that the doublet in our sample of N-methylacetamide coalesces at about 160°C; this seems to be a result of chemical exchange because the doublet is also reduced to a single line at 29°C by the addition of HCl, but the details remain to be established.

[18] S. Mizushima, *Structure of Molecules and Internal Rotation* (Academic Press, Inc., New York, 1954), pp. 117–152.

N-Methylformanilide and N-Methylacetanilide

The situation with this pair of compounds is identical with that of N-methylformamide and N-methylacetamide except that there are no multiplets. However, whereas there is independent evidence supporting the existence of only one stable configuration for NMA, there appears to be none for either NMFA or NMAA. In addition, the phenyl group on the nitrogen in the latter compounds could compete with the oxygen for the unshared pair of electrons on the nitrogen, which would tend to decrease the double bond character of the C—N bond and promote more rapid reorientations.

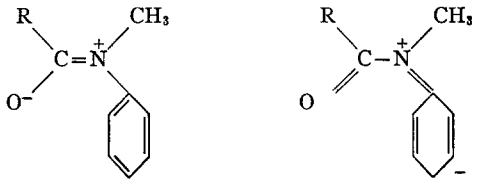

If it is assumed that the interpretations based on the existence of only one configuration are correct, a lower limit can be set on the free energy difference between the *cis* and *trans* forms of NMF, NMA and NMFA. As a conservative estimate, 10% of a second form would have been detectable, giving

$$K_{eq} \geq 10 \quad \text{and} \quad |\Delta F^\circ| \geq 1.4 \text{ kcal.}$$

General Comments

The planar configurations found in this research for the $R_1CONR_2R_3$ skeletons of DMF and DMA are consistent with the microwave results on formamide[19] and with the broad line proton magnetic resonance studies of solid urea,[20] which have shown both molecules to be planar. It is clear that the oxygen of the amide group contributes a significant amount of double bond character to the C—N amide bond. The added stability afforded in this way should be closely related to the internal barrier to reorientation, because the transition state most likely involves the structure with a single C—N bond. Pauling estimated[14] the resonance energy associated with the C—N double bond in amides to be about 21 kcal. This value compares favorably with the values of 22 and 19 kcal we find for the free energy of activation, $\Delta F\ddagger$, associated with the molecular reorientations in DMF and DMA.

The activation energies and frequency factors differ markedly for DMF and DMA. DMF has a low activation energy and a low frequency factor while DMA has a higher activation energy and a much higher frequency factor. This is consistent with the elementary theory of absolute reaction rates, but the effect observed is off by a few orders of magnitude. Equation (9) for the reorientation rate may be written as

$$k \cong \nu_t \exp(-E_a/RT) \qquad (11)$$

where the frequency factor is the internal torsional frequency ν_t. ν_t will be larger for a greater E_a, but for DMA it would be only about twice as great as for DMF, while the observed ratio is the order of 10^4. The uncertainty in the experimental values is large enough that further discussion of the matter seems unwarranted except to note that similar effects have been found and treated in detail for *cis-trans* isomerization reactions[21] which require reorientations about double bonds.

Because of the importance of amides in biological systems and the general lack of quantitative data on the rigidity of the amide group, we are continuing these studies with the hope that better values can be obtained for DMF and DMA and that the effects of other substituents can be determined.

IV. ACKNOWLEDGMENT

Several people contributed to the development of the apparatus. J. C. Buchta was responsible for the electronics; J. P. Heeschen, the thermoregulation of the permanent magnet; and R. L. Rutledge, the construction of the saw tooth field sweep generator. A. Saika assisted in the experiments on NMF, NMA, NMFA and NMAA. We are grateful to the E. I. duPont de Nemours and Company for a grant-in-aid supporting the research.

[19] R. J. Kurland, J. Chem. Phys. **23**, 2202 (1955).
[20] E. R. Andrew and D. Hyndman, Discussions Faraday Soc. **19**, 195 (1955).
[21] Douglas, Rabinovitch, and Looney, J. Chem. Phys. **23**, 315 (1955).

mixture was allowed to cool to room temperature and directly applied to a Sephadex G-25 gel filtration column and eluted with water. The desired metalloprotein complex was then separated from the small amounts of unreacted peptide using ion exchange chromatography on CM-Sephadex C-25 with a 0–2 M NaCl salt gradient in 50 mM MES pH 6.5 buffer. Final purification as well as desalting was performed using RP HPLC to afford about 15 mg of the desired metalloprotein. Formation of the desired complex was established by FIB mass spectroscopy m/z = 5563 (Figure 5) and the following characteristic ultraviolet and visible absorption bands: λ_{max} (nm) 255, 300, and 470 br.

Acknowledgment. The Searle Scholars Program/The Chicago Community Trust and the Arnold and Mabel Beckman Foundation are gratefully acknowledged for their support for of this work. We are also grateful to Dr. C. Singh and V. N. Balaji for the computer-generated model, M. Pique for the graphics presentation, Dr. G. Siuzdak for mass spectroscopic analysis, and colleagues B. Oskouian for help in the design and R. Lerner, K. C. Nicolaou, P. Wright, L. Walters, and J. Skolnick for valuable discussions.

Registry No. 2,2'-Bipyridyl-5-carbonyl-GELAQKLEQALQKLA-NH_2, 138060-62-5; ethyl 6-chloronicotinate, 49608-01-7; 2-(trimethylstannyl)pyridine, 13737-05-8; 5-(ethoxycarbonyl)-2,2'-bipyridine, 56100-24-4; 5-carboxy-2,2'-bipyridine, 1970-80-5.

Resonance Interactions in Acyclic Systems. 3. Formamide Internal Rotation Revisited. Charge and Energy Redistribution along the C–N Bond Rotational Pathway

Kenneth B. Wiberg* and Curt M. Breneman†

Contribution from the Department of Chemistry, Yale University, New Haven, Connecticut 06511.
Received January 24, 1991

Abstract: The changes that occur during the rotation of the amino group of formamide have been studied in some detail. Geometry optimizations at the MP2/6-31G* level confirmed the relatively large increase in C–N bond length but small decrease in the C–O length on going from the planar structure to the rotational transition state. A calculation of the force constants for formamide and for the transition state showed that the carbonyl force constant changed relatively little, but the C–N constant changed by about 30%. The path followed in the rotation was studied starting with the saddle point geometry and following it computationally down to the ground state. The geometrical changes are discussed. The electron populations were calculated for a number of structures along the reaction coordinate by numerical integration of the charge density within uniquely defined atomic volumes. The oxygen population was little affected by the rotation and the main charge shift was between carbon and nitrogen. The electrostatic potentials for the structures also were examined and converted to effective charges for spherically symmetrical atoms. All of the analyses indicated that essentially all of the interactions leading to the rotational barrier originate in the C–N bond and that the oxygen does not participate to a significant extent. The direction of the charge shift between C and N was in opposite directions for the electron populations derived by integration of the charge density, and by fitting the electrostatic potentials. However, this was due to the difference in the definition of the atoms, being anisotropic in the first case and spherically symmetrical in the second. All of the observations can be rationalized on the basis of the assumption that stabilization of the lone pair on nitrogen is the most important factor in determining both structures and energies.

1. Introduction

The amide group is one of the most important functional groups in chemistry. Its planarity and relatively high barrier to rotation about the C–N bond are important factors in determining the conformations of peptides and related compounds. Most of the properties of amides are readily rationalized by postulating amide resonance of the type

Invocation of partial double bond character for the C–N bond allows one to account for the rotational barrier, since this presumably stabilizing interaction would be lost when the amino group is rotated by 90°. Similarly, planarity of the amino group would be required in order to achieve a maximum resonance interaction. Addition of a nucleophile to the carbonyl group would result in loss of the resonance interaction, and so one would correctly predict that these additions would be unfavorable. The resonance interaction model also provides a convenient explanation for the observed stabilization achieved by the combination of an amino group and a carbonyl group. The magnitude of this interaction can be estimated from the following hypothetical reaction (kcal/mol)[1]

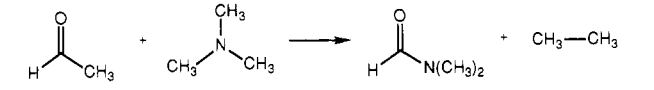

ΔH_f = −39.37 ΔH_f = −5.67 ΔH_f = −45.8 ΔH_f = −20.24

$\Delta\Delta H$ = −21.0 kcal/mol

The energy change is close to that for the rotational barrier, indicating that the corresponding reaction forming the 90° rotated structure would be close to thermoneutral.

Despite the success of the above resonance picture in explaining a large body of data, there are some observations which cast doubt on this simple interpretation. In an earlier investigation of the rotational barrier in formamide, in which the observed barrier was successfully reproduced via ab initio molecular orbital calculations using the 6-31G** basis set, the changes in electron population and structure on rotation were found not to be in accord with an electron donation from the amino group to the carbonyl

† Present address: Department of Chemistry, Rensselaer Polytechnic Institute, Troy, NY 12180.

(1) Cox, J. D.; Pilcher, G. *Thermochemistry of Organic and Organometallic Compounds*; Academic Press: New York, 1970.

0002-7863/92/1514-831$03.00/0

Table I. Structural Parameters of Formamide Conformers[a]

parameter	planar			90° structure (A)		270° structure (B)	
	HF	MP2	obs[4]	HF	MP2	HF	MP2
energy (6-31G*)	−168.93070	−169.40538		−168.90569	−169.37878	−168.90114	−169.37462
ΔE (kcal/mol)	0.0	0.0		15.69	16.69	18.55	19.30
energy (6-31G**)	−168.94048			−168.91510		−168.91072	
ΔE (kcal/mol)	0.0			15.98		18.67	
$r_{C=O}$	1.1927	1.2238	1.219	1.1832	1.2169	1.1789	1.2124
r_{CN}	1.3489	1.3606	1.360	1.4273	1.4421	1.4230	1.4368
r_{CH}	1.0910	1.1046	1.098	1.0876	1.1004	1.0943	1.1090
r_{NH}	0.9957[b]	1.0107[b]	1.002	1.0055	1.0225	1.0046	1.0220
	0.9929[c]	1.0084[c]	1.002				
∠N–C–O	124.95	124.73	124.5	125.05	125.38	123.27	122.83
∠H–C–N	112.66	112.37	112.7	113.48	113.06	116.39	116.71
∠C–N–H	119.33[b]	118.95[b]	118.8	108.48	107.24	106.78	108.35
	121.79[c]	121.83[c]	121.4				
	0.0	0.0	0.0	57.06	55.74	121.71	123.27

[a] Total energies are in hartrees, bond lengths in Å, and bond angles in deg. Geometries were determined using the HF/6-31G* method except where noted. [b] Hydrogen eclipsed with carbonyl. [c] Hydrogen eclipsed with aldehyde hydrogen. [d] O=C—N—H torsional angle.

oxygen.[2] First, it was found that whereas the C–N bond increased in length by 0.08 Å on a 90° rotation, the carbonyl bond length decreased by only 0.01 Å (Table I). If the resonance model were really descriptive, one might have expected a more equal change in bond lengths. Second, the integrated electron population[3] at the nitrogen was found to be greater in the lower energy planar form than in either of the rotated saddle point structures.[2] The electrons were taken from the carbon, and the electron population at the carbonyl oxygen was almost unchanged during the rotation. Here, the direction of the charge shift is opposite to that expected from the resonance formulation, and the oxygen does not appear to be significantly affected by the rotation.

2. Structural Data

Before proceeding to an interpretation of the origin of the properties of formamide, it appeared necessary to be sure that the calculated structural changes on rotation were correct. It is possible (although unlikely) that they were an artifact resulting from the use of an RHF treatment. In order to see whether or not correction for electron correlation would affect the calculated structural changes, we have carried out geometry optimizations at the MP2/6-31G* level which has been found to give bond lengths and angles that are in very good agreement with experimental data.[4] The structural parameters for formamide and the saddle point rotamers A and B are compared with the RHF results and the experimental data in Table I. It can be seen that although the bond lengths increase somewhat on correction for electron correlation, the difference in the calculated changes in C–N and C–O bond lengths persists. Again, it appears that the main changes are in the C–N bond and that the C–O bond is relatively unaffected by rotation.

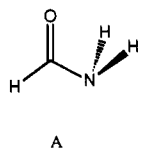

A

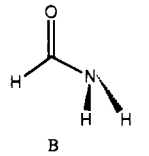

B

The calculated barrier height at the MP2/6-31G* level (16.7 kcal/mol) is in good agreement with the experimental barrier (18–19 kcal/mol).[5]

Information has been obtained on the geometrical changes that occur for formamide vibrationally excited for the CN bond rotation, and they involve significant stretching of the CN bond and a decrease in HNH angles,[6] as has been found in the above calculations. Structural data for amides that are prevented from achieving planarity because of geometrical constraints have recently been reported.[7] In both cases, the CN bond was found to have lengthened without much of a change in the CO bond length. Thus, these data are in very good accord with the theoretical predictions.

Table II. Some Significant Force Constants (mdyn/Å) in Formamide Conformers

force constant	planar	90° structure (A)	270° structure (B)
C—N stretch	8.22	6.15	6.20
C=O stretch	15.80	16.95	17.30
C=O/C—N interaction	1.59	1.01	1.00

3. Vibrational Spectrum

It is well-established that the rotation of the amino group of an amide leads to a significant change in the carbonyl stretching frequency.[8] This increase in frequency could be caused by either a change in the carbonyl stretching force constant or a change in the interaction between the carbonyl group and other groups such as the C–N bond. Since the magnitude of a stretching force constant can, in a qualitative sense, be related to the strength of a bond, any change in bond order which occurs during rotation about the C–N bond should be reflected in the calculated force constants. In order to explore this problem, we have investigated the infrared spectrum of formamide. Since it is not possible to observe the spectrum of the saddle point conformers A and B, it was necessary to make use of theoretical calculations in order to obtain the desired information.

The HF/6-31G* frequency calculations lead to force constants that are about 20% too large because the theoretical geometry has bond lengths that are somewhat too short and the observed vibrational frequencies are for anharmonic vibrations whereas the theoretical force constants and are for harmonic vibrations which have a higher frequency. Nevertheless, it is generally found that the force constants for corresponding modes are overestimated by essentially the same amount,[9] and so the calculated values may usefully be compared. The force constants of interest are those

(2) Wiberg, K. B.; Laidig, K. E. *J. Am. Chem. Soc.* **1987**, *109*, 5935.
(3) (a) Bader, R. F. W. *Acc. Chem. Res.* **1985**, *18*, 9. (b) Bader, R. F. W. *Atoms in Molecules: A Quantum Theory*; Oxford University Press: Oxford, 1990.
(4) Hehre, W. J.; Radom, L.; Schleyer, P. v. R.; Pople, J. A. *Ab Initio Molecular Orbital Theory*; Wiley: New York, 1986; Chapter 6.
(5) Sunner, B.; Piette, L. H.; Schneider, W. G. *Can. J. Chem.* **1960**, *38*, 681. Kamei, H. *Bull. Chem. Soc. Jpn.* **1968**, *41*, 2269. Drakenberg, T.; Forsen, S. *J. Phys. Chem.* **1970**, *74*, 1.
(6) Brown, R. D.; Godfrey, P. D.; Kleibömer, B. *J. Mol. Struct.* **1987**, *124*, 34.
(7) Bennet, A. J.; Wang, Q.-P.; Slebocka-Tilk, H.; Somayaji, V.; Brown, R. S.; Santarsiero, B. D. *J. Am. Chem. Soc.* **1990**, *112*, 6383. Shea, K. J.; Lease, T. G.; Ziller, J. W. *J. Am. Chem. Soc.* **1990**, *112*, 8627.
(8) Greenberg, A. In *Structure and Reactivity*; Liebman, J. F., Greenberg, A., Eds.; VCH Publishers: New York, 1988.
(9) Sellers, H.; Pulay, P.; Boggs, J. E. *J. Am. Chem. Soc.* **1985**, *107*, 6487.

Table III. Calculated and Experimental Vibrational Frequencies of Formamide (cm^{-1})

exptl[a]	planar[b]	90° structure (A)[b]	270° structure (B)[b]
289	99	444*i*	398*i*
565	544	565	595
602	593	850	833
1030	1021	904	836
1059	1041	1068	1029
1255	1213	1216	1213
1378	1380	1363	1384
1572	1575	1573	1583
1734[c]	*1760*[c]	*1788*[c]	*1816*[c]
2852	2923	2962	2880
3451	3492	3362	3368
3545	3614	3433	3440

[a] Data from: Evans, J. C. *J. Chem. Phys.* **1954**, *22*, 1228. King, S. T. *J. Phys. Chem.* **1971**, *75*, 405. [b] Corrected by multiplying all values under 2000 cm^{-1} by 0.88 and all those over 2000 cm^{-1} by 0.91. [c] Carbonyl stretching mode.

involving the C, N, and O, and they are summarized in Table II. It can be seen that the carbonyl stretching force constant does not change much and the major changes are found with the C—N stretching force constant and the C=O/C—N interaction constant. The carbonyl force constant for rotamer A is close to that calculated for acetaldehyde using the same basis set (16.58 mdyn/Å).[10] The CO force constant decreases only by 7% on going to the planar form, whereas the CN constant increases by 32%.

In using theoretically calculated force constants, it has been found that a simple scaling scheme normally reproduces the experimental frequencies with a root-mean-square error of only about 25 cm^{-1}.[11] The application of these scaling factors leads to the scaled frequencies that are given together with the observed values in Table III. Except for the lowest frequency band, there is quite good agreement. This low-energy band corresponds to an NH_2 wagging mode which is known to have positive anharmonicity resulting from a stiff quartic potential which is not represented in a harmonic frequency analysis.[12]

Analysis of the vibrational data given in part in Table II suggests that the increase in carbonyl stretching frequency in the rotated conformers arises from changes in the C=O force constant and through the significant coupling interaction of the carbonyl stretch with the C–N bond stretching mode. The small change in the carbonyl stretching force constant upon rotation about C–N bond suggests that the nature of that bond is not largely affected, while the C–N bond becomes much softer in the transition structures. This is consistent with the large observed lengthening of the C–N bonds in structures A and B and the relatively insensitivity of the C=O bond length to the C—N bond changes.

The carbonyl vibrational frequency was calculated to increase by 28 cm^{-1} on going from the planar to the 90° rotated form (A) and by 56 cm^{-1} in going to the 270° rotated form (B). These changes are consistent with the ca. 60 cm^{-1} higher carbonyl stretching frequency seen in the twisted bridgehead lactam 1-azabicyclo[2.2.2]octan-2-one compared to open chain amides.[7]

Even though the change in the carbonyl force constant is small, it actually predicts a somewhat greater change in the calculated difference in the harmonic carbonyl vibrational frequencies between the planar and rotated conformers than is found. Consequently, the large C=O/C—N cross-term must also be taken into account when comparing these data. In this case, the cross-term serves to reduce the difference between the calculated carbonyl stretching frequencies of the planar and transition-state forms. It might also be noted that the ~60-cm^{-1} change in vibrational frequency is small in comparison to the difference between C=O and C—O stretching frequencies (~600 cm^{-1}).

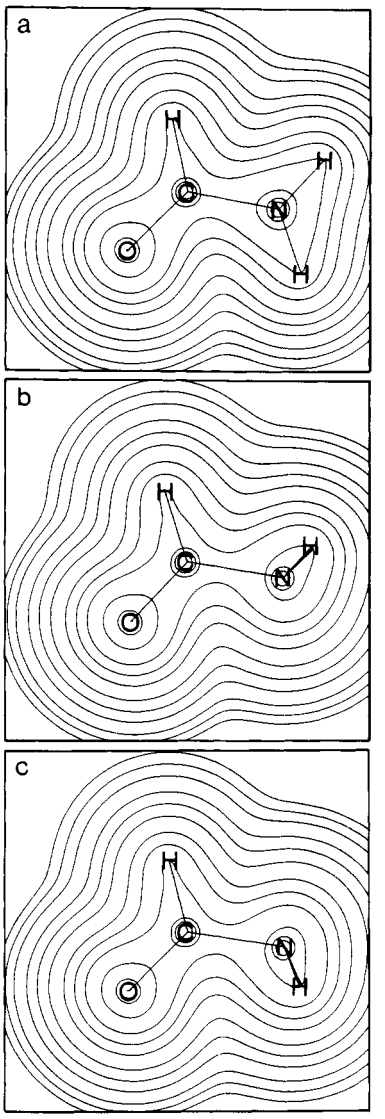

Figure 1. Projection density plots for all the electrons of (a) formamide, (b) rotamer B, and (c) rotamer A. The amino group is to the right and the oxygen is to the left.

Although the force constants are interesting and provide some indication of the changes in bonding on rotation, it would be more useful to have a direct measure of the bond orders. The force constants are affected by bond orders, bond lengths, and other factors and are therefore at best an indirect indicator of bond order. Some time ago, we proposed a bond index that was the covalent bond order in zero differential overlap semiempirical MO calculations.[13] This has been extended to ab initio calculations by others,[14] but we have not been satisfied with these procedures because they have the inherent problems associated with the use of atomic orbitals in calculating populations and other properties.[15] Recently, Cioslowski[16] has proposed a related covalent bond order based on the atomic overlap matrix as defined in the theory of

(10) Wiberg, K. B.; Walters, V.; Colson, S. D. *J. Phys. Chem.* **1984**, *88*, 4723.

(11) Vibrational frequencies calculated using the HF/6-31G* level of theory compare very well with experimental values if all frequencies below 2000 cm^{-1} are scaled by 0.88 and all higher frequencies scaled by 0.91. Cf.: Wiberg, K. B.; Walters, V.; Colson, S. D. *J. Phys. Chem.* **1984**, *88*, 4723. Wiberg, K. B.; Dempsey, R. C.; Wendoloski, J. J. *J. Phys. Chem.* **1984**, *88*, 5596. Wiberg, K. B.; Walters, V. A.; Wong, K. N.; Colson, S. D. *J. Phys. Chem.* **1984**, *88*, 6067.

(12) Hirota, E.; Sugisaki, R.; Nielsen, C. J.; Sorensen, G. O. *J. Mol. Spectrosc.* **1974**, *49*, 251.

(13) Wiberg, K. B. *Tetrahedron* **1968**, *24*, 1083.

(14) Gopinathan, M. S.; Jug, K. *Theor. Chim. Acta* **1983**, *63*, 497, 511. Jug, K. *J. Comput. Chem.* **1984**, *5*, 555. Jug, K.; Fasold, E.; Gopinathan, M. S. *J. Comput. Chem.* **1989**, *10*, 965.

(15) Cf.: Glaser, R. *J. Comput. Chem.* **1989**, *10*, 118.

(16) Cioslowski, J.; Mixon, S. T. *J. Am. Chem. Soc.* **1991**, *113*, 4142.

Table IV. Calculated Covalent Bond Orders for Formamide Conformers[a]

	planar			90° (A)			270° (B)		
bond	π	σ	total	π	σ	total	π	σ	total
C–O	0.458	0.668	1.127	0.571	0.677	1.248	0.584	0.666	1.249
C–N	0.229	0.655	0.884	0.046	0.844	0.891	0.048	0.839	0.887
C–H	0.003	0.895	0.898	0.004	0.917	0.921	0.004	0.920	0.924
NHa	0.029	0.745	0.775			0.830			0.841
NHb	0.031	0.760	0.792						
N···O	0.134	0.154	0.288	0.057	0.157	0.215	0.061	0.153	0.214

[a] Separation into σ and π is not easily defined for out-of-plane hydrogens in the rotated forms.

atoms in molecules.[3] We have applied this procedure to the three rotamers of formamide giving the results shown in Table IV.

The carbon–carbon double bond in ethylene is calculated to have a covalent bond order of 1.96, close to the nominal 2.0.[15] One might then note the relatively small covalent bond order for the carbonyl group, suggesting that it has considerable ionic character. This is in good accord with the large C=O bond dipole,[17] and with calculations of the electron populations at C and O of carbonyl groups.[18] The much greater electronegativity of oxygen as compared with carbon leads to a charge shift from C to O. This may be seen in projection density[19] plots in which all of the charge density above and below the molecular plane is collapsed onto that plane. Plots for the total charge density are shown in Figure 1, and those for just the π electrons are shown in Figure 2. It might be noted that both the σ and π components of the bond are polarized, and so the total covalent bond order is divided approximately equally between σ and π.

In Figure 1 it can be seen that the oxygen contours occupy most of the volume associated with the C=O bond leading to a large electron population for the oxygen and a small population for the carbon. In this way, a carbonyl group is best written as C^+–O^-, and the relatively short bond length may be attributed to a coulombic attraction between C and O. The contours in the vicinity of the carbonyl group are essentially unchanged on rotation about the CN bond, again indicating a lack of participation of this bond in the C–N bond rotation process.

The resonance picture is concerned with the π electrons, and their contours in Figure 2 again show a large shift in charge density from carbon to oxygen. However, there is essentially no change for the C=O bond on rotation about the CN bond. It is clear that the carbonyl group is a spectator and not an active participant in the C–N bond rotation. The small change in C–O bond order on rotation may be attributed to the changes in charge at the atoms and a change in the ionic character of the bond.[20] There is no significant change in the C–N covalent bond order on rotation. However, in the planar form there is a significant π-covalent bond order (0.229) which almost disappears in the 90° rotated form. In the latter, this is compensated for by an increase in the σ bond order. This is in agreement with the finding that there is less C–N charge separation in the rotated form than in the planar form (see below).

All of these data are consistent with the proposal that any resonance interactions present in formamide do not affect the carbonyl C=O bond to the large extent required to support the standard resonance model. Recent VB calculations on formamide also support this view.[21]

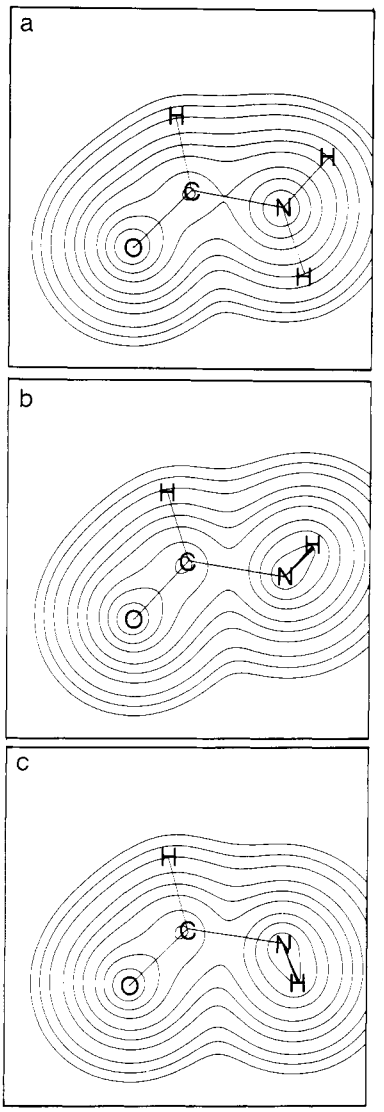

Figure 2. Projection density plots for the π electrons of (a) formamide, (b) rotamer B, and (c) rotamer A.

4. Atomic and Structural Changes during Rotation

It was of interest to us to see how the structural parameters and atomic properties change during rotation about the C–N bond. To accomplish this, we started with the lower energy saddle point conformer (A) and carried out a search for the path connecting this conformer to the planar form using a highly damped mode-walking algorithm with the force constants evaluated analytically (HF/6-31G*) at each point.[22] The calculated rotational pathway was found to begin with the amino hydrogens gauche to the carbonyl group, followed by rotation of the pyramidal NH_2 with little change in hybridization until the hydrogen

(17) Aldehydes and ketones have dipole moments of 2.6–2.7 D, most of which may be attributed to the carbonyl group.

(18) Slee, T.; Larouche, A.; Bader, R. F. W. *J. Phys. Chem.* **1988**, *92*, 6219.

(19) Streitwieser, A., Jr.; Collins, J. B.; McKelvey, J. M.; Grier, D.; Sender, J.; Toczko, A. G. *Proc. Natl. Acad. Sci. U.S.A.* **1979**, *76*, 2499.

(20) The electron populations for planar formamide were as follows: C, 4.023; H, 1.035; O, 9.392; N, 8.476; H, 0.529 and 0.544. For 90° rotated formamide they were as follows: C, 4.249; H, 1.005; O, 9.341; N, 8.222; H, 0.592. We have examined the populations and bond orders for a number of types of compounds containing groups and have found a linear relationship between the population at oxygen and the C–O bond order (Wiberg, K. B.; Hadad, C. M.; Rablen, P. R.; Cioslowski, J. To be published).

(21) Flegg, R. H.; Harcourt, R. D. *J. Mol. Struct. (Theochem)* **1988**, *164*, 67.

(22) The calculation was performed using a harmonic mode-walking algorithm implemented in the developmental version of GAUSSIAN90.[29]

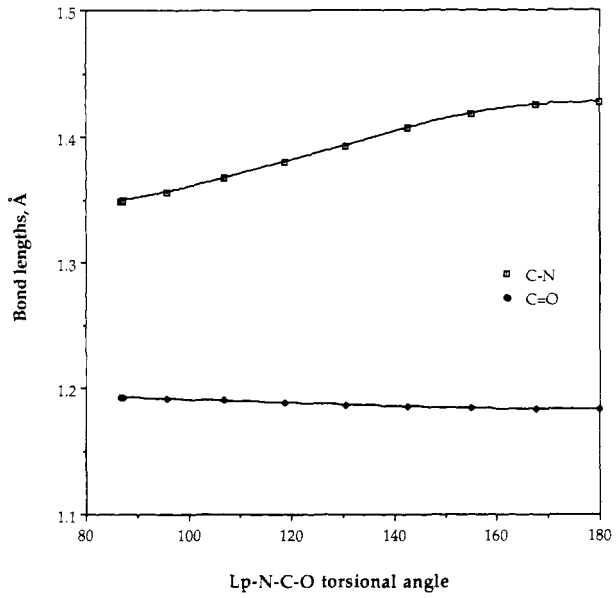

Figure 3. Bond length changes for formamide on rotation about the C–N bond.

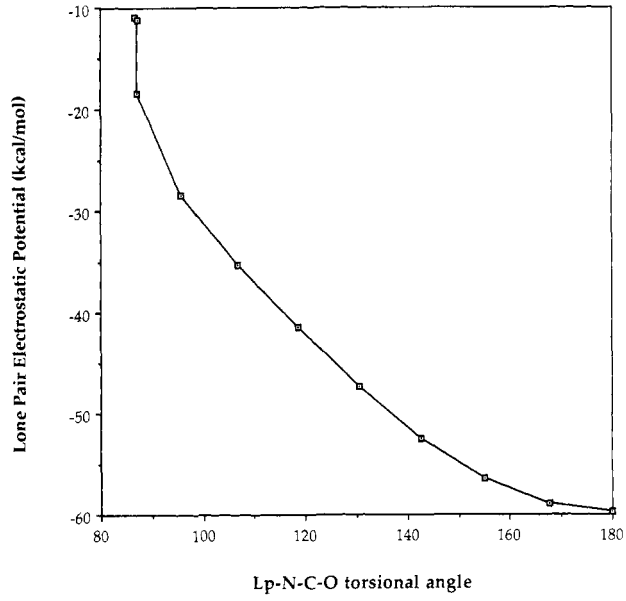

Figure 4. Electrostatic potential minima in the vicinity of the amide nitrogen.

rotating toward the carbonyl group overshoots by about 8°. At this point, the hydrogen becoming anti to the carbonyl is still about 25° out of plane, but the calculated energy of this structure is within 0.5 kcal/mol of the planar form. This demonstrates that considerable distortion of the amino group in the planar structure is possible with little energy cost.

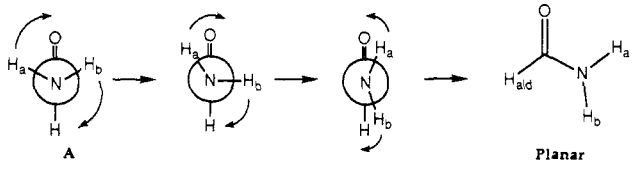

The mode-walk technique resulted in our finding 33 intermediate structures, from which 11 were chosen for further study using the 6-31G** basis set. The reaction coordinate was taken as the torsional angle between the carbonyl and the nitrogen "lone pair". The latter was defined by a line from the nitrogen to the point at which the electrostatic potential was most negative. The C=O and C—N bond length changes that occur during rotation are shown in Figure 3 as a function of this reaction coordinate. Whereas the C–N bond length increases significantly on rotation from the planar to rotamer A, the changes in the C—O bond length are negligible.

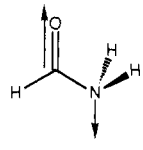

Nitrogen lone-pair dihedral angle with C=O bond

Figure 4 shows the dependence of the "lone pair" electrostatic potential value on the progress of the transition from the planar form to rotational transition state A. It can be seen from the figure that when the amide is close to planar the electrostatic potential well is quite shallow, with a potential minimum of only −10.9 kcal/mol. The electrostatic potential well deepens considerably even with small, energetically-negligible deformations from the planar structure, and finally arrives at a value of −59.7 kcal/mol at the rotational transition structure. This potential well is more shallow than the value expected for a typical primary amine such as methylamine, which has an electrostatic potential well value of −82.5 kcal/mol, presumably as a result of the proximity of the orthogonal electronegative carbonyl group.

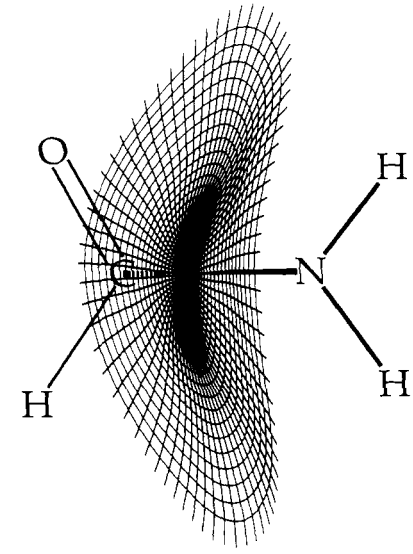

Figure 5. An example of an interatomic surface.

5. Electron Populations

We may now turn to one of our special concerns, the flow of electron population and electronic kinetic energy between the atoms in the structures connecting the planar and saddle point conformers. The 6-31G** atomic electron populations were evaluated at each of the 11 selected intermediate structures using Bader's theory of atoms in molecules.[3]

Direct analysis of the electron density is capable of providing all pertinent information concerning molecular behavior and energetics. To understand this technique, one must envision the molecule as a collection of atomic "attractors" (nuclei) surrounded by a sea of charge density. Between each pair of bonded atoms, there exists a pathway of greatest charge density called the *bond path*. Somewhere along this path there is a point of minimum density known as the *bond critical point*. A bond path connecting atoms A and B containing just such a critical point is illustrated below:

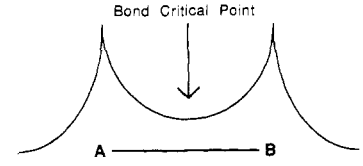

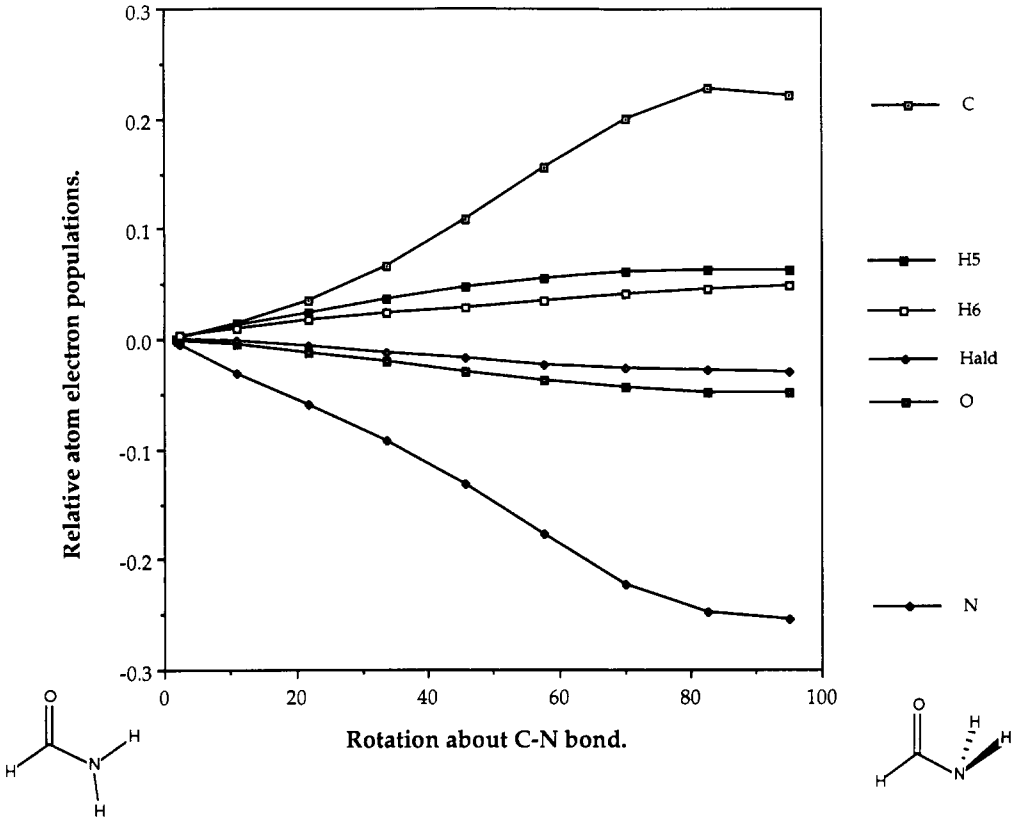

Figure 6. Changes in electron population on rotation about the C–N bond.

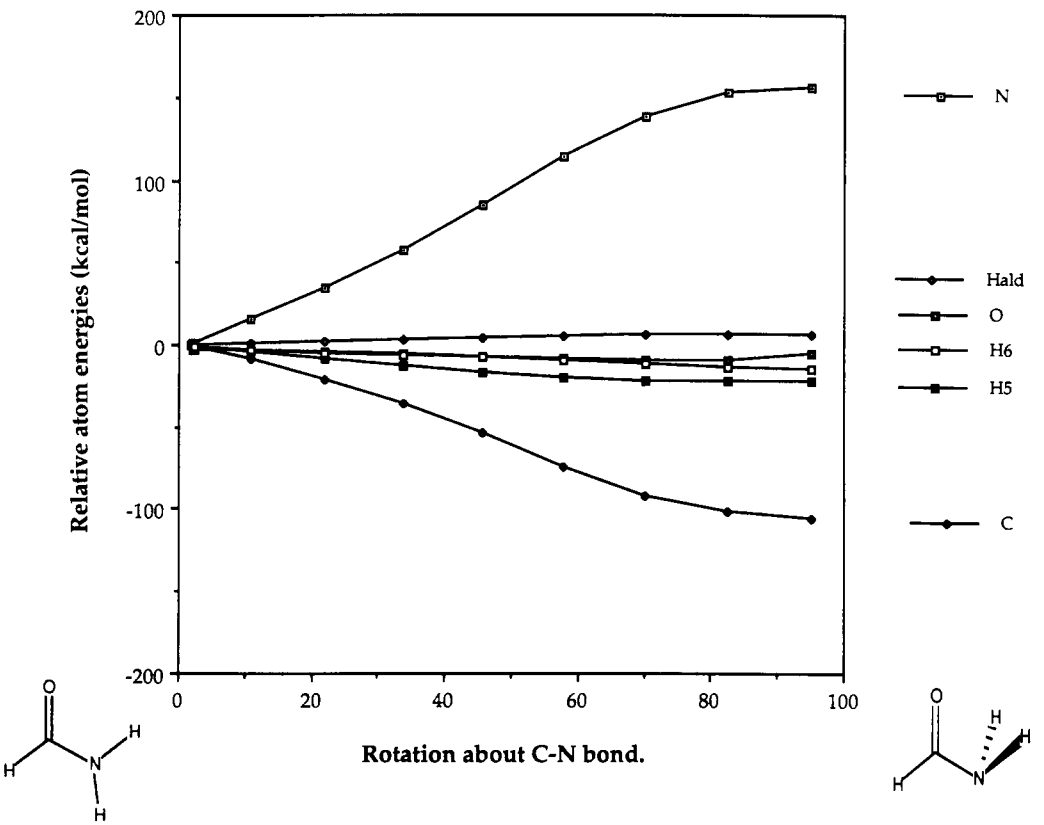

Figure 7. Changes in energy on rotation about the C–N bond.

Within the density analysis method, the bond critical point represents a special point where the electron populations of atoms A and B join. If one then starts at the bond critical point and constructs a set of rays normal to the bond path for which the charge density decreases most rapidly, an interatomic surface can be defined as shown in Figure 5. A set of surfaces may be constructed, one for each bond, which serve to separate the molecule into a set of atomic domains.

By integrating the appropriate function of the charge density over each atomic domain, the electronic properties of each atom

can be calculated. The most obvious of these properties is the atomic electron population, but the method has the added capability of calculating other properties such as the atomic electronic kinetic energies for each atom in a molecule. It is this capability that allows us to describe the rotational barrier in formamide from an *intramolecular* perspective.

As shown in Figures 6 and 7 the flow of charge and energy between atoms proved to be smooth during the rotation.[19] It is significant that most of the changes involve only the carbonyl carbon and the amide nitrogen. The data in Figure 6 show that as the structure changes from the planar amide form to the rotated structure the carbonyl carbon gains electronic population at the expense of the amide nitrogen. This result is consistent with the earlier work of Wiberg and Laidig[2] and suggests that the barrier to rotation is due largely to the amino group being destabilized near the transition structure. This destabilization is clearly shown in the kinetic energy flow in Figure 7, where there is a smooth destabilization of the amide nitrogen and a smaller stabilization of the carbonyl carbon during the conformational change. This can be interpreted as being indicative of the relative electronegativities of the nitrogen and the carbonyl carbon, since the amount of stability that a particular type of atom can derive from a given amount of electron density provides a fundamental description of electronegativity. Figures 8 shows the relationship between changes in electron population and atomic stability for the amide nitrogen, the carbonyl carbon, and the carbonyl oxygen, respectively. The abscissa of each of these graphs indicates the relative stability of each atom with increasing electron population. The origins are with respect to the planar formamide values. It is significnt that the slope of the nitrogen line is 1.38 times greater than that of carbon, while the changes at oxygen are small. These data are also consistent with the view that a carbonyl oxygen is very nearly saturated with electron density, and increasing the electronic population of this kind of atom does not give it extra stability. Recent work on enolate electronic structures supports this view.[23]

We have noted that the nitrogen in the planar form appears more electronegative than that in either saddle point conformer and has a larger electron population. The change in population at nitrogen can be accommodated by a simple hybridization argument. In the planar amino group, the hybridization at nitrogen would be close to sp^2. However, on rotation, the amino group undergoes pyramidalization, leading to H–N–H bond angles of 106° and bond path angles (102°) that are even smaller. Here, the hybridization would correspond to less than 25% s-character, and the nitrogen would be much less electronegative than in the planar form. This would lead to the calculated change in structure and electron population, since in the planar form the greater electronegativitiy of the sp^2 hybridized nitrogen shortens the C–N bond and allows the nitrogen to withdraw more electron density from the carbonyl carbon. As a check on this hypothesis, we have carried out a geometry optimization for 90° rotated formamide in which the amino group was forced to be planar. This raised the energy by 6.6 kcal/mol above the transition structure (A) and led to electron populations that are between those of the planar form and the pyramidal saddle point form. It would appear that one reason why the planar transition form is not favored is because the nitrogen prefers to place its lone pair electrons in an orbital with high s-character which requires a pyramidal structure.

It is possible to separate the electron populations of the planar form into σ and π components.[2] The π populations are 1.866 (NH_2), 0.408 (CH), and 1.710 (O). In the absence of any interactions, the populations would have been 2.0, 1.0, and 1.0, respectively. Therefore, the π system charges are NH_2, +0.134 (NH_2), +0.592 (C), and −0.710 (O). This may be compared with rotamer A for which the π populations are 1.990 (NH_2), 0.406 (CH), and 1.604 (O). There is essentially no change at carbon, but the oxygen gains 0.106 π electron in the planar form. At the same time, it loses 0.054 σ electron on going from the rotated to planar forms, leaving a net change of only 0.05 electron. All of the relatively large shift in electron population at carbon is found in the σ system as would be expected for an inductive effect.

It is also of interest to look at the changes which occur in atomic sizes during rotation about the C–N bond. Figure 9 shows the distances from each atom of the C—N and C═O bonds to each bond critical point. Examination of this figure reveals that the largest change is in the radius of the carbonyl carbon atom bonding to the amide nitrogen. The nitrogen atom is somewhat affected, but not to as large an extent.

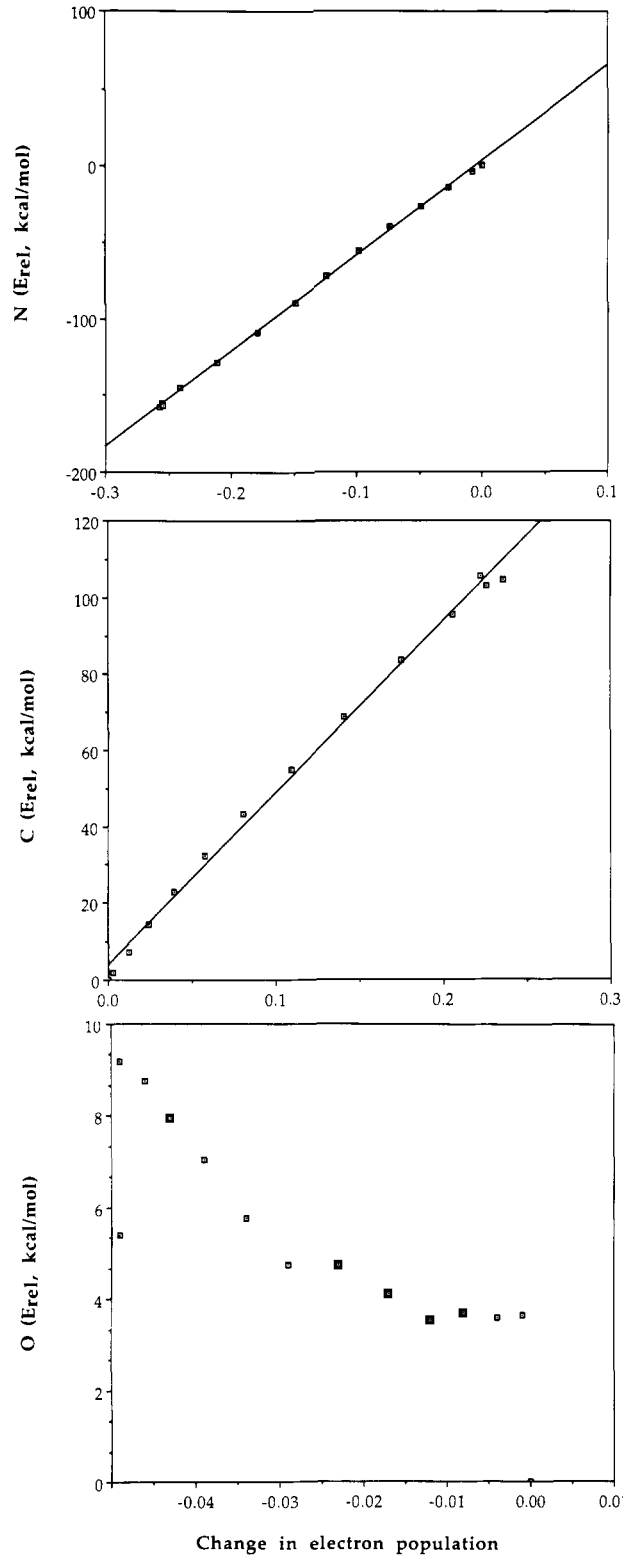

Figure 8. Relationship between the electron population and the kinetic energy for the C, N, and O atoms of formamide. Note that the energy scale for O is much different than that for C or N.

(23) Breneman, C. M. Unpublished work.

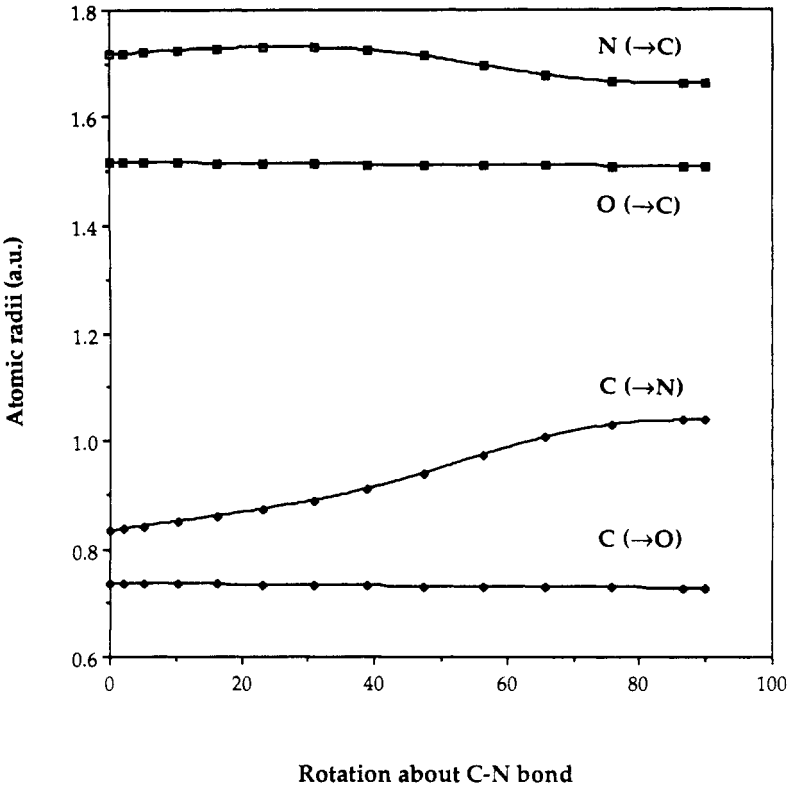

Figure 9. Changes in atomic sizes (distances from the atoms to the bond critical points) on rotation about the C–N bond.

6. A View from the Outside

The analysis given above is concerned with the molecule as seen by its nuclei. The population calculations are in good accord with simple hybridization arguments, as is usually found to be the case.[24] However, for intermolecular interactions, this approach may sometimes be inconvenient since the atomic charge, atomic dipoles, and higher terms must be considered. Here, it is helpful to view the molecule from the outside in order to see what an approaching reagent would experience. Two pertinent quantities are readily obtained from the wave functions: the Laplacian of the charge density ($\nabla^2\rho$) and the electrostatic potential. The Laplacian of ρ has been used to predict regions of higher reactivity,[25] and the electrostatic potential has frequently been used to predict the regiochemistry of intermolecular interactions.[26]

To simplify the analysis, the electrostatic potential field can be used to define effective point charges for spherically symmetrical atoms. We have used a version of the CHELP program[27] (CHELPG), modified to be nearly rotationally invariant, to calculate nuclear-centered effective point charges that reproduce the electrostatic potential field outside the molecular van der Waals radius to a high degree of accuracy.[28] These charges, while not strictly representative of the interior charge distribution of the molecule, do convey a qualitative picture of what the molecule looks like to its surroundings. As indicated in Figure 10, the calculated CHELPG charges show that the amino group externally appears more positive in the planar structure than in the pyramidal transition state, as predicted by the resonance model, while the carbonyl carbon appears to become considerably more electrophilic in the rotated structure, also in accord with experiment. The data show that the carbonyl oxygen remains relatively unchanged throughout the rotation. In each case, the Mulliken population analysis data are also included on the figures for comparison, even though Mulliken charges are known to be considerably basis-set dependent.[29]

In an effort to visualize the external view of the electrostatic potential and the Laplacian of the charge density ($\nabla^2\rho$), we have calculated these properties at about 30 000 points on the molecular van der Waals surface (defined as the 0.002 e/au^3 surface in ρ). The calculated values are represented by a color scale superimposed on the closely-spaced 3-D contours which represent the molecular surface in ρ (Figure 11). The electrostatic potential values at the VDW surface are in accord with intuition; the lowest values of the electrostatic potential are found in the molecular plane near the carbonyl oxygen in all three conformers, while in the rotated structures A and B a second region of low potential is seen near the nitrogen, where a "lone pair" might be expected to exist. There is a somewhat larger region of negative potential around the carbonyl oxygen in the planar structure than in either of the rotational transition-state structures, as predicted by the resonance model, but this is not reflected in the change in atomic charge at oxygen.

The Laplacian of ρ is normally examined in terms of its critical points, which lie closer to the nuclei than the VDW surface.[24] Nevertheless, we thought it might be of interest to see if there is any relationship between $\nabla^2\rho$ at the critical points and at the VDW surface. It can be seen from Figure 11 that the nature of the Laplacian field around the carbonyl oxygen at the van der Waals radius is in conflict with the electrostatic potential; in the region where "lone pairs" might be expected, there are weak areas of greater positive $\nabla^2\rho$, implying regions of relative charge depletion, although at much shorter distances from the oxygen nucleus (<0.5 au) there are two negative peaks in the Laplacian field. These observations suggest that the critical points in $\nabla^2\rho$ may predict the nature of the electrostatic potential at the VDW surface. This question will receive further study.

(24) Cf.: Wiberg, K. B.; Breneman, C. M. *J. Am. Chem. Soc.* **1990**, *112*, 8765.
(25) Carroll, M. T.; Chang, C.; Bader, R. F. W. *Mol. Phys.* **1988**, *63*, 387 and ref 3b.
(26) Scrocco, E.; Tomasi, J. *Adv. Quantum Chem.* **1978**, *11*, 115.
(27) Chirlian, L. E.; Francl, M. M. *J. Comput. Chem.* **1987**, *6*, 894. QCPE program No. 524. Our modification consists of selecting points for fitting from a 3-D grid of 5000 points placed around the molecule with a point spacing of 0.3 Å. Points within a 2.0-Å radius from any atom are excluded.
(28) Breneman, C. M.; Wiberg, K. B. *J. Comput. Chem.* **1990**, *11*, 361.
(29) Mulliken, R. S.; Politzer, P. *J. Chem. Phys.* **1971**, *55*, 5135. Grier, D. D.; Streitwieser, A., Jr. *J. Am. Chem. Soc.* **1982**, *104*, 3556.

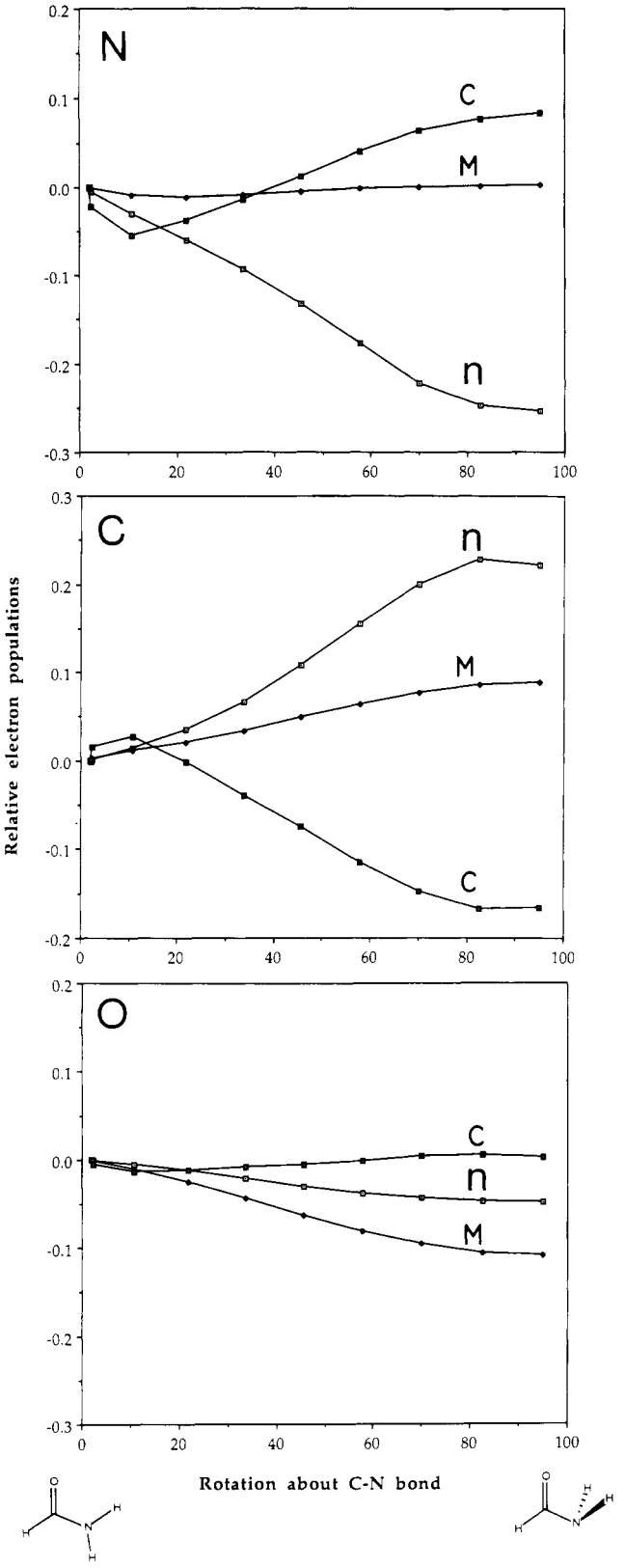

Figure 10. Changes in electron populations caused by rotation about the C–N bond. The lines are indicate (n) the changes in electron population as determined by the theory of atoms in molecules, (C) the changes in effective charges determined by fitting the electrostatic potentials, and (M) the changes in the Mulliken populations.

It is important to note the anisotropy of the electrostatic potential near the nitrogen (Figure 11). *The only way in which this anisotropy can be reproduced by charges for spherically symmetrical atoms is to have part of it associated with other atoms such as the hydrogens attached to the nitrogen.* Thus, the charges derived from the electrostatic potential are effective charges which will reproduce the data, and should not be thought of as correctly representing the charge at a given atom.

7. Conclusions

All of the results, including the geometry changes, the changes in force constants, and the changes in electron populations or effective charges, indicate that the oxygen in formamide does not play an active role in determining the rotational barrier and that the principal interactions involve only the carbon and nitrogen. A reasonable hypothesis is that the main determining factor is the need for the nitrogen to stabilize its lone pair electrons as well as possible. In the rotated form, A, the nitrogen places its lone pair electrons in an orbital with as much s-character as possible since the s-electrons are more strongly bound than are p-electrons, and as a result the other bonds are formed with orbitals having higher p-character. This may be seen in the less than tetrahedral observed H–N–H angles which correspond to even smaller bond path angles.[30] The nitrogen will then have relatively low electronegativity since this quantity decreases with increasing p-character. In the planar form, the nitrogen has an opportunity to use its lone pair to interact with the adjacent electron deficient carbon, and this will lead to stabilization. The interaction is seen in the CN π bond order of 0.229 in the planar form. In order to allow this interaction, the lone pair must occupy a p-orbital, which results in approximately 120° bond angles at nitrogen and sp^2 hybridization. The increase in electronegativity of the nitrogen results in a charge shift from the carbon to the nitrogen in the σ system. The shift in charge density is in part due to a shift in the bond critical point toward the carbon leading to a larger volume element for the nitrogen. The role of the oxygen is mainly to polarize the carbonyl group and make the carbon able to interact with the nitrogen.

The atoms defined in this way are far from spherical, and the center of charge does not coincide with the nuclear position. As a result, there are atomic dipoles and higher terms, which may readily be calculated along with the populations derived from integration of the charge density. The dipole moment may be reproduced by summing the charge-distance products and adding the atomic dipoles.[31] Similarly, if one also includes the quadrupole terms, it is possible to reproduce the electrostatic potential outward from the van der Waals surface.

It is also possible to reproduce the electrostatic potential using a set of nuclear centered charges, and the values of these effective charges may be derived from the electrostatic potential. The charges defined in this way are for nonphysical spherically symmetrical atoms. They also are in agreement with the conclusion that the oxygens is not significantly involved in determining the barrier to rotation. The direction of charge flow between C and N derived from the effective charges is opposite from that obtained from the electron populations found by integration of the charge density. This is a result of the difference in the way the atoms are defined, and formamide is probably an extreme example of this difference. The electrostatic energy plots (Figure 11) illustrate the difficulty in representing the nitrogen by an effective charge. The electrostatic potential in the vicinity of the nitrogen is markedly anisotropic. *As a result, the effective charges must be balanced among the several atoms in such a way as to reproduce the anisotropy.*

It is important to note that the electrostatic potential outward from the van der Waals surface may be well reproduced either by the terms obtained using the theory of atoms in molecules or by the effective charges derived by fitting the electrostatic potential. The molecular dipole moment may also be reproduced in the same fashion. Thus, there is no fundamental conflict between the two sets of charges, despite the differences seen in Figure 10. The charges designated as "n" are for anisotropic (nonspherical) quantum mechanically defined atoms, and are the

(30) Wiberg, K. B.; Murcko, M. A. *J. Mol. Struct.* **1988**, *169*, 355.
(31) Cf.: Bader, R. F. W.; Larouche, A.; Gatti, C.; Carroll, M. T.; MacDougall, P. J.; Wiberg, K. B. *J. Chem. Phys.* **1987**, *87*, 1142.

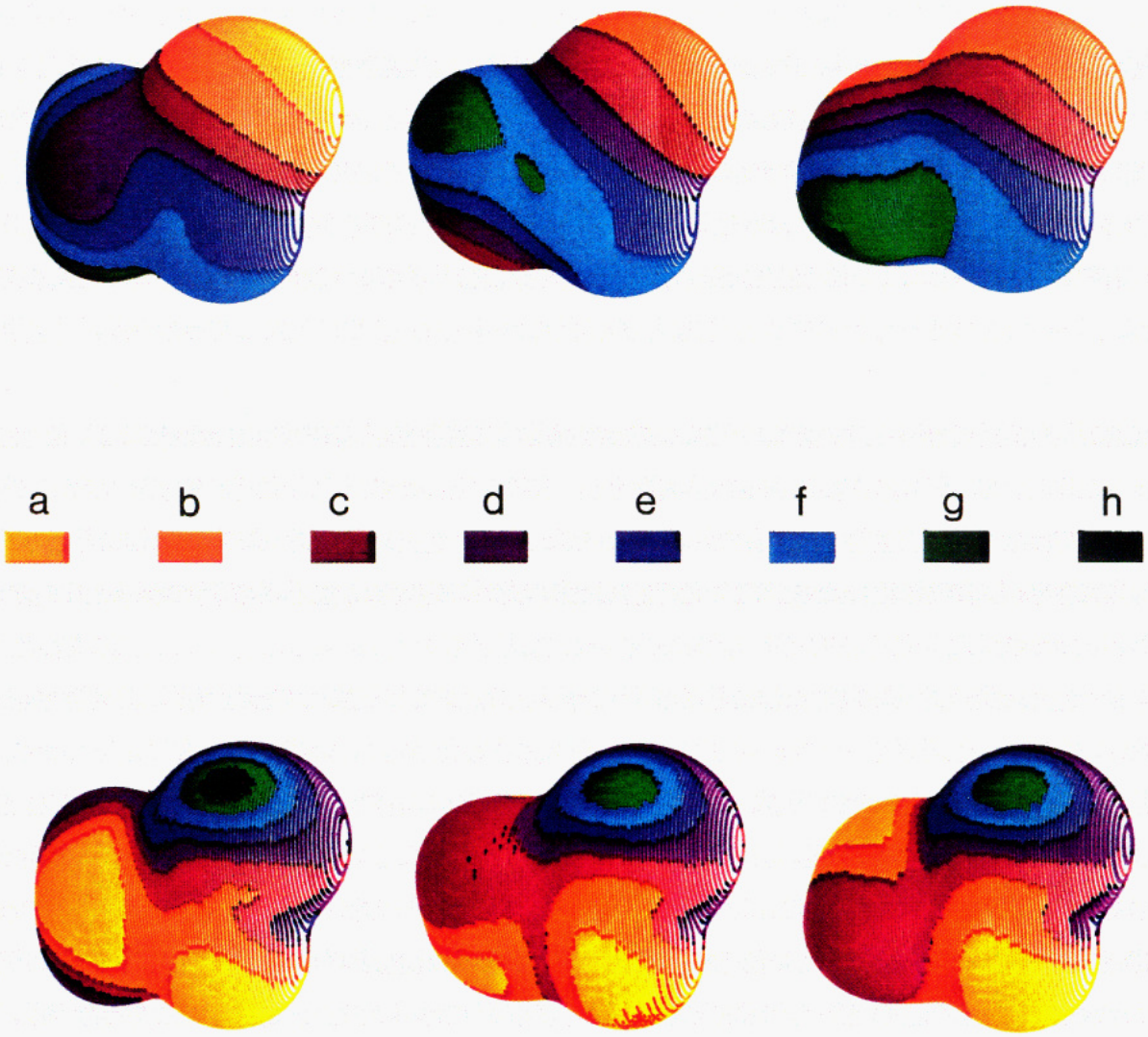

Figure 11. Electrostatic potential maps (upper) at the van der Waals surface (0.002 e/B^3) for planar formamide (left), conformer A (center), and conformer B (right). The color code is (kcal/mol) as follows: (a) −52 to −38; (b) −38 to −24; (c) −24 to −10; (d) −10 to +4; (e) 4 to 18; (f) 18 to 32; (g) 32 to 46; and (h) 46 to 60. Values of the Laplacian of ρ at the van der Waals surface are given in the lower plot. The color code (e/B^5) is as follows: (a) 0.0065 to 0.0077; (b) 0.0077 to 0.0089; (c) 0.0089 to 0.0101; (d) 0.0101 to 0.0113; (e) 0.0113 to 0.0125; (f) 0.0125 to 0.0137; (g) 0.0137 to 0.0149; (h) 0.0149 to 0.0160. The molecule is oriented with the oxygen at the upper right, the amine group at the left, and the aldehydic proton to the lower right.

leading terms of a series expansion that includes atomic dipoles, quadrupoles, etc. They correctly represent the charge distribution as seen by the atomic nuclei and reflect changes in hybridization. The effective charges marked "c" are for spherical *nonphysical* atoms and give a simple representation of the electrostatic potential at the VDW surface. As such, they provide a convenient way in which to think of the molecule in terms of intermolecular interactions.

8. Calculations

The calculations were carried out using GAUSSIAN-90[32] and standard basis sets.[33] The electron populations and kinetic energies were calculated using PROAIM.[34] The bond orders were calculated using BONDER.[35]

Acknowledgment. This investigation was supported by a grant from the National Institutes of Health. We thank Prof. Cioslowski for providing information on the bond order calculations prior to publication.

Registry No. $HC(O)NH_2$, 75-12-7.

(32) Frisch, M. J.; Head-Gordon, M.; Schlegel, H. B.; Raghavachari, K.; Binkley, J. S.; Gonzolez, C.; Defrees, D. J.; Fox, D. J.; Whitehead, R. A.; Seeger, R.; Melius, C. F.; Baker, J.; Martin, R. L.; Kahn, L. R.; Stewart, J. J. P.; Fleuder, E. M.; Topiol, S.; Pople, J. A. GAUSSIAN 90, Developmental version, revision A, Gaussian, Inc.: Pittsburgh, PA, 1988.

(33) Hehre, W. H.; Radom, L.; Schleyer, P. v. R.; Pople, J. A. *Ab Initio Molecular Orbital Calculations*; Wiley: New York, 1986.

(34) Biegler-König, F. W.; Bader, R. F. W.; Tang, T.-H. *J. Comput. Chem.* **1982**, *3*, 317. Bader, R. F. W.; Tang, T.-H.; Tal, Y.; Biegler-König, F. W. *J. Am. Chem. Soc.* **1982**, *104*, 946.

(35) Cioslowski, J. Florida State University, SCRI, 1990.

JOURNAL OF MAGNETIC RESONANCE 46, 319-321 (1982)

NOTES

A Simple Multinuclear NMR Thermometer

CLAUDE AMMANN, PIERRE MEIER, AND ANDRÉ E. MERBACH*

Institut de Chimie Minérale et Analytique, Université de Lausanne, Place du Château 3, CH-1005 Lausanne, Switzerland

Received June 22, 1981

For many years we have been performing multinuclear kinetic NMR measurements and for the purpose of temperature measurement we currently utilize a simple, accurate Pt-resistance thermometer assembly. The method involves a substitution technique, possible nowadays because of the good stability of commercial NMR thermostating units.

The thermometer assembly is made of a temperature sensor contained in an NMR tube (Fig. 1) and connected to a readout device by an insulated cable. The temperature sensor consists of a 2-mm-diameter Pt 100-Ω resistor (J) at the end of an alumina rod (H). The sensor head (B) supports the connection plug (A) and can be fixed to tubes of either 5 or 10 mm external diameter by means of O-rings (C). The weight of the temperature sensor, 5 g only, permits rotation with the gas turbine. The resistance measurement is made with a digital ohmmeter (for example, Dana 4600 multimeter, 4½ digits). After subtraction of the small resistance of the connecting wire (typically 0.5 Ω), the resistance is converted to temperature by means of DIN 43760 tables. If one uses devices giving the temperature directly (for example, Hewlett-Packard 2802 A), account must be taken of the diversity of temperature coefficients of resistors of different origins.

To measure the temperature the sensor is placed in a tube of the same diameter as that of the sample. The liquid surrounding the sensor should have the same physical properties as those of the sample. The temperature measuring tube is placed in the probe head and is rotated if the following NMR measurement is to be done with rotation. After temperature equilibration (less than 3 min for 5-mm and 10 min for 10-mm tubes) the rotation, if used, is stopped, the sensor connected to the readout device, and the reading made within the 5 sec following the stoppage of rotation. The tube is replaced by the sample tube, the NMR measurement made, and the temperature rechecked at the end for higher accuracy.

No changes of the observed temperatures attributable to tube nonuniformity (Wilmad Glass Co.) have been detected (*1*, *2*). However, in nonspinning samples the temperature was found to depend (±1 K) on its angular position; this is attributed to poor axial symmetry of the tube and probe-head assembly. Rotation of the sample eliminates this problem and gives excellent reproducibility (±0.2 K).

* To whom all correspondence should be addressed.

0022-2364/82/020319-03$02.00/0

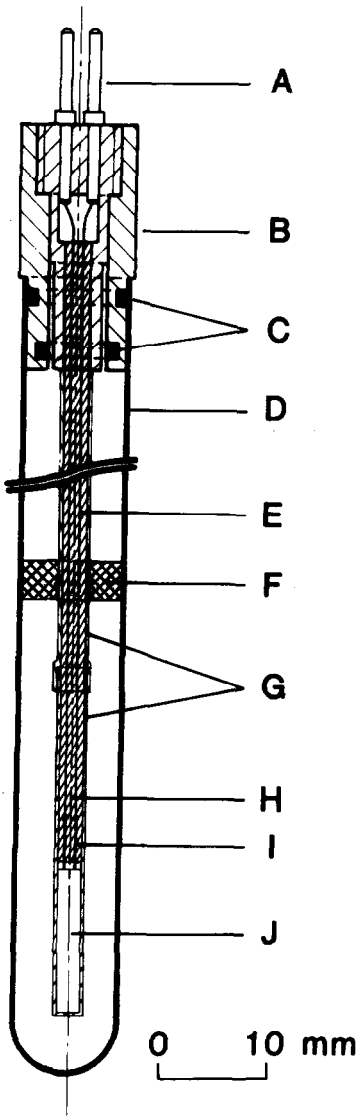

FIG. 1. Pt-resistor temperature sensor in a 10-mm-diameter NMR tube. (A) Connecting plug, (B) sensor head (Teflon), (C) O-rings, (D) 10-mm NMR tube, (E) Cu wires, (F) centering ring (Teflon), (G) thermoretractable protection sheath, (H) alumina rod with two holes, (I) connection wires, (J) Pt 100-Ω resistor (W 60150 Degussa Switzerland AG, Zurich).

It has been established that introduction of the sensor into the liquid of the temperature-measuring tube does not produce any detectable temperature changes in the liquid from, for example, modification of convection currents or loss of heat along the sensor length.

For the Bruker WP-60 spectrometer the difference between the temperature of a nonspinning sample and that of a spinning sample is at maximum 1 K from 150

to 460 K for 5-mm tubes, and from 150 to 370 K for 10-mm tubes. For the latter, above 370 K, the difference increases considerably to reach 5 K at 460 K. It is therefore recommended that the temperature-measuring tube be rotated before measurements. The rotation speed (15 to 60 Hz) does not affect the measured values. The magnitude of the vertical temperature gradients at the level of the NMR measuring coil depends on the difference between the experimental and ambient temperatures. In the 5-mm proton NMR probe head, the vertical gradients were ± 0.4 K cm^{-1} at 180 and 400 K.

In contrast to the magnetic field H_0 and the radiofrequency pulsed field H_1, the high-power radiofrequency decoupling field H_2 can cause large changes of the sample temperature, up to 50 K (*3*). Therefore, for measurements using H_2, it is essential that the liquid surrounding the temperature sensor be identical to the sample to be measured. Moreover H_2 must remain on during the thermostating of the temperature tube (like the sample tube) and turned off just before the reading so as not to perturb it.

In proton NMR the temperature is usually determined by means of two thermometric solutions: methanol and ethylene glycol. Numerous calibration equations have been proposed relating the chemical shift differences $\Delta\delta$ (ppm), and the temperature for these compounds (*4*). Our multinuclear thermometer yields the following equations:

$$T\,(\mathrm{K})\ (\text{methanol}) = 409.0 - 36.54\,\Delta\delta - 21.85\,(\Delta\delta)^2, \quad \text{between 178 and 330 K,}$$

$$T\,(\mathrm{K})\ (\text{ethylene glycol}) = 466.5 - 102.00\,\Delta\delta, \quad \text{between 273 and 416 K.}$$

These results agree to within ± 0.5 K with those obtained by Van Geet ((*5*); see also (*1*)).

ACKNOWLEDGMENTS

This work is supported by the Swiss National Science Foundation under Grant 2.870-0.80.

REFERENCES

1. M. L. KAPLAN, F. A. BOVEY, AND H. N. CHENG, *Anal. Chem.* **47,** 1703 (1975).
2. D. W. VIDRINE AND P. E. PETERSON, *Anal. Chem.* **48,** 1301 (1976).
3. J. J. LED AND S. B. PETERSEN, *J. Magn. Reson.* **32,** 1 (1978).
4. D. S. RAIFORD, C. L. FISK, AND E. D. BECKER, *Anal. Chem.* **51,** 2050 (1979).
5. A. L. VAN GEET, *Anal. Chem.* **42,** 679 (1970).

CONTENTS

1 SAFETY

The following general safety precautions must be observed during the operation, service and repair of this instrument.

1.1 Protective Ground

To minimise shock hazard the instrument must be connected to an electrical ground. The ground wire (green/yellow) in the instrument AC power cable must be connected to the installation electrical ground system. Do not use extension cords without a protective earth conductor. Do not disconnect the protective ground inside or outside the instrument. Do not have external circuits connected to the instrument when its protective ground is disconnected.

1.2 Repair and Adjustment

Ensure that the instrument is disconnected from the AC power supply (switching off the front panel ON-OFF switch is not sufficient) before the covers are removed or fuses are replaced, otherwise dangerous voltages are accessible. Capacitors inside the instrument and power connector filter, if fitted, may remain charged after removal of AC power. These should be discharged before starting work.

For fault finding and calibration the AC power supply may require reconnection. This work may only be carried out by skilled personnel who are aware of the hazard involved.

2 INTRODUCTION

This manual provides operating and service information for the Oxford Instruments VT Controller model VTC4.

The Variable Temperature Controller (VTC) is intended for use in conjunction with a Varian NMR spectrometer. It is designed to control the sample temperature within the NMR probe. Heating of the sample is by means of a nitrogen gas stream which is warmed by a heater within the probe. The heater is supplied with 0-40v DC from the VTC. For operation below room temperature the gas stream is precooled by passing it through a heat exchanger immersed in liquid nitrogen.

The sample temperature is sensed by two thermocouples mounted in the gas stream between the heater and the sample. These are connected in parallel via a potentiometer which allows the ratio of their contributions to be adjusted.

An additional platinum resistance safety sensor is mounted directly on the heater assembly. This enables the heater power to be shut down in the event of a failure of the gas flow. Additional safety features are incorporated to protect the VT probe against operator errors and system faults.

The VTC employs a 4 digit display of temperature covering the range -150.0 to +200.0 degrees C. In addition a Status Lamp allows an operator to observe the current VT status. All control of the VTC is by serial data sent from the spectrometer computer via an RS232C data link. This link also allows the computer to interrogate the VTC. The same link may be used, connected either to a computer or to a standard 9600 baud terminal, to effect a full calibration of the VTC.

The following error conditions may be detected and produce an status message to the computer.

- o/c Thermocouple
- o/c Safety Sensor
- s/c Safety Sensor
- Over-temp at safety sensor
- s/c Output transistor
- Software/uProcessor failure

Over-temperature at the safety sensor initially turns the heater off. If this fails to correct the condition within 5 seconds, it is assumed that either the gas flow has been interrupted, or that an output transistor failure has occurred. In this case a protective relay operates, isolating the heater from the control electronics. Sensor failure on any of the sensors also results in this relay operating.

Once the protective relay has operated the output will remain off. A power down, or an "N" or "C" instruction from the computer is required to release the relay.

An auxillary output port is available on the VTC for control of a gas solenoid of other external devices.

3 INSTALLATION

3.1 Supply Connection

Before applying power to the instrument, ensure that the voltage selector on the rear panel is correctly set for the intended supply voltage.
If necessary, open the voltage selector panel using the slot provided, withdraw the voltage selector and replace it in the correct orientation for the intended voltage. Check that the correct fuses are fitted, then close the voltage selector panel.

Fuse ratings are:

100-120v	1.6A Type T (Slow Blow)
200-240v	0.8A Type T (Slow Blow)

3.2 Heater and Sensor Connections

Connections to the heater, the main sensor (Copper/Constantan Thermocouple) and the safety sensor (Platinum Resistance Thermometer) are by means of a 9 way D-socket on the rear panel. Pin connections are:

1 Thermocouple +ve
2 0v
3 Thermocouple -ve
4 n/c
5 n/c
6 Heater Output +ve
7 Heater Output -ve
8 Platinum Resistance Thermometer -ve
9 Platinum Resistance Thermometer +ve

SANK AT PROBE 6 WAY CONNECTOR

The Heater Output connections are electrically isolated from the controller ground and from the power supply ground within the temperature controller.

The Input connections and the 0v connection on the 9 pin socket, share a common ground with the temperature controller electronics and are linked to the RS232 socket signal ground within the temperature controller. Both are isolated from power supply ground within the controller, though signal and power grounds may be linked within the computer.

It is important to note that the the room temperature compensating sensor for the main sensor thermocouple is mounted at the rear panel of the VTC. To get accurate compensation it is essential that the thermocouple reference junction is at the same temperature. This in turn means that the cable linking the probe to the VTC must use thermocouple compensating cable for

the main sensor leads. If the rear panel in the region of the connector is likely to be exposed to temperature fluctions, it will be an advantage if a draught shield is placed around the plug, and the RT sensor, positioned immediately to its right.

3.3 Serial Data Line Connections

The bi-directional serial data link from the computer is connected via a 25 way D-socket on the rear panel.

Pin connections at this socket are:

2	Received Data (From Computer)
3	Transmitted Data (To Computer)
4	Linked to 5
5	Linked to 4
6	+5V when VTC is powered up
7	Signal Ground
8	+5V when VTC is powered up

All other pins are open circuit.

Voltage levels for the transmitted and received data are:

Tx Data High	> +5.5V
Tx Data Low	< -5.5V
Rx Data High Threshold	< +2.6V
Rx Data Low Threshold	> +1.4V
Max Rx Input Voltage	+/-30V

Data protocols are:

Baud Rate	9600
Tx Start Bits	1
Tx Data Bits	8
Tx Stop Bits	2
Rx Start Bits	1
Rx Data Bits	8
Rx Stop Bits	>=1

For normal ASCII exchanges the 8th data bit is treated as a parity bit. It is always set to "0" on transmitted data. It is ignored on received data.

3.4 Auxilliary Port Connections

The auxilliary port is provided primarily for the control of a gas solenoid. However it has up to 8 independant output lines and 4 input lines available. Connections to the port are by means of a 15-way D-socket on the rear panel.

The outputs are open-collector transistors. (Specification as for ULN2803A). These may be used to drive solenoids etc.

directly. The solenoids should be supplied from an external supply of 25 volts maximum and the maximum current per line should not exceed 500mA. The solenoid supply ground should be linked directly to the 0v pin of the Auxilliary socket.

Inductive loads such as solenoids must be protected by diodes to prevent the driver transistors being damaged by inductive spikes. This may either be achieved by individual diodes directly across the loads, or alternatively the +ve solenoid supply may be linked directly to pin 15 of the auxillary socket, in which case the protection diodes within the VTC will operate.

For low power loads, current may be drawn directly from pin 15, which is connected via a diode and fuse, to the internal unregulated 11 volt line. A maximum total current of 500mA may be drawn from this source.

The input lines on the auxilliary socket are suitable for either TTL level inputs or contact closures to 0v. The input device is a 74HC244 and 100K ohm pull-up resistors are fitted to the internal 5v line.

Pin connections at this socket are:

1	Output Bit 0
9	Output Bit 1
2	Output Bit 2
10	Output Bit 3
3	Output Bit 4
11	Output Bit 5
4	Output Bit 6
12	Output Bit 7
5	Input K4
13	Input K5
6	Input K6
14	Input K7
7	+5v
15	Driver Protection / +11v unregulated.
8	0v

4 OPERATION

4.1 First Time Operation

For first time operation it will be probably simplest to connect the VTC directly to a data terminal. Any terminal capable of operating at 9600 baud should be suitable.
Once familiar with the operation of the various commands and responses, software may be written for the computer to perform the required functions.

With the terminal connected to the VTC the latter may be switched on using the POWER switch on the front panel. This switch should illuminate. If it fails to do so, check the power connection and the fuses.
At switch on, the VTC first performs a self test of its internal memory and its back-up battery. If all is well the display shows the message "PASS" for 2 seconds. If hardware errors are detected the message "Err" followed by a number is displayed for 10 seconds. If the back-up battery is aging the message "batt" is displayed for 10 seconds. (See below for the significance of this message).

On completion of the self test the display is blanked whilst the analogue circuits are given time to stabilise and the sensors are checked for error conditions.

If the sensors are within range the output safety relay is closed and the VTC enters its Stand-By state. In this state the STATUS indicator is unlit and the the heater and gas-control solenoid are un-energised.

If a sensor error condition is encountered the relay is not closed and the status indicator flashes at a fast rate (2Hz).

In either case the display illuminates and indicates the measured probe temperature.

If the display blinks on then immediately goes out for another 1-2 seconds and continues to cycle on and off, check that the supply voltage is adequate. (The VTC automatically senses low supply volts and performs a reset function, to protect the data stored in memory). If necessary operate the instrument on a lower voltage setting.

Once the display is lit, the VTC should be fully operational. To test the serial link, type a "V" at the terminal (must be upper-case letters). The VTC should respond by sending two lines of text, describing the software and its version number. Provided this message is correctly printed the communication link is fully operational. The other commands given below may then by tried to gain familiarity with the system operation.

In the Stand-By state, manual control of the heater and gas solenoid is possible by means of the "O" and "G" commands. To

leave the Stand-By state and commence Automatic Control, the "A" command may be used. To provide full system operation, it will be necessary to have a VT probe connected with gas flowing. However most of the commands may be tested by placing a s/c across the thermocouple input terminals and a 100 ohm resistor across the safety sensor terminals.

Note that if an error condition is detected on the sensor assembly the safety relay may operate making it impossible to obtain any output. After clearing the problem the the "N" command may be used to reset the safety relay.

4.2 Communication Protocols

All dialogue with the computer is in 9600 baud serial form.

Data is sent as a start bit, 8 data bits plus two stop bits.

All normal user commands to the VTC and responses received, are sent as strings of ASCII characters. Where numeric values are required, these are also sent as ASCII strings representing the number in normal, decimal format. Numbers are preceeded where appropriate by a "+" or "-" sign. To simplify interfacing, the VTC is fairly flexible in the format of numbers it will accept from the computer. Characters sent by the VTC have the MSB (parity bit) set to "0". If parity is sent by the computer it is ignored.

None of the Modem control lines of the RS232C interface are used. The VT controller will accept serial data at all times. In its default state it will only send data to the computer in response to a specific command. If however the computer is able to accept serial data at all times, the VT controller can be instructed to send a status message spontaneously whenever the status changes. This is done by means of the "Q" command, see below. The same command may also be used to control the sequence of characters returned by the VTC in response to a command. These may consist of any combination of:

Single Letter Echo
<CR> . Prompt String
EOM character (ctrl-C)
<LF> after all <CR>

If the computer used does not have adequate buffering it may be possible for messages from the controller to over-run this. To overcome this problem, the data rate from the controller may be slowed down to any chosen speed by means of the W command. This introduces a delay, before each character is sent. With this feature it is possible to accomodate computers with no input buffering.

4.3 Commands and Responses

Commands to the controller consist of a single upper case letter A-Z, optionally followed by a parameter sent as an ASCII decimal string. Where a parameter is required, it must be terminated by an ASCII <RETURN> character. <LINE FEED> characters, if sent are ignored. Commands not requiring a parameter, need no terminator. Only the single command letter is required. Again if a terminator is sent it will be echoed, but otherwise ignored.

The VTC may respond to a command to indicate that it has been correctly received. In some cases the response is to return a requested value. In cases where no other specific response is required, the controller may be instructed to remain silent, to echo the command letter or to issue a prompt string. In addition, if required the VTC may issue an EOM character after a command letter to indicate that its parameter may be sent. (It is however not necessary for the computer to await the EOM, the VTC will accept the parameter immediately after the command letter). merely echos the command letter.

Any commands which are not understood or cannot be obeyed in the current state of the instrument result in a "?" being echoed, followed by the command string as received. The "?" will always be the first character returned to simplify error handling by the computer. Again an EOM may optionally be sent following an error message.

Apart from responses to specific commands, the VTC will not normally issue messages. However another option in the Q command allows the VTC to send a status message spontaneously whenever the status changes.

Section 5 gives a list of the available commands and details of each.

5 COMMAND LIST

A list of all the currently active commands is given below, followed by a more detailed description of each of these,

In the list which follows the symbol n is used to indicate a decimal digit in the range 0-9.

1. COMMANDS NOT REQUIRING A PARAMETER

A	COMMENCE AUTOMATIC CONTROL
M	RETURN TO MANUAL CONTROL
B	RETURN TO STANDBY STATE
R	SEND READING (MEASURED TEMPERATURE)
E	SEND ERROR (BETWEEN MEASURED AND SET TEMPERATURES)
H	SEND HEATER OUTPUT (Range 0-100%)
S	SEND STATUS
V	SEND VERSION NUMBER FOR SOFTWARE
C	INITIATE CALIBRATION DIALOGUE
N	RESTORE NORMAL OPERATION

2. COMMANDS REQUIRING A PARAMETER & TERMINATOR

Tnnnnn	SET TEMPERATURE (See note 1)
Pn	SET PROPORTIONAL BAND (See note 2)
In	SET INTEGRAL ACTION TIME (See note 2)
Dn	SET DERIVATIVE ACTION TIME (See note 2)
Onnnnn	SET OUTPUT VOLTAGE (In MANUAL mode only)
Gnnn	SET GAS SOLENOID (In MANUAL mode only)
Qn	SET "QUIET" STATUS (See Note 3)
Fnn	SET FRONT PANEL DISPLAY
Wnnnn	SET WAIT INTERVAL BETWEEN OUTPUT CHARACTERS
Unnnn	UNLOCK MEMORY PROTECTION

3. CHARACTERISATION AND DIAGNOSTIC COMMANDS

L	LOAD LINEARISER DATA TABLE
X	LOAD PATCH MEMORY
Y	LOAD WHOLE MEMORY
Z	DUMP WHOLE MEMORY

6. COMMAND SYNTAX

A COMMAND

The AUTO command sets the VTC into automatic control. It should be followed by a "T" command to select a desired temperature. After power-up or a "B" command the assumed set temperature will be 0.0 degrees. Otherwise the set point will remain at the last value selected. Note that it is possible to give the "T" command whilst in standby, but in this case the facility to automatically set the gas solenoid on the basis of the temperature requested will be lost. (See "T" command below).

M COMMAND

The MANUAL command returns the VTC from automatic to manual control. A fully "bumpless" auto-manual transition is effected. i.e. at switch-over the heater output is maintained at its current value and the state of the gas solenoid is unchanged. Similarly the transition from manual back to auto is also made "bumpless", by precharging the integrator to the current manual output. Thus if the temperature is being manually controlled at the desired set-point, there will be no change in heater output when switching to auto. (If the temperature is not at the set point when the switch to auto is made, there will of course be a change in output as the VTC attemps to move towards the set point).

B COMMAND

The BEGIN command performs a complete power-up and initialisation sequence, and returns the controller to the stand-by state with heater and gas solenoid both off. It is exactly equivalent to switching the controller off and then on again.

R COMMAND

The READ command instructs the computer to send the measured temperature. This is sent in the form of a signed integer giving the temperature in tenths of a degree, followed by a <CR> character.

E COMMAND

The ERROR command sends the temperature difference between measured and set temperatures in the same format.

H COMMAND

The HEATER command sends the heater voltage as a percentage of full output. (Note that this value is only approximate, it is not a calibrated parameter.)

S COMMAND

The STATUS command instructs the controller to send its current status. This is sent as a response consisting of S followed by a signed, single decimal digit and a <CR> character. Positive values of status indicate normal operation whilst a negative value normally indicates that a fault has been detected. When a negative status occurs, the output safety relay operates, to isolate the heater and prevent any possible damage to the VT probe. This relay may be reset by means of the "N" command (or by performing a calibration).

The following status reports are currently defined.

S+0	Control in Stand-By or Manual Control
S+1	Temperature Stable at Set Point
S+2	Temperature Changing
S+3	Safety Sensor limiting output
S-1	Gas not flowing or o/p stage fault (turn up or check gas flow)
S-2	Main Sensor on Bottom Limit
S-3	Main Sensor on Top Limit (o/c Thermocouple)
S-4	s/c Safety Sensor
S-5	o/c Safety Sensor

V COMMAND

The VERSION command results in the Software title, and version being sent as two lines of ASCII text, each terminated by a <CR>.

C COMMAND

The CALIBRATE command initiates a calibration dialogue where the controller issues messages requesting various input conditions to be applied, on the basis of which the internal calibration constants are set up. Once set, these are retained in non-volatile memory. Recalibration will normally only be necessary if sensors are changed or servicing work is carried out on the analogue portions of the controller.

To reduce the possibility of inadvertant loss of calibration, a "U" command is required before the "C" command will be recognised. See section 7.

N COMMAND

The NORMAL command restores a normal operation of the controller. Specifically it resets the output safety relay. Before issuing this command the cause of the relay operating should be investigated, and a "S" command issued to ensure that the controller is in a normal state. The "N" command also resets the front panel display to show Measured Temperature (equivalent to "F0" command).

Tnnnn COMMAND

The TEMPERATURE command instructs the controller to set a specific target temperature. Temperatures may be set in the range -150C to +200C. (The indication range is made larger than this to allow for overshoot etc.)

The format of the parameter following the T command has been made flexible to cope with a variety of computer output formats. The parameter required is a signed integer, representing the temperature in tenths of a degree. A decimal point, a +ve sign or leading zeros are all optional and will be ignored. However a digit for the tenths of degrees must be included even if this is zero. Thus the following formats will be accepted for a set temperature of 38.0 degrees.

```
38.0
0038.0
+ 38.0
380
```

whilst

```
38
38.
```

will be accepted but will give rise to a set point of 3.8 degrees. Other characters within a number will give rise to an error message.

If the "T" command is issued whilst under automatic control, the state of the Gas Control solenoid will be selected automatically on the basis of the temperature requested. For temperatures of 25.0 Celcius and below, the solenoid will be energised, to provide cooling. Above this temperature it will be un-energised.

If non-standard control of the gas solenoid is required, an "M" command should be issued to select the manual state, before issuing separate "T" and "G" commands to set the target temperature and gas solenoid respectively. Automatic operation may then be resumed by means of an "A" command.

Pn,Inand Dn COMMANDS

This family of three commands set the PROPORTIONAL, INTEGRAL and DERIVATIVE control terms. The commands are followed by a single digit specifying the value required, as shown in the following table. At power up the P,I and D values are set to defaults of 4, 4 and 0 respectively.

VALUE of n	P COMMAND	I COMMAND	D COMMAND
0	100%	32 min	OFF
1	50%	16 min	8 sec
2	25%	8 min	16 sec
3	12%	4 min	32 sec
4	6%	2 min	1 min
5	3%	1 min	2 min
6	1.5%	32 sec	4 min
7	-	16 sec	8 min
8	-	8 sec	16 min
9	-	4 sec	32 min

Onnnnn COMMAND

The OUTPUT command allows the output voltage to be set directly when in manual mode. (Status S=0). The command is not recognised in auto mode. The parameter may take values of 0 to 32767. (Note that output voltage is not directly proportional to nnnnn. There will be a dead bands at the end for which changes of nnnnn will not produce output changes.

Gnnn COMMAND

The GAS control command allows the state of the auxillary output port to be set directly when in manual mode. (Status S=0). The command is not recognised in auto mode. The parameter may take values of 0-255, allowing each of the eight lines of the auxilliary output port to be controlled directly. Each line is represented as ont bit of an 8-bit binary number. Any line that is active (i.e. pulled low) is represented by a binary 1. Then the required parameter nnn is the decimal equivalent of this 8-bit binary number.

In normal use only the least significant line is used, to control the gas solenoid. Hence the only two options will be G0 for solenoid off and G1 for solenoid energised.

Qn COMMAND

The "QUIET" command controls the responses generated by the VTC. The parameter n may take any value in the range 0-255. With n=0 or omitted. The VTC is totally quiet, the only data transfered

to the computer are the actual number strings in response to a measure command. Non-zero values for the parameter, result in a selection of any combination of 8 independant response options. Each is given a value (in a binary sequence) and the required Q parameter is obtained by adding together the values for each of the options required to be active. The list below shows the options available.

VALUE	OPTION
1	Echo Single Command letter on command-completed
2	Echo each character as received
4	Send "<CR>." prompt on command-completion or after STATUS sent automatically
8	Send <EOM> after initial command letter received
16	Send <EOM> after illegal-command error message
32	Send STATUS message whenever status changes
64	Send <EOM> after automatic status message
128	Send <LF> after every <CR>

At power-up the VTC is in the Q254 state, which is believed to be the state requested by Varian. ✓ (AS SHOWN ON ACQ DIAG PORT)

Fn COMMAND

The FRONT PANEL command determines which of the internal variables is displayed on the front panel LED display. The parameter normally displayed is measured temperature. For diagnostic purposes it can be useful to have a display of various other parameters. The following may be displayed:

F0	MEASURED TEMPERATURE
F1	SET TEMPERATURE
F2	ERROR (SET TEMP. - MEASURED TEMP.)
F3	HEATER VOLTS (AS A PERCENTAGE OF FULL OUTPUT)
F4	SAFETY SENSOR RESISTANCE (OHMS)
F5	RT SENSOR VALUE (DEGREES)
F6	CH1 INPUT FREQ/4
F7	CH2 INPUT FREQ/4
F8	CH3 INPUT FREQ/4
F9	P PARAMETER
F10	I PARAMETER
F11	D PARAMETER

NOTES
1. F2 is currently on an expanded scale (x20 approx) for dignostic purposes.
2. The values for F3, F4 and F5 are approximate readings, intended for diagnostic purposes only.
3. F6, F7 and F8 provide a measure of the frequencies of the input V/F converters. Again these are intended for service diagnostic purposes only.
4. F9, F10 and F11 serve as a reminder of the current values of the P, I and D control parameters. Note that unlike the other values above, the displayed value is not continuously updated.

Thus after a P command it will be necessary to repeat the F9 command if the new value of P is to be displayed.

Wn COMMAND

The WAIT command is provided to simplify interfacing to slow computers, with no input buffering. For example a computer running a simple logging program in basic, may take several milliseconds between issuing an R command and being ready to accept the resulting response. The W command introduces a fixed delay before every character sent. The value of nnnnn specifies the delay in milliseconds. (Leading zero's may be omitted). Delays may extend from zero to 1 minute. (Though the latter is not recommended!).

Unnnn COMMAND

The VTC holds a number of key parameters in non-volatile memory. These can however be overwritten by specific sequences of commands, in order to reconfigure the instrument. To prevent erroneous commands causing such a corruption, a lock is built into the software. As supplied, the L, X and Y commands will not be recognised and produce an error message. To Unlock these commands the command Unnnn must be issued, where nnnn is the correct key-value.

To prevent inadvertant operator error a second lower level of locking is incorporated. This is used for example on the "C" command. At power up the command is locked but it can be unlocked by a U1 command. Almost any non-zero U parameter will open this lock. It is not necessary to know the full four digit key-value.

L COMMAND

The L command allows data to be sent to load the lineariser data table. The data is sent as a series of 257 decimal values in the range 0 to 65535. These represent the start and end points for the 256 segments into which the working range of the controller is divided. A relatively simple program written in Basic, is available from Oxford Instruments to transfer a data table from a computer to the VTC. To avoid the data table becoming corrupted by an inadvertant L command, this command is normally "locked" (see above).

X,Y & Z COMMANDS

This family of commands are provided purely for software diagnostic purposes. They transfer pure binary data (ie non-ASCII) between the controller and a computer. The X and Y commands overwrite areas of the non-volatile memory and could

therefore have a serious effect if misused. For this reason they are "locked". The Z command performs a binary RAM dump. It will produce confusing output at a terminal but can do no harm to the controller and is therefore left unlocked.

7. CALIBRATION

All linearisation data and calibration constants are held in NONVOL RAM (Mostek 480-Z-02, internal dual Lithium Battery with retention life >10 years). New linearisation tables can be loaded from the computer and all other calibration is handled by an interactive dialogue with the computer.

Minimal equipment required for a full calibration is:

Millivolt Calibration Source
Resistance box (to simulate safety sensor)
Thermometer (to measure Room Temperature)
9600 Baud Terminal (or the spectrometer computer)

To reduce the chances of a calibration sequence being started inadvertantly, the calibration command is "locked" at switch-on. Before calibration can take place a "U1" command must be given. (Almost any non-zero parameter will suffice, it is not necessary to know the unique key required for the "X" and "Y" commands).

Following the "U1" command, calibration is initiated by sending a "C" command. The VTC then conducts a dialogue in which it requests that various input conditions are applied in sequence. Once the specified condition has been applied the operator responds by pressing <RETURN>. After a pause to ensure that conditions have settled, the parameter is measured and the appropriate calibration constant is stored in non-volatile memory.

The calibration sequence is split into 3 sections covering the safety sensor, the main sensor and the room temperature sensor. Any section may be omitted by entering a <SPACE> rather than a <RETURN> for the first step of its sequence. However once a calibration sequence has been started for a sensor it must be completed. If any errors are made, the sequence for that sensor should be completed and then the calibration routine restarted to correct the error.

When calibration is complete, the "C" command may be relocked by means of a "U0" command. The "C" command automatically becomes locked if the instrument is switched off or if a "B" command is issued.

The following is an example of the calibration dialogue conducted in response to a C command. The operators responses are underlined and the symbol <RET> is used to denote a carriage return entered by the operator.

U1
C
CALIBRATION SEQUENCE

Apply Input Condition specified, then press RETURN. To skip any step, press SPACE.

Safety Sensor = 20 ohms<RET>,wait
Safety Sensor = 210 ohms<RET>,wait
Safety Sensor = 199 ohms<RET>,wait
RT sensor TP = 0.35 volts<RET>,wait
RT sensor TP = 1.55 volts<RET>,wait
Isolate RT sensor TP<RET>,wait
Enter Room Temp in form XX.X 24.3<RET>
Main sensor = -5.603 mV<RET>,wait
Main sensor = +9.827 mV<RET>,wait
CALIBRATION COMPLETE
U0

8. CALIBRATION CONSTANTS AND NOTES

ROOM TEMP SENSOR TEST POINTS

Voltages are applied between TP1 (+ve) and TP0 (-ve) on the input board. (The smaller board at the left-hand side of the instrument. Positions of the test points are shown on the PCB silk-screen.

MAIN SENSOR INPUT VOLTAGES

(Apply these voltages direct to 9 way D socket. The calibration logic takes care of any RT corrections required.)

The values given calibrate the instrument for a range from -200C to +210C. In general it will not be possible to obtain readings down to -200C with the reference junction at room temperatures. The input amplifier will normally limit at around -190C. Calibration down to at least -150C is guaranteed with ambient temperatures up to 40C at the rear panel.

RESTORATION OF ORIGINAL CALIBRATION

If calibration has been lost for any reason and a suitable voltage source is not available, it may be expedient to restore the original calibration settings determined when the equipment was initially tested. To this end, a copy of the original calibration data is contained within the program memory EPROM U2. Use of this facility is described in section 10.3.

In instruments prior to serial number 07/006 this calibration data was supplied in a separate EPROM.

9. THEORY OF CONTROL

9.1 General

The aim of a controller is to maintain the temperature of a system as close as possible to some desired temperature (the SET POINT) and as far as possible to eliminate the effect of changes in the heat loss from the system. When a steady state is established, the heating provided by the controller will exactly balance the heat lost by the system to its surroundings. A further function of the controller is to follow any changes in the set point as rapidly as possible. Thus the criteria for good control are:

CONTROL ACCURACY	The mean temperature of the system should be as close as possible to the desired temperature.
CONTROL STABILITY	The fluctuations above and below the mean temperature should be small.
CONTROL RESPONSE	The system should follow changes in the set point as rapidly as possible.

In the following sections a number of possible control systems of increasing complexity are described, culminating in 3-TERM or P.I.D. control, as used in the VTC4.

9.2 Open Loop Operation

In an open loop system, a fixed heater power is applied and the system is allowed to come to equilibrium. There is no control as such, since the heater power can only be changed by the intervention of a hman operator. The system takes a long time to reach equilibrium and any changes in the heat loss from the system, produce corresponding changes in the system temperature. The hot plates on a domestic cooker form an example of this form of "control". This mode of operation can be obtained with the VTC in its MANUAL mode.

9.3 On-Off Control

In an on-off (or "bang-bang") control system the heater power is either full on, if the temperature is below the set point; or off, if it is above. The control accuracy and response can be made very good with this form of control and the system can be made largely immune to changes in heat loss. However the control stability can never be made very good since the system temperature must always cycle above and below the set point. The magnitude of the temperature fluctuations depends on the thermal

properties of the system. For some systems, where temperature fluctuations are not important, this is a perfectly satisfactory and simple system of control. (e.g. the domestic electric oven).

9.4 Proportional Control

A proportional control system overcomes the problems of temperature cycling by allowing the heater power to be continuously varied. The heater voltage at any instant is proportional to the error between the measured and desired temperatures. Thus a large negative error will produce a large heater voltage in order to correct that error.

If the output voltage were proportional to the error over the whole range of the instrument, a negative error equal to half the total span of the instrument would be required in order to generate a full output voltage. Thus, although the control stability might be good, the accuracy would be very poor.

By increasing the GAIN of the controller the output can be made proportional to the error over part of the total range of the instrument. Outside this range the output is either fully on or completely off. The range over which the output is proportional to the input is the PROPORTIONAL BAND. This is normally expressed as a percentage of the total span of the instrument. Thus a Proportional band of 100% is equivalent to a gain of unity.

By reducing the proportional band, the accuracy of the controller may be improved since a smaller error will then be necessary to produce a given change in output.

This would seem to imply that, by sufficiently reducing the proportional band, any required accuracy could be obtained. Unfortunately as the proportional band is progressively reduced, there will come a point at which temperature oscillations reappear. (In the limit a controller with a proportional band of 0% is an on-off controller, as described above).

The reduction in proportional band which can be achieved before the onset of oscillations, will depend largely on the design of the system being controlled. In some systems it may be possible to achieve the required control accuracy without oscillations but in most cases this will not be so.

9.5 Integral Action

To overcome this problem, INTEGRAL ACTION is introduced. Consider a system controlled by proportional action as described above, with the proportional band sufficiently large to prevent oscillation. The result will be stable control but with a residual error between the measured and desired temperatures. Suppose this error signal is fed to an integrator, the output of

which is added to the existing controller output. The effect of this will be to vary the overall output until control is achieved with no residual error. At this point the input to the integrator will be zero and this will therefore maintain a contant output. Integral action has thus served to remove the residual error. Provided the contribution from the integrator is only allowed to vary slowly, proportional action will prevent the occurrence of oscillations. The response of the integrator is characterised by the INTEGRAL ACTION TIME. This is defined as the time taken for the output to vary from zero to full output, in the presence of a fixed error equal to the proportional band.

To ensure that the integrator itself does not give rise to oscillations, it is usual to employ an Integral Action Time of at least twice the response time constant of the system.

9.6 Derivative Action

The combination of Proportional and Integral Action will suffice to ensure that accurate and stable control can be achieved at a fixed temeprature. However when the set point is changed many systems will tend to overshoot the required value. By means of Derivative Action this effect may be reduced or eliminated completely. Derivative Action monitors the rate at which the measured temperature is changing and modifies the control output such as to reduce this rate of change. (Derivative Action is exactly analogous to the use of velocity feedback in servo systems and serves the same function).

Like Integral Action, Derivative Action is charcterised by an action time. If the measured temperature is changing at a rate of one proportional band per DERIVATIVE ACTION TIME, Derivative Action will contribute a signal sufficient to reduce a full output to zero or vice versa.

10 THE NON-VOLATILE MEMORY

All the sensor linearisation tables, calibration data and long-term parameters such as the prompt string are held in a non-volatile memory, so that they are retained when power is removed. This memory is contained in the integrated circuit U3 on the main circuit board.

Retention of the memory in the absence of power is achieved by means of a small lithium battery built into the memory package. Thus data is retained even when the integrated circuit is removed from its socket. The battery has sufficient capacity to retain the memory contents for at least 10 years.

Under exceptional circumstances, it is possible that some or all of the contents of the non volatile memory may be lost. Indications that this has occurred are a sudden change in calibration or a string of random characters, returned in place of the normal "." prompt, after every response.

Should this occur, follow the procedure given in section 10.3 below, to restore the calibration. If the fault re-appears after the instrument has been switched off, the non-volatile memory chip has failed and should be replaced.

10.1 "batt" warning message

Every time power is applied to the controller, internal circuitry within the memory tests the state of the battery. If this is starting to fail the normal "PASS" message obtained at power-up is replaced by a "batt" message. The letters are rather stylised and appear as:-

This message is held for 10 seconds instead of the normal 2 seconds. If this message is obtained, it is an indication that the memory chip needs replacing. There is a large voltage margin between the point at which the low battery warning is obtained and the point at which data is lost. Thus it will normally be possible to obtain and fit a replacement memory chip before data has been lost from the old one.

10.2 Memory Replication

If calibration data is not to be lost it is obviously necessary that the contents of the old memory chip must be copied into the new one. This may be done automatically by the VTC itself. The procedure to be followed is:

1. Disconnect the instrument from the mains supply and remove the top cover. (Once the four screws have been removed, the cover may be slid towards one corner, and the opposite corner lifted clear of the frame.)

2. Mark the old and new memory chips to avoid confusing them.

3. Carefully remove the program memory chip U2 from its socket and put it somewhere safe.

4. Carefully remove the old data memory chip U3 from its socket and install it in the U2 socket. Make sure it is the same way round. There will be a mark in one corner, or a notch at one end, which should be towards the front of the VTC. The data memory chip is a 24 pin device, whereas in later instruments the program memory chip is a 28 pin device. In this case the data memory chip should be mounted at the rear of the U2 socket, with the unused four positions towards the front of the instrument.

5. Install the new memory chip in the U3 socket. Again make sure it is the right way round.

6. Now reconnect the mains and switch the instrument on for 5 seconds, then switch it off again and disconnect from the mains once more. (Provided fingers are kept clear it is not necessary to replace the cover for this operation.). Apart from the mains indicator lighting, there will be no indication that anything is happening. The displays will not light. However a special piece of code contained within the memory chip will have copied its entire contents into the new chip.

7. Finally remove the old memory chip from the U2 socket and replace the original program memory chip in the socket. Replace the top cover and test the instrument. It should now operate normally and will still be fully calibrated.

10.3 Restoration of Original Memory Content

1

If the calibration of an instrument has been lost for any reason, it is possible to restore the original calibration parameters determined during manufacture. On units from serial number 07/006 onwards, having software version 5.01 or later, this calibration data is incorporated in the program memory EPROM U2, which is a 28 pin device type 2764.

To restore the original calibration, the red button SW1 on the main PCB should be pressed, whilst the unit is switched on. Data from U2 will automatically be copied into U3.

2

On instruments prior to serial number 07/006, with software version 4.xx, U2 is a 24 pin device type 2732. In this case the calibration data is written in a separate calibration EPROM supplied with the instrument.

To use this EPROM, follow the procedure given in section 10.2 but use the calibration EPROM in U2 socket rather than the old memory chip.

In either case it is important to use the correct calibration data for a specific instrument. Check that the label on the EPROM containing the calibration matches the serial number of the instrument it is to be used with.

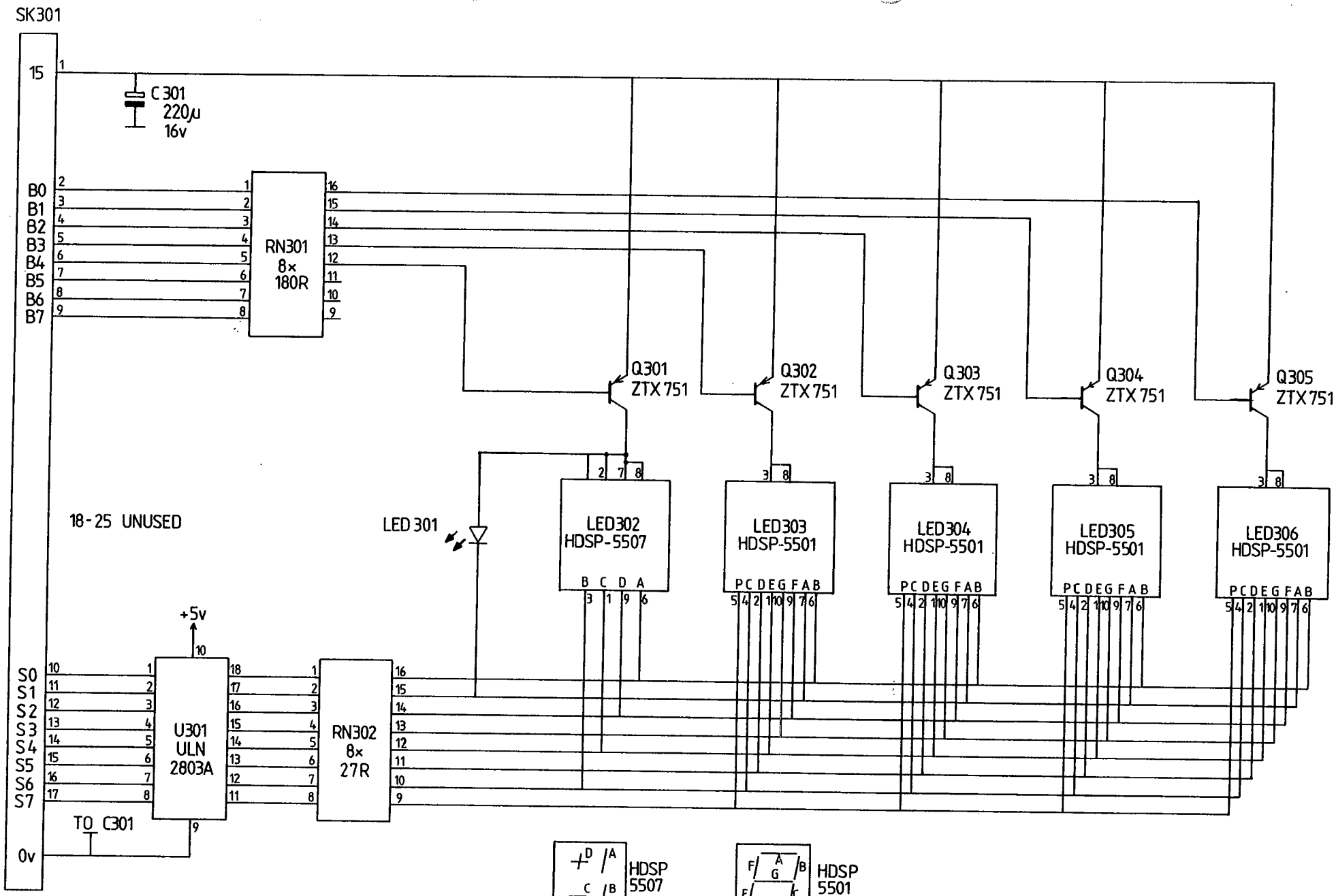

SEGMENT ALLOCATION

CQA0102 (SHEET 1 OF 1) VTC DISPLAY PCB

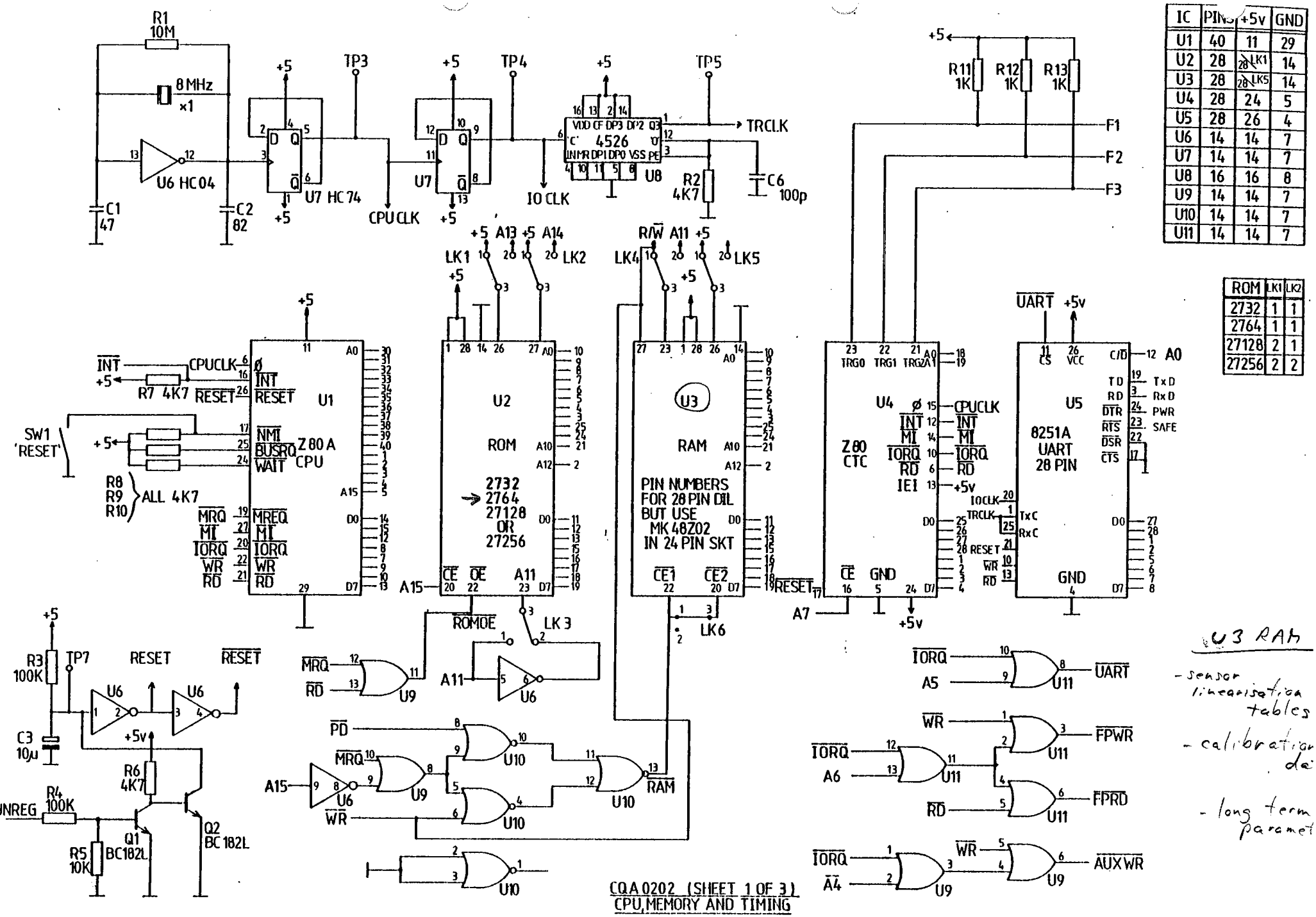

IC	PINS	+5v	GND
U1	40	11	29
U2	28	28 LK1	14
U3	28	28 LK5	14
U4	28	24	5
U5	28	26	4
U6	14	14	7
U7	14	14	7
U8	16	16	8
U9	14	14	7
U10	14	14	7
U11	14	14	7

ROM	LK1	LK2
2732	1	1
2764	1	1
27128	2	1
27256	2	2

U3 RAM

- sensor linearisation tables
- calibration da
- long term paramet

CQA 0202 (SHEET 1 OF 3)
CPU, MEMORY AND TIMING

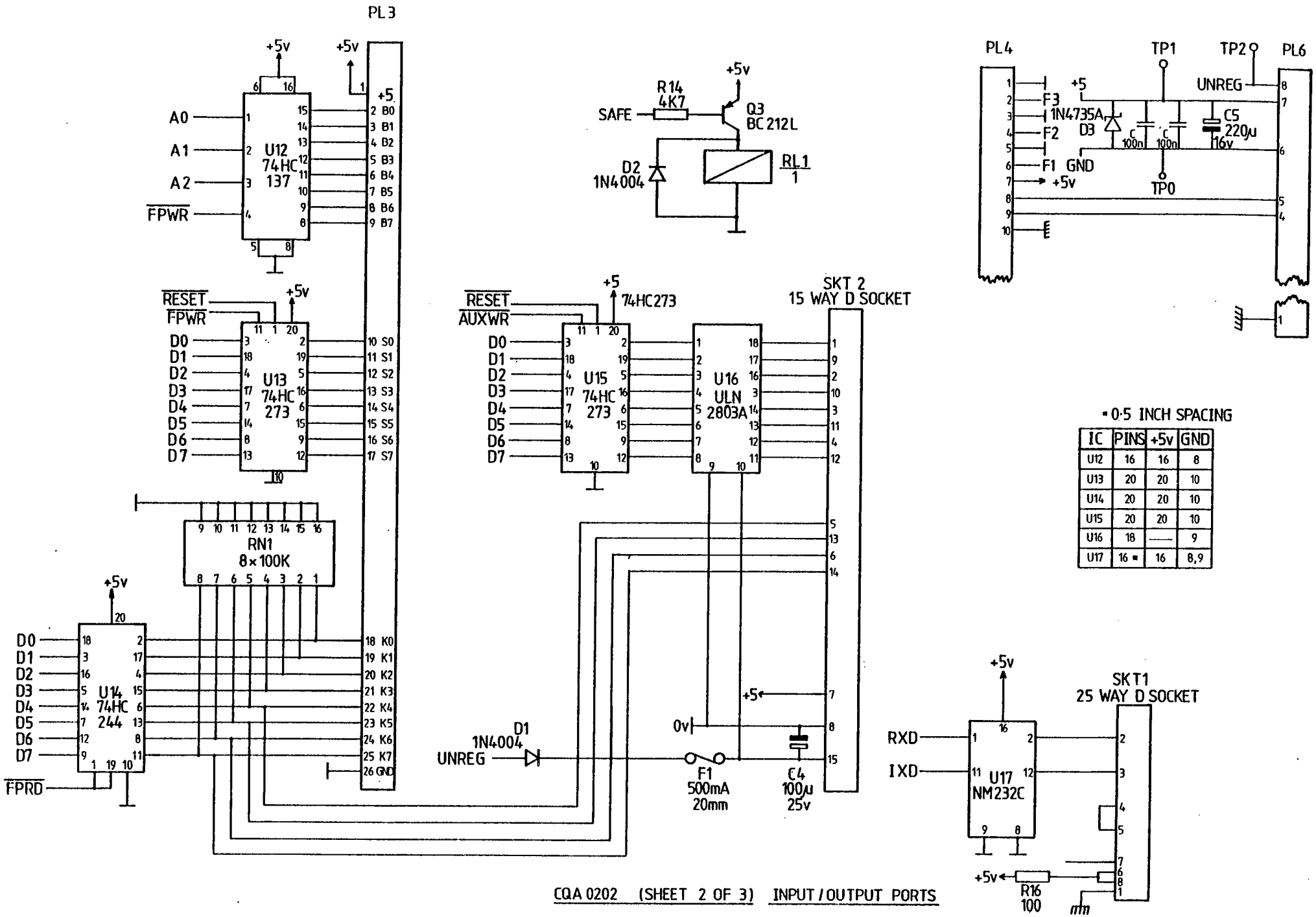

IC	PINS	+5v	GND
U12	16	16	8
U13	20	20	10
U14	20	20	10
U15	20	20	10
U16	18	—	9
U17	16 •	16	8,9

CQA 0202 (SHEET 2 OF 3) INPUT/OUTPUT PORTS

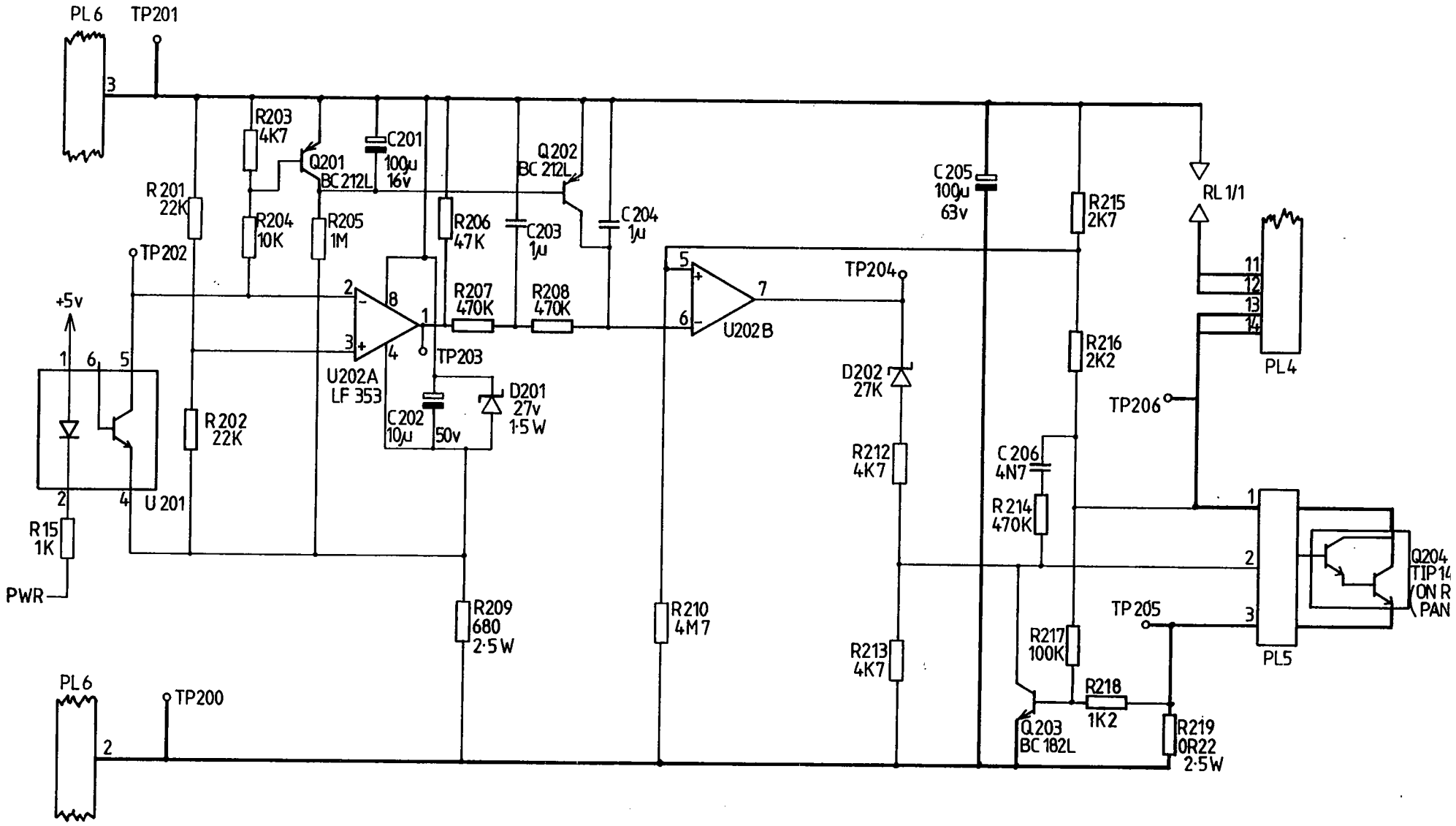

CQA 0202 (SHEET 3 OF 3) OUTPUT STAGE

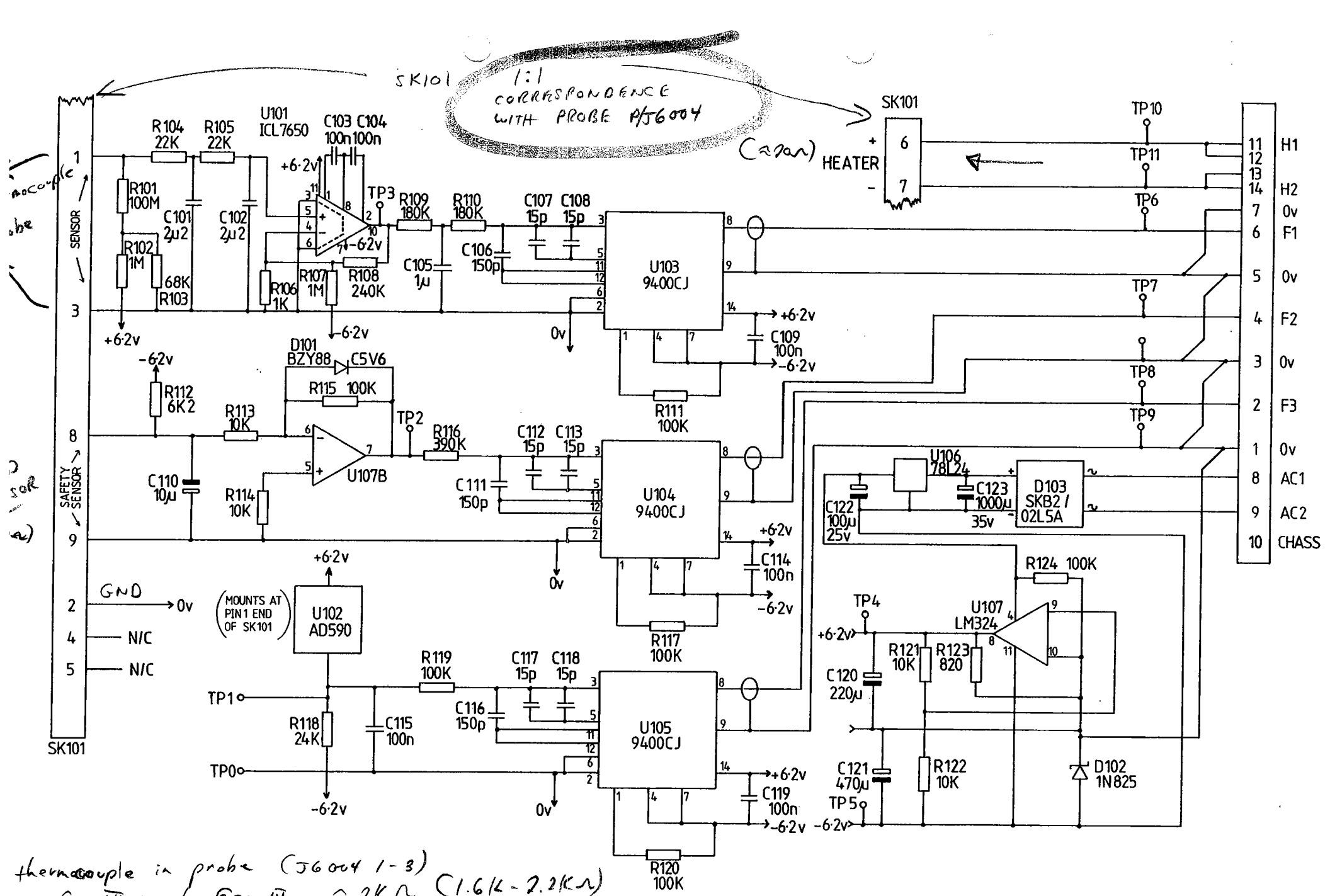

thermocouple in probe (PJ6004 1-3)
Gen III & early Gen IV ≈ 2KΩ (1.6K - 2.2KΩ)

new Gen IV 1-3 ≤ 100Ω (typ. 28Ω)

CQA 0302 (SHEET 1 OF 1) VTC INPUT PCB

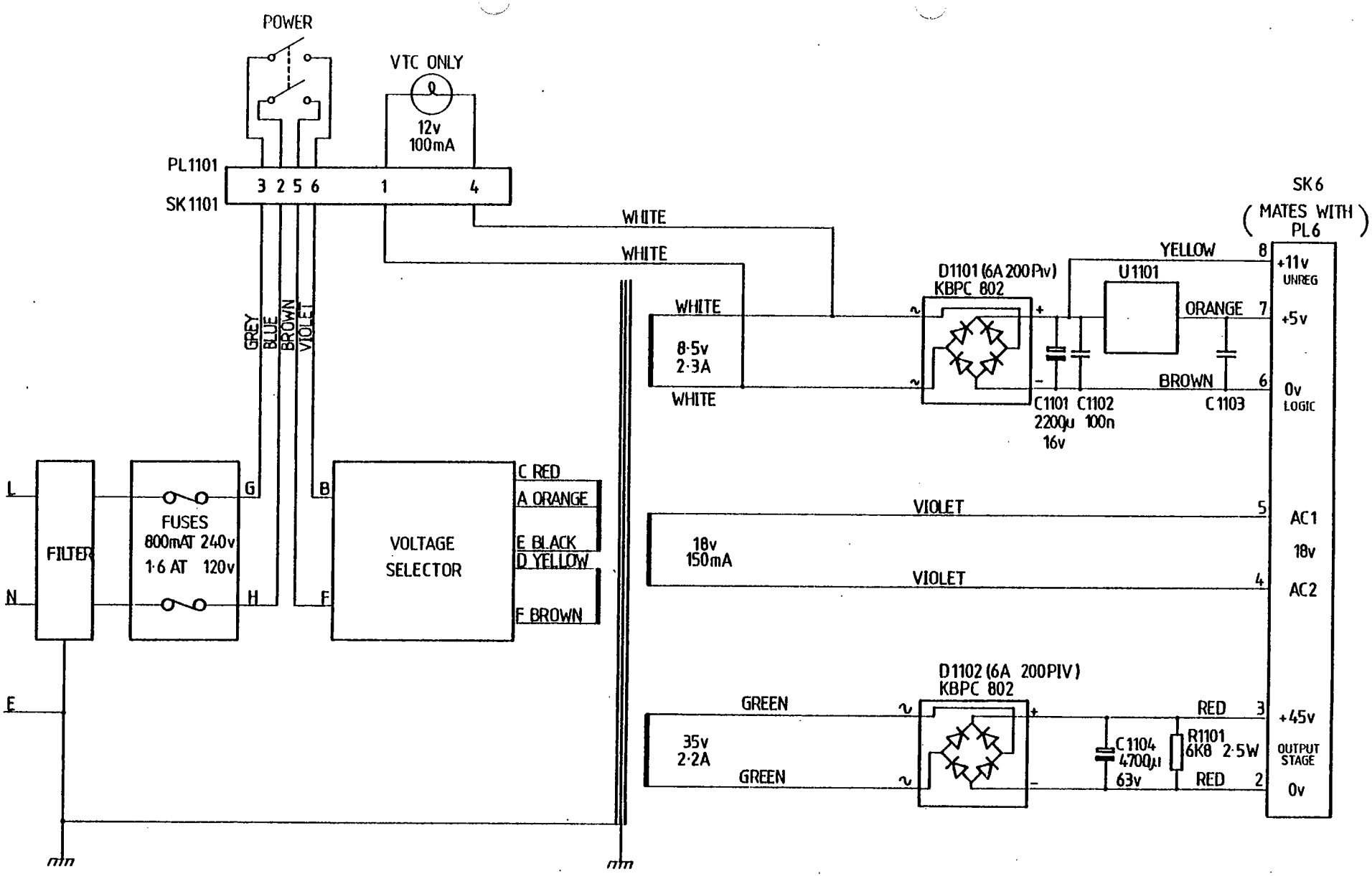

CQA 1102 (SHEET 1 OF 1) POWER SUPPLY

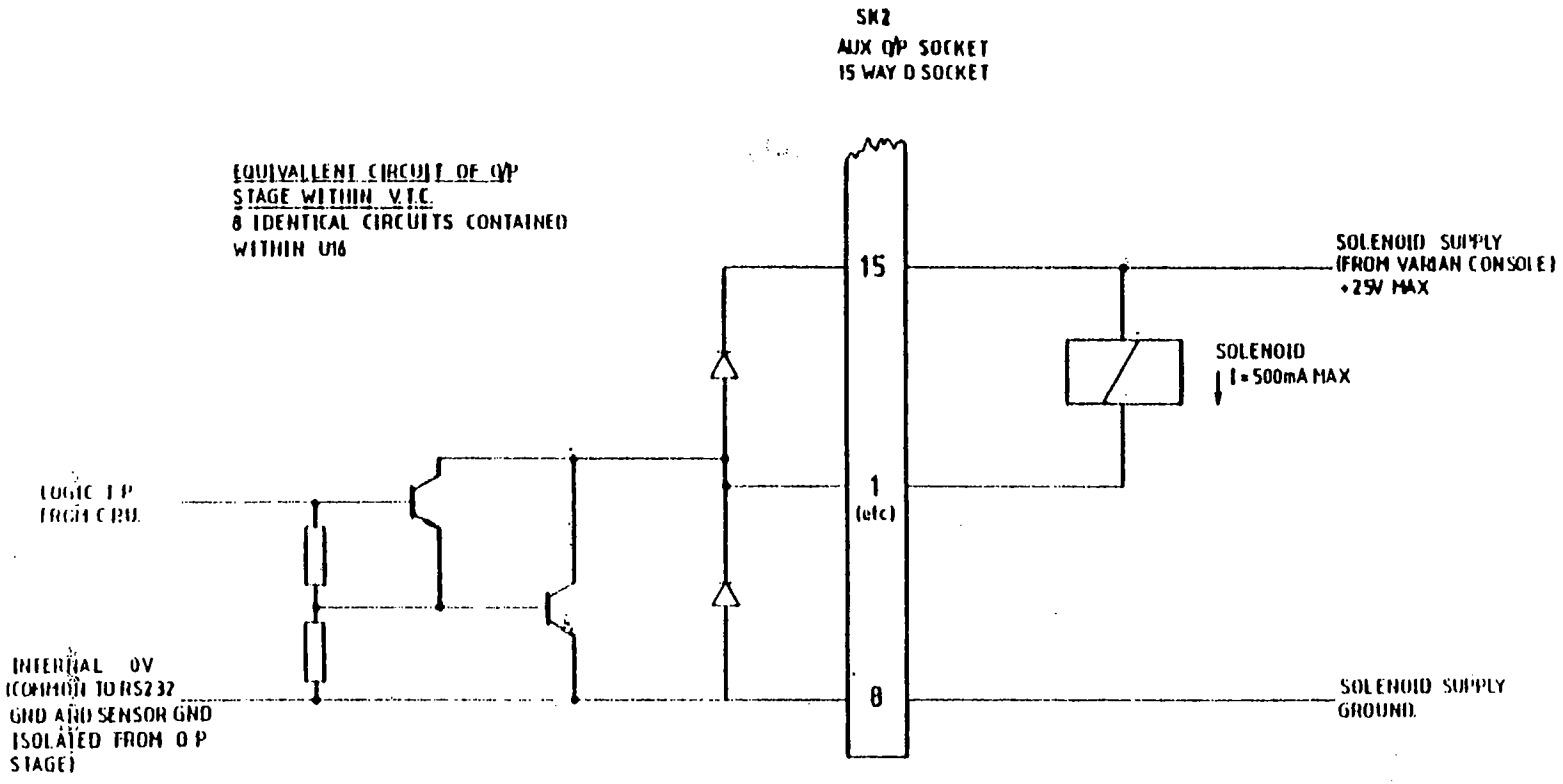
SK2
AUX O/P SOCKET
15 WAY D SOCKET
EQUIVALENT CIRCUIT OF O/P STAGE WITHIN V.T.C.
8 IDENTICAL CIRCUITS CONTAINED WITHIN U16
15
1
(etc)
8
SOLENOID SUPPLY
(FROM VARIAN CONSOLE)
+25V MAX
SOLENOID
I = 500mA MAX
LOGIC I/P
FROM CPU.
INTERNAL 0V
(COMMON TO RS232
GND AND SENSOR GND
ISOLATED FROM O/P
STAGE)
SOLENOID SUPPLY
GROUND.

CQA0200 VT CONTROLLER MAIN PCB ASSY

PART NUM	DESCRIPTION	REFERENCE DESIGNATOR
CQA0010	VTC PCB MOUNTING BLOCK	
CQA0201	VTC MAIN PCB MAN. DETAILS	
ECC0147	CAP 47p CER N150 2% 63V	C1
ECC0182	CAP 82p CER N150 2% 63V	C2
ECC0210	CAP 100p CER N150 2% 63V	C6
ECC0347	CAP 4n7 CER MED-K 10% 63V	C206
ECD0510	CAP 100n MONOCER -20+80% 50V	C10-14, C16-20.
ECP0610	CAP 1u0 POLYESTER 10% 100V	C203,204
ECR0710	CAP 10u LOWLEAK*ELEC 20% 50V	C3,C202
ECS0810	CAP 100u ELEC -10+50% 25V	C4,C201
ECS0812	CAP 100u ELEC -10+50% 63v	C205
ECS0822	CAP 220u ELEC -10+50% 16V	C5
EDA4004	DIODE 1N4004 400V 1A	D1&D2
EDR6127	ZENER 1N4750A BZX61 27V 1.3W	D201 D202
EFF2205	FUSE 20mm GLASS QUICK 500mA	F1
EFH2300	FUSEHOLDER 20mm PCB MTG	
EHN0300	FULL NUT B/Zn M3	
EHP4300	FEMALE SCREWLOCK (D TYPE)	
EHS0207	SCREW PAN-POZI B/Zn M2.5x6mm	
EHS0310	M3x10mm PAN-POZI B/Zn SCREW	
EHW3300	WASHER FIBRE M3.	
EHW4201	WASHER WAVY B/Zn M2.5	
EHW4300	WASHER WAVY B/Zn M3	
EHZ0000	SELF ADHESIVE FOAM 25x12mm 0.8	UNDER CRYSTAL
EIA0353	IC LF353 DUAL J FET AMP 8 DIL	U202
EIG0526	IC HC14526 COUNTER 16 DIL	U8
EIH0002	IC 74HC02N 14 DIL	U10
EIH0004	IC 74HC04N 14 DIL	U6
EIH0032	IC 74HC32N 14 DIL	U9&U11
EIH0074	IC 74HC74N 14 DIL	U7
EIH0137	IC 74HC137N 16 DIL	U12
EIH0244	IC 74HC244N 20 DIL	U14
EIH0273	IC 74HC273N 20 DIL	U13&U15
EIM2732	IC 2732 EPROM 450nS 24 DIL	U2
EIM4802	IC NOVRAM 2K X8 MK48Z02B	U3
EIQ0035	IC OPTO-ISOLATOR 4N35 6 DIL	U201
EIU8251	IC 8251A USART 28 DIL	U5
EIU8400	IC Z80A CPU 40 DIL	U1
EIU8430	IC Z80A CTC 28 DIL	U4
EIZ0232	IC HM232C TTL/RS232 C'INTFACE	U17
EIZ2803	IC OPTO DRLGTON DRIVER ARRY 5V	U16
EPA0000	TEST POINT (SPACE INVADER)	TP'S
EPI0025	SOCKET IC TURNED PIN 24 DIL	
EPI0028	SOCKET IC TURNED PIN 28 DIL	
EPI0040	SOCKET IC TURNED PIN 40 DIL	
EPM0303	PLG AMP .100 PCB 3P S	PL5
EPM0308	PLG AMP .100" PCB 8P S	PL6
EPM1615	SKT D TYPE PCB PLASTIC 15P 90	SK2
EPM1625	SKT D TYPE PCB PLASTIC 25P 90	SK1
EPR0314	PLG IDC PCB LOCKING 14P S	PL4
EPR0326	PLG IDC/PCB LOCKING 26P S	PL3
EQA0080	QUARTZ CRYSTAL 8MHz HC18U WRES	X1
ERB0210	RES MF 100R 1% 0.25W 50PPM	R16
ERB0247	RES MF 470R 1% 0.25W 50PPM	R214
ERB0310	RES MF 1K0 1% 0.25W 50PPM	R11,12,13, R15
ERB0312	RES MF 1K2 1% 0.25W 50PPM	R218
ERB0322	RES MF 2K2 1% 0.25W 50PPM	R216
ERB0339	RES MF 3K9 1% 0.25W 50PPM	R215
ERB0347	RES MF 4K7 1% 0.25W 50PPM	R2,R6-10, R14,R203 R212,213
ERB0410	RES MF 10K 1% 0.25W 50PPM	R5,R204
ERB0422	RES MF 22K 1% 0.25W 50PPM	R201,202
ERB0447	RES MF 47K 1% 0.25W 50PPM	R206
ERB0510	RES MF 100K 1% 0.25W 50PPM	R3,4,R217
ERB0547	RES MF 470K 1% 0.25W 50PPM	R207,208
ERB0610	RES MF 1M0 1% 0.25W 50PPM	R205
ERC0647	RES MF 4M7 5% 0.25W 100PPM	R210
ERC0710	RES MF 10M 5% 0.25W 100PPM	R1
ERM2522	RES WW 0R22 2.5W 10%	R219
ERN8510	RES NETWORK 8x100K D.I.L.	RN1
ERP2268	RES WW 680R 2.5W 5%	R209
ESR1106	RELAY MINI 3A 6V SPC/O 100R	RL1
ESZ0102	SWITCH SPST MINI .100 PCB RED	SW1
ETB0182	TR BC182L NPN 300mW TO92	Q1,2,203
ETB0212	TR BC212L PNP 300mW TO92	Q3,201,202
EZB0001	CERAMIC BEAD SDP1	FOR ITEMS 17 & 23

CQA0300 VT CONTROLLER INPUT PCB ASSY

PART NUM	DESCRIPTION	REFERENCE DESIGNATOR
CQA0010	VTC PCB MOUNTING BLOCK	
CQA0301	VTC INPUT PCB MAN. DETAILS	
ECC0115	CAP 15p CER NP0 2% 63V	C107,108 C112,113 C117,118
ECC0215	CAP 150p CER N150 2% 63V	C106,111 C116
ECD0510	CAP 100n MONOCER -20+80% 50V	C109,114 C119
ECP0510	CAP 100n POLYESTER 10% 100V	C103,104 C115
ECP0610	CAP 1u0 POLYESTER 10% 100V	C105
ECP0622	CAP 2u2 POLYESTER 10% 100V	C101,102
ECR0710	CAP 10u LOWLEAK ELEC 20% 50V	C110
ECS0810	CAP 100u ELEC -10+50% 25V	C122
ECS0822	CAP 220u ELEC -10+50% 16V	C120
ECS0847	CAP 470u ELEC -10+50% 16V	C121
ECS0912	CAP 1m0 ELEC -10+50% 40V	C123
EDB0220	DIODE BRIDGE 1.6A 200v	D103
EDR0825	DIODE REF. 1N825 6.2V 20ppm	D102
EDR8805	ZENER BZY88 C5V6 500mW	D101
EHN0300	FULL NUT B/Zn M3	
EHP4300	FEMALE SCREWLOCK (D TYPE)	
EHS0207	SCREW PAN-POZI B/Zn M2.5x6mm	
EHS0310	M3x10mm PAN-POZI B/Zn SCREW	
EHW3300	WASHER FIBRE M3.	
EHW4201	WASHER WAVY B/Zn M2.5	
EHW4300	WASHER WAVY B/Zn M3	
EIA0324	IC QUAD OP-AMP LM324 LOW POWER	U107
EIA7650	IC OP-AMP ICL 7650 U-LOW DRIFT	U101
EID9400	IC 9400CJ V/F CONV. 14 DIL	U103,104 U105
EIV7825	IC VOLT REG. 78L24 24V 100mA	U106
EPA0000	TEST POINT (SPACE INVADER)	
EPM1609	SKT D TYPE PCB (PLASTIC) 9P 90	SK102
EPR0314	PLG IDC PCB LOCKING 14P S	SK101
EQT0590	THERM SENSR AD590JH -55to+150C	U102 POSITION AS DRAWN
ERB0282	RES MF 820R 1% 0.25W 50PPM	R123
ERB0310	RES MF 1K0 1% 0.25W 50PPM	R106
ERB0362	RES MF 6K2 1% 0.25W 50PPM	R112
ERB0410	RES MF 10K 1% 0.25W 50PPM	R113,114 R121,122
ERB0422	RES MF 22K 1% 0.25W 50PPM	R104,105
ERB0424	RES MF 24K 1% 0.25W 50PPM	R118
ERB0468	RES MF 68K 1% 0.25W 50PPM	R103
ERB0510	RES MF 100K 1% 0.25W 50PPM	R111,117 R119,120 R124
ERB0516	RES MF 160K 1% 0.25W 50PPM	R115
ERB0518	RES MF 180K 1% 0.25W 50PPM	R109,110
ERB0524	RES MF 240K 1% 0.25W 50PPM	R108
ERB0539	RES MF 390K 1% 0.25W 50PPM	R116
ERB0610	RES MF 1M0 1% 0.25W 50PPM	R107
ERC0710	RES MF 10M 5% 0.25W 100PPM	R102
ERC0810	RES CA 100M 5% .5W	R101

CQA1000 VT CONTROLLER FRONT PANEL ASSY

PART NUM	DESCRIPTION	REFERENCE DESIGNATOR
CQA1J00	VTC FRONT PANEL SUB ASSY	
EFB3210	INS BOOT 32mm FUSE (BLACK)	
EFL1014	BULB 14V HIGHLAND	
EPM3306	PLG TRI-DENT,CABLE,6WAY	
EPT0520	CONNECTOR PIN SIZE 20 BICC	
ESZ3240	SWITCH SERIES 31 H'LAND ROUND	
ESZ3242	LENS ROUND RED,FOR ESZ3240	
EWS0301	WIRE 3A 16/0.2 PVC BROWN	
EWS0306	WIRE 3A 16/0.2 PVC BLUE	
EWS0307	WIRE 3A 16/0.2 PVC VIOLET	
EWS0308	WIRE 3A 16/0.2 PVC GREY	

EWS0309	WIRE 3A 16/0.2 PVC WHITE	2 LENGTHS
EWT3095	CABLE TYRAP 2.5x95mm	

CQA1400 VT CONTROLLER REAR PANEL ASSY

PART NUM	DESCRIPTION	REFERENCE DESIGNATOR
CQA1100	VTC TRANSFORMER MTG ASSY	
CQA1401	VTC REAR PANEL DETAILS	CQA1405
EHN0300	FULL NUT B/Zn M3	
EHS1310	SCREW CSK-POZI B/Zn M3x10mm	
EHW5300	WASHER STAR B/Zn M3	
EWZ2015	INS SLEEVE 20mmX1.5mm I/D BLK	
EZF3786	FILTER 240V AC FUSED FN378-6	

CQA1500 VTC INPUT/MAIN PC HARNESS

PART NUM	DESCRIPTION	REFERENCE DESIGNATOR
EPR2014	SKT.IDC 14W STRAIN RELIEF.	
EWR0114	RIBBON CABLE GREY 14 WAY	

CQA1600 HEATSINK/TRANSISTOR ASSY

PART NUM	DESCRIPTION	REFERENCE DESIGNATOR
CQA0420	HEATSINK 3E-1 MACHINED 1.7c/W	
EHS0306	M3x6mm PAN-POZI B/Zn SCREW	
EPM0203	SKT AMP .100 PCB 3P S	
ETP0141	TR TIP141 DPN 125W 80V TO220	
EWS0151	WIRE 1.4A 7/0.2 PVC BROWN	
EWS0152	WIRE 1.4A 7/0.2 PVC RED	
EWS0153	WIRE 1.4A 7/0.2 PVC ORANGE	
EWT3095	CABLE TYRAP 2.5x95mm	
EWZ2015	INS SLEEVE 20mmX1.5mm I/D BLK	
EZS1032	INS.WASH MICA TO3P	
EZS1033	INS.BUSH NYLON TO3P	

CQA0000 V.T. CONTROLLER FINAL ASSY (EA)

PART NUM	DESCRIPTION	REFERENCE DESIGNATOR
CQA0020	VTC MTG. EARS 2U	
CQA0099	VT CONTROLLER SPARES KIT	
CQA0100	VT CONTROLLER DISPLAY PCB ASSY	
CQA0200	VT CONTROLLER MAIN PCB ASSY	
CQA0300	VT CONTROLLER INPUT PCB ASSY	
CQA1000	VT CONTROLLER FRONT PANEL ASSY	
CQA1400	VT CONTROLLER REAR PANEL ASSY	
CQA1500	VTC INPUT/MAIN PC HARNESS	
CQA1600	HEATSINK/TRANSISTOR ASSY	
EEA0200	TAPPED STRIP BITE M2.5 (411mm)	
EJC2319	CASE HARMONIE 20x19"x261mm	
EHS0207	SCREW PAN-POZI B/Zn M2.5x6mm	
EHS0306	M3x6mm PAN-POZI B/Zn SCREW	
EHS0308	M3x8mm PAN-POZI B/Zn SCREW	
EHS1211	SCREW CSK-POZI B/Zn M2.5x10mm	
EHS8211	M2.5x10mm SCREW R'SED CSK BLCK	
EHW4201	WASHER WAVY B/Zn M2.5	
EHW5201	WASHER STAR B/Zn M2.5	
EHW5300	WASHER STAR B/Zn M3	

CQA0099 VT CONTROLLER SPARES KIT

PART NUM	DESCRIPTION	REFERENCE DESIGNATOR
CQA0999	VTC4 MANUAL	
EFF2308	FUSE 20MM GLAS ANTISURGE800N/A	
EFF2316	FUSE 20MM GLASS ANTISURGE 1.6A	

CQA0100 VT CONTROLLER DISPLAY PCB ASSY

PART NUM	DESCRIPTION	REFERENCE DESIGNATOR
CQA0010	VTC PCB MOUNTING BLOCK	
CQA0101	VTC DISPLAY PCB MAN. DETAILS	CQA0103
CQA1200	VTC DISP/MAIN PCB HARNESS	
ECS0822	CAP 220n ELEC -10+50% 16V	C301
EDL0002	LED GREEN STD .2"	LED301
EHS0207	SCREW PAN-POZI B/Zn M2.5x6mm	
EHW4201	WASHER WAVY B/Zn M2.5	
EIP5501	LED DIGIT 7 SEG .56 HE RED AN	LED303-306
EIP5507	LED SIGN DISPLAY .5o HE RED AN	LED302
EIZ2803	IC OPTO DRLGTON DRIVER ARRY 5V	U301
EPI0025	SOCKET IC TURNED PIN 24 DIL	
EPI0028	SOCKET IC TURNED PIN 28 DIL	
ERN0133	RES.NETWORK 8x33R D.I.L.	RN302
ERN0218	RES NETWORK 8X180R D.I.L.	RN301
ETB0751	TR ZTX 751 PNP BI-POLAR	Q301-305

CQA1100 VTC TRANSFORMER MTG ASSY

PART NUM	DESCRIPTION	REFERENCE DESIGNATOR
CQA1101	VTC TRANSFORMER MTG PLATE	
CQA1110	MTG. PLATE HARNESS SKT (VTC)	
ECD0510	CAP 100n MONOCER -20+80% 50V	C1102,1103
ECS0922	CAP 2m2 ELEC -10+50% 16V	C1101
ECS0947	CAP 4700uF ELEC -10+50% 63V	C1104
EDB0260	DIODE BRIDGE RECT. 6A 200V	D1101,1102
EHN0300	FULL NUT B/Zn M3	
EHS0205	SCREW PAN-POZI B/Zn M2.5x4mm	
EHS0304	M3x4mm PAN-POZI B/Zn SCREW	
EHS0312	M3x12mm PAN-POZI B/Zn SCREW	
EHS0405	SCREW PAN POZI B/Z M4x5mm	
EHW5300	WASHER STAR B/Zn M3	
EHW5400	WASHER STAR B/Zn M4	
EHZ0000	SELF ADHESIVE FOAM 25x12mm	PUT ON TOP OF ITEM 4
EHZ0005	CLAMP CAP (16mm DIA) BLACK	
EHZ0009	CLAMP CAP, 35mm DIA JO'	
EIV7805	IC VOLTAGE REG. 1A +5V	U1101
ELS0001	TRANSFORMER VT CONTROLLER	T1101
EPA0110	SOLDER TAG (EYELET) 4DA	
EPM0208	SKT AMP .100"PCB 8P S	SK6
EPM3206	SKT TRI-DENT,CABLE,6 WAY	SK1101
EPT0420	CONNECTOR SKT SIZE 20 BICC	
ERP0368	RES WW 6K8 2.5W 5%	R1101
EWS0150	WIRE 1.4A 7/0.2 PVC BLACK	
EWS0150	WIRE 1.4A 7/0.2 PVC BLACK	
EWS0151	WIRE 1.4A 7/0.2 PVC BROWN	
EWS0152	WIRE 1.4A 7/0.2 PVC RED	
EWS0152	WIRE 1.4A 7/0.2 PVC RED	
EWS0153	WIRE 1.4A 7/0.2 PVC ORANGE	
EWS0154	WIRE 1.4A 7/0.2 PVC YELLOW	
EWS0301	WIRE 3A 16/0.2 PVC BROWN	
EWS0306	WIRE 3A 16/0.2 PVC BLUE	
EWS0307	WIRE 3A 16/0.2 PVC VIOLET	
EWS0308	WIRE 3A 16/0.2 PVC GREY	
EWS0310	WIRE 3A 16/0.2 PVC GRN/YLLW	
EWT2101	'P'CLIP SIZE Nx1 BLACK	
EWT2102	'P'CLIP SIZE Nx2 BLACK	REAR
EWT3095	CABLE TYRAP 2.5x95mm	
EZS1220	INS.WASH MICA TO220AB	
EZS1221	INS.BUSH NYLON TO220AB	